STP-NU-018

# CREEP-FATIGUE DATA AND EXISTING EVALUATION PROCEDURES FOR GRADE 91 AND HASTELLOY XR

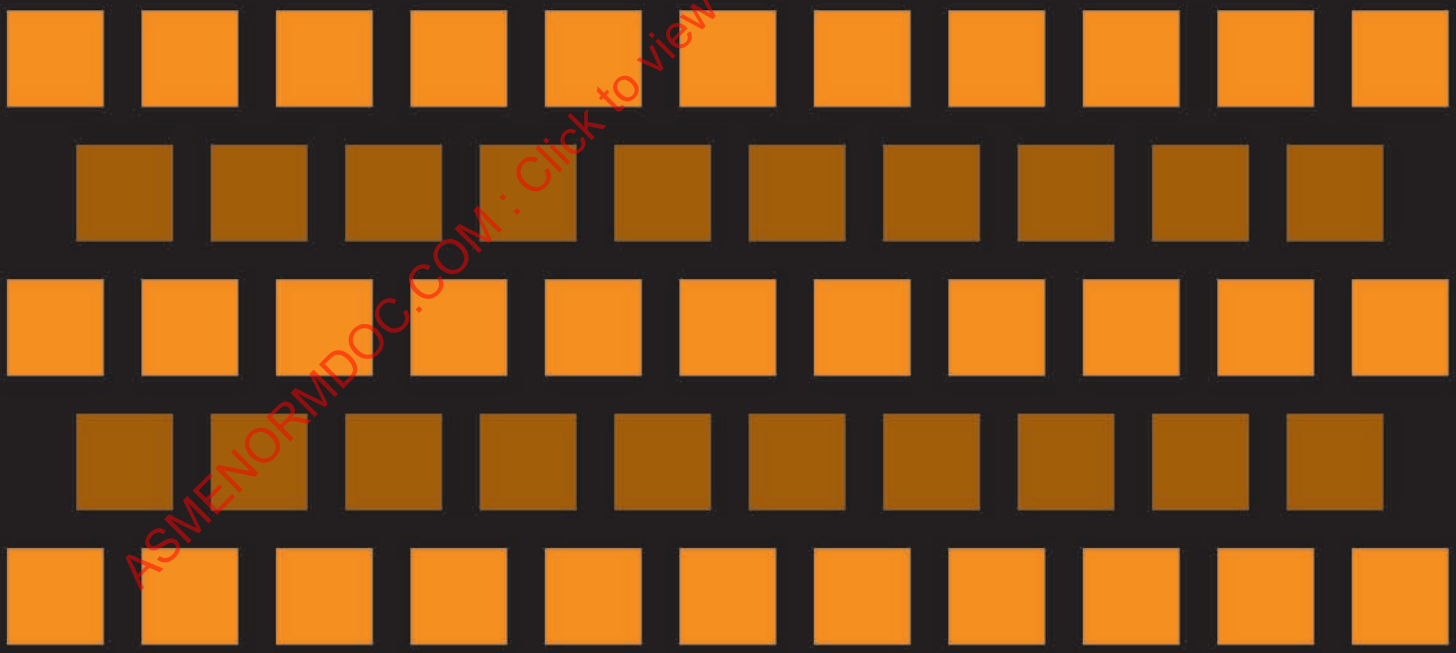

INTENTIONALLY LEFT BLANK

STP-NU-018

# CREEP-FATIGUE DATA AND EXISTING EVALUATION PROCEDURES FOR GRADE 91 AND HASTELLOY XR



*Prepared by:*

Tai Asayama and Yukio Tachibana

Japan Atomic Energy Agency

ASME STANDARDS TECHNOLOGY, LLC

Date of Issuance: May 21, 2009

This report was prepared as an account of work sponsored by U.S. Department on Energy (DOE) and the ASME Standards Technology, LLC (ASME ST-LLC).







ASME Standards Technology, LLC
Three Park Avenue, New York, NY 10016-5990

ISBN No. 978-0-7918-3184-7

# TABLE OF CONTENTS

## LIST OF TABLES

## LIST OF FIGURES

## FOREWORD

This report describes the results of investigation on Task 5 of DOE/ASME Materials Project based on a contract between ASME Standards Technology, LLC (ASME ST-LLC) and Japan Atomic Energy Agency (JAEA). Task 5 is to collect available creep-fatigue data and study existing creep-fatigue evaluation procedures for Grade 91 steel and Hastelloy XR. Part I of this report is devoted to Grade 91 steel. Part II of this report is devoted to Hastelloy XR.

The American Society of Mechanical Engineers (ASME) is a not-for-profit professional organization promoting the art, science and practice of mechanical and multidisciplinary engineering and allied sciences. ASME develops codes and standards that enhance public safety, and provides lifelong learning and technical exchange opportunities benefiting the engineering and technology community. Visit www.asme.org.

The ASME Standards Technology, LLC (ASME ST-LLC) is a not-for-profit Limited Liability Company, with ASME as the sole member, formed in 2004 to carry out work related to newly commercialized technology, expanding upon the former role of ASME's Codes and Standards Technology Institute (CSTI). The ASME ST-LLC mission includes meeting the needs of industry and government by providing new standards-related products and services, which advance the application of emerging and newly commercialized science and technology and providing the research and technology development needed to establish and maintain the technical relevance of codes and standards. Visit www.stllc.asme.org for more information.

## EXECUTIVE SUMMARY

This report describes the results of investigation on Task 5 of DOE/ASME Materials Project based on a contract between ASME Standards Technology, LLC (ASME ST-LLC) and Japan Atomic Energy Agency (JAEA). Task 5 is to collect available creep-fatigue data and study existing creep-fatigue evaluation procedures for Grade 91 steel and Hastelloy XR. Part I of this report is devoted to Grade 91 steel. Existing creep-fatigue data were collected (Appendix A) and analyzed from the viewpoints of establishing a creep-fatigue procedure for VHTR design. A fair amount of creep-fatigue data has been obtained and creep-fatigue phenomena have been clarified to develop design standards mainly for fast breeder reactors. Following this, existing creep-fatigue procedures were studied and it was clarified that the creep-fatigue evaluation procedure of the ASME-NH has a lot of conservatisms and they were analyzed in detail from the viewpoints of the evaluation of creep damage of material. Based on the above studies, suggestions to improve the ASME-NH procedure along with necessary research and development items were presented. Part II of this report is devoted to Hastelloy XR. Existing creep-fatigue data used for development of the high temperature structural design guideline for High Temperature Gas-cooled Reactor (HTGR) were collected. Creep-fatigue evaluation procedure in the design guideline and its application to design of the intermediate heat exchanger (IHX) for High Temperature Engineering Test Reactor (HTTR) was described. Finally, some necessary research and development items in relation to creep-fatigue evaluation for Gen IV and VHTR reactors were presented.

# PART I
# GRADE 91

# 1 COLLECTION OF AVAILABLE DATA

## 1.1 Outline of Collected Data

Data obtained in various organizations such as Japan Atomic Energy Agency (JAEA), Electric Power Research Institute (EPRI), Oak Ridge National Laboratory (ORNL), Central Research Institute of Power Industry in Japan (CRIEPI), National Institute of Material Science in Japan (NIMS) and the University of Tokyo were collected from available sources as listed in Table 1 Data collected include 205 creep data, 281 fatigue data and 78 creep-fatigue data. Product forms include plate, forgings and pipe. Chemical compositions available in the data sources are summarized in Table 2. Most of the data are considered to have been obtained for the application to the development of fast breeder reactors.

## 1.2 Evaluation of Collected Data

Collected data were evaluated in terms of creep properties, fatigue properties and creep-fatigue properties. Details are described below.

### 1.2.1 Creep Properties

*(a)* General trend

Creep rupture life is shown in Figure 1. All the collected data showed a uniform trend and there were no data that showed obvious discrepancy compared to other data.

*(b)* Environmental effect in sodium

In Figure 1, data in sodium are plotted for comparison at a temperature range from 450 to 600˚C. Although creep rupture time was slightly longer in sodium at 600˚C, basically it was same both in air and sodium environments, and environmental effects due to sodium were not observed.

### 1.2.2 Fatigue Properties

*(a)* General trend

Fatigue life is plotted against total strain range in Figure 2 to Figure 7. All the collected data were obtained under completely reversed strain controlled conditions using uniaxial push-pull specimens. Along with the experimental data, an average trend derived from the DDS procedure (See Reference. Outline of the procedure is shown in Chapter 2 of this report.) by substituting safety margins from design curves are shown in the figures. In general, fatigue life showed clear strain rate dependency. As strain rate becomes slower, fatigue life becomes shorter. EPRI data showed shorter fatigue life at 550˚C but the reason is not clear.

*(b)* Effect of thermal aging

In Figure 5, available data with thermal aging at 550˚C are plotted. As far as these data are concerned, no effect of thermal aging on fatigue life was observed.

*(c)* Effect of environment

From Figure 3 to Figure 6, it is shown that fatigue life in sodium is obviously longer than that in air. This trend is the same for a vacuum environment but the difference is more pronounced in a vacuum than in sodium as shown in Figure 6. The difference of fatigue life in air and vacuum environments is as much as an order of magnitude. This is attributed to the fact that oxidation of test specimens is negligible in vacuum.

*(d)* Stress-strain relationship

Figure 8 and Figure 12 show stress-strain relationships at mid-life. The slower the strain rate, the smaller the stress ranges. This tendency is more pronounced at higher temperatures. Although from Figure 11, is not clear if additional softening occurs due to aging, this point will be further addressed in Section 2.5 of this report. Effects of environments do not exist for stress-strain response because they are identical irrespective of environments under which they were obtained.

### 1.2.3 Creep-Fatigue Properties

Available creep-fatigue data are plotted in Figure 13 to Figure 15. Along with the experimental data, average trends derived from DDS procedure by substituting safety margins are shown in the figures. All the collected data were obtained under completely reversed strain controlled conditions using uniaxial push-pull specimens, and strain was held either at a tensile peak, at a compressive peak or at both tensile and compressive peaks.

*(a)* Reduction of creep-fatigue life due to strain hold

Creep-fatigue life reduction occurs due to introduction of strain hold period. At 500˚C, creep-fatigue life is almost identical to fatigue life as long as a hold time is less than 60 minutes. Tests with a compressive hold period showed greater life reduction than those with a tensile hold period.

*(b)* Effect of strain hold period

Creep-fatigue life is plotted against strain hold time in Figure 16 to Figure 18. Most of the data were obtained with a hold time not larger than 60 minutes and the saturation of creep-fatigue life is not clearly observed.

### 1.2.4 Points to be Addressed

As described above, a fair amount of creep-fatigue data have been obtained. However, most of the data were originally obtained for the application to fast breeder reactors and the temperature range is limited to 400 to 650 degrees C. Within this temperature range, creep-fatigue data have been accumulated to the extent that they serve to clarify the mechanisms of creep-fatigue life reduction of this steel, if not sufficient in quantity. Tests with a tensile hold time, a compressive hold time and both tensile and compressive hold times have been conducted. Most of the data were obtained in an air environment but data in sodium and vacuum environments are also available, and they give us valuable information. For the effect of aging, available data is not necessarily sufficient to clarify the effects on stress-strain response and creep-fatigue life.

**Table 1 - Mod. 9Cr-1Mo Material Data Source List (Temp is 400˚C or higher)**

| Research Laboratories | Creep | Fatigue | Creep Fatigue | Reference |
|---|---|---|---|---|
| EPRI | 3 | 15 | - | (1) |
| CRIEPI | 6 | 12 | 9 | (1) |
| ORNL | 3 | 9 | 17 | (2) |
| Univ. of Connecticut | - | 3 | - | (3) |
| Univ. of Tokyo | - | 13 | 3 | |
| JAEA | 176 | 161 | 27 | (4) |
| NIMS | 17 | 68 | 22 | (5),(6),(7),(8) |
| Total | 205 | 281 | 78 | |

(1) M. Ruggles and T. Ogata, Creep-Fatigue Criteria and Inelastic Behavior of Modified 9Cr-1Mo Steel at Elevated Temperatures, ORNL/M-3198.

(2) B. Giseke, C. Brinkman and P.. Maziasz, The Influence of Thermal Aging the Microstructure and Fatigue Properties of Modified 9Cr-1Mo Steel, ORNL, TN 37831-6155, 1993.

(3) J. McEvily and J. Bunch, Fatigue Behavior of Chromium-Containing Ferritic Steels at Elevated Temperature, IMS, 1985.

(4) Japan Atomic Energy Agency, Material Test Data of 2.25Cr-1Mo and Mod.9Cr-1Mo Steels, TN9450 2003-004, 2003.

(5) NRIM, Fatigue Dat a Sheet No. 49, 1985.

(6) NRIM, Fatigue Data Sheet No. 15, 1979.

(7) NRIM, Fatigue Data Sheet No. 78, 1993.

(8) NRIM, Fatigue Data Sheet No. 43, 1996.

**Table 2 - Chemical Composition of Mod. 9Cr-1Mo**

| Heat | Research laboratories | C | Si | Mn | P | S | Ni | Cr | Mo | V | Nb | Al | N |
|---|---|---|---|---|---|---|---|---|---|---|---|---|---|
| F2 | JAEA | 0.1 | 0.4 | 0.43 | 0.01 | 0 | 0.07 | 8.73 | 0.96 | 0.22 | 0.09 | 0.01 | 0.051 |
| F3 | JAEA | 0.09 | 0.41 | 0.42 | 0.01 | 0 | 0.09 | 8.83 | 0.98 | 0.21 | 0.07 | 0.02 | 0.04 |
| F4 | JAEA | 0.1 | 0.25 | 0.37 | 0.01 | 0.03 | 0.08 | 9.1 | 0.93 | 0.22 | 0.09 | 0 | 0.043 |
| F5 | JAEA | 0.1 | 0.24 | 0.38 | 0.01 | 0 | 0.08 | 8.99 | 0.95 | 0.22 | 0.09 | 0 | 0.042 |
| F6 | JAEA | 0.1 | 0.39 | 0.42 | 0.01 | 0 | 0.06 | 8.75 | 0.97 | 0.21 | 0.089 | 0.01 | 0.051 |
| F7 | JAEA | 0.1 | 0.39 | 0.43 | 0.01 | 0 | 0.06 | 8.69 | 0.93 | 0.2 | 0.09 | 0.01 | 0.052 |
| F8 | JAEA | 0.09 | 0.23 | 0.37 | 0.02 | 0 | 0.18 | 8.82 | 0.97 | 0.2 | 0.066 | 0 | 0.048 |
| F9 | JAEA | 0.1 | 0.26 | 0.42 | 0.01 | 0 | 0.1 | 8.84 | 0.96 | 0.22 | 0.08 | 0 | 0.068 |
| F10 | JAEA | 0.09 | 0.24 | 0.44 | 0 | 0 | 0.04 | 8.76 | 0.94 | 0.21 | 0.08 | 0.01 | 0.054 |
| F11 | JAEA | 0.1 | 0.25 | 0.42 | 0.01 | 0 | 0.13 | 8.67 | 0.98 | 0.19 | 0.09 | 0.01 | 0.06 |
| 30394 | ORNL | 0.084 | 0.4 | 0.46 | 0.01 | 0.003 | 0.09 | 8,57 | 0.198 | 0.198 | 0.073 | 0.014 | 0.053 |
| ORNL | Univ. of Connecticut | 0.09 | 0.19 | 0.37 | | 0.02 | 0.09 | 8.47 | 0.88 | 0.21 | 0.07 | 0 | 0.54 |
| Tokyo | Univ. of Tokyo | 0.08 | 0.26 | 0.45 | 0.006 | 0.001 | 0.1 | 8.89 | 0.95 | | | | |
| NRIM1 | NIMS | 0.09 | 0.34 | 0.46 | 0.005 | 0.004 | 0.09 | 8.43 | 0.9 | 0.2 | 0.079 | 0.01 | 0.062 |

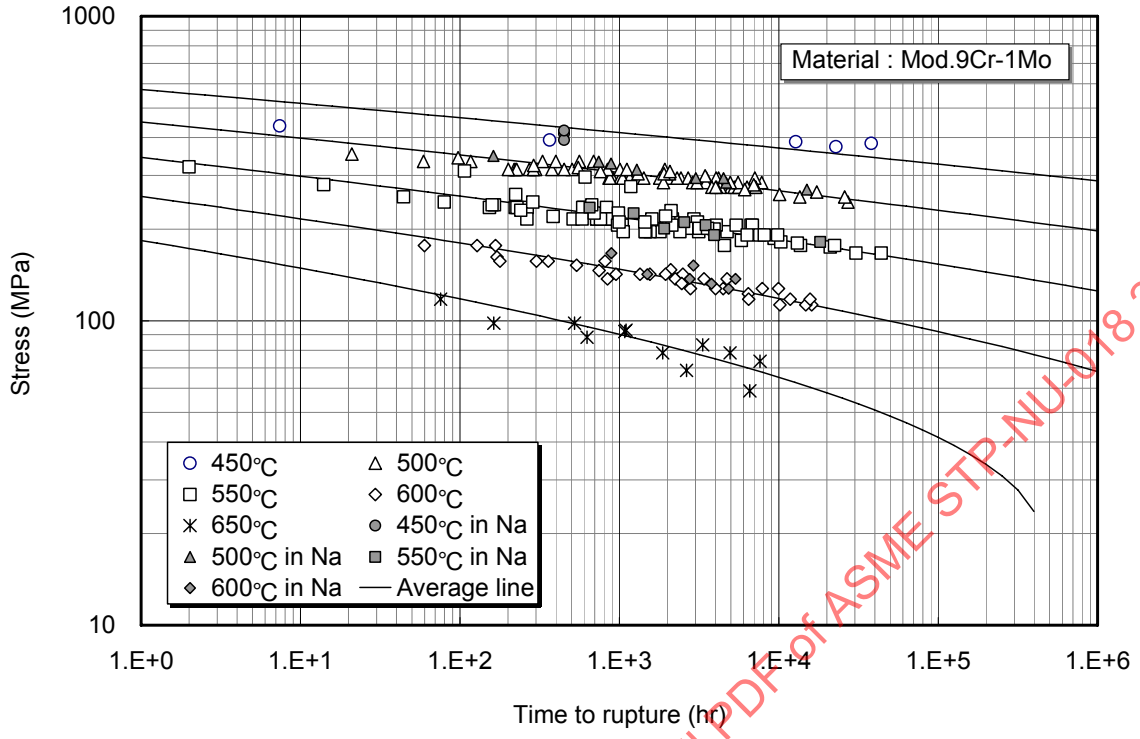


**Figure 1 - Creep Rupture: Average Curves and Experimental Values**

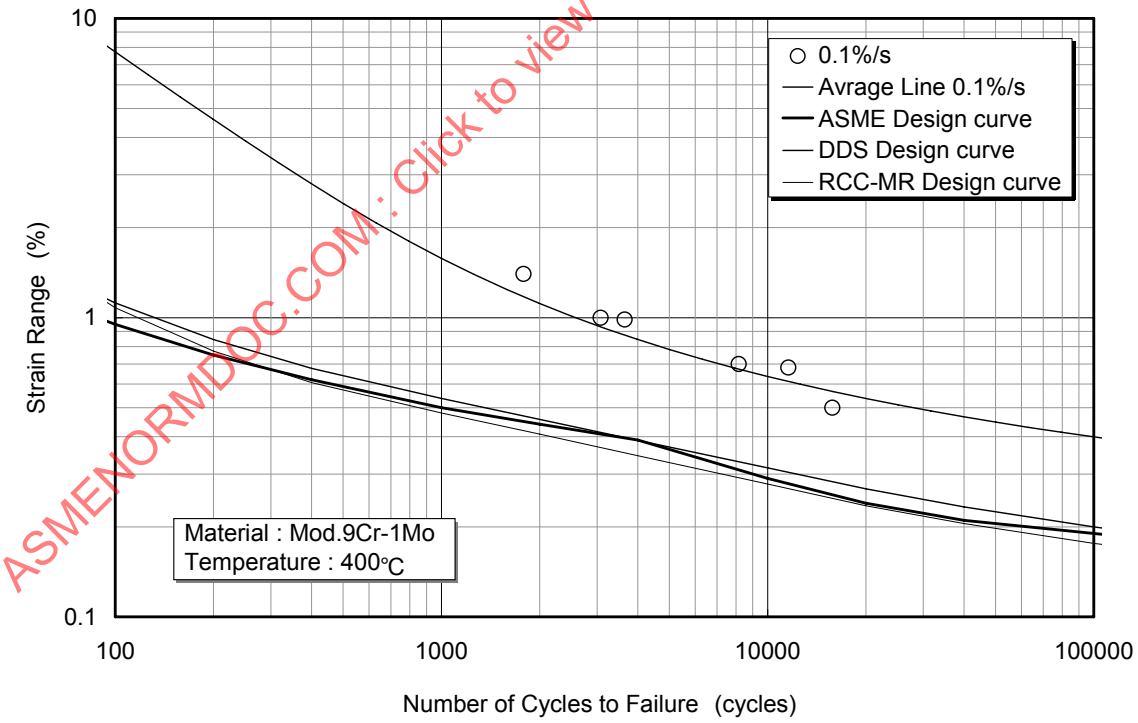


**Figure 2 - Fatigue Life: Average Curves and Experimental Values at 400˚C**

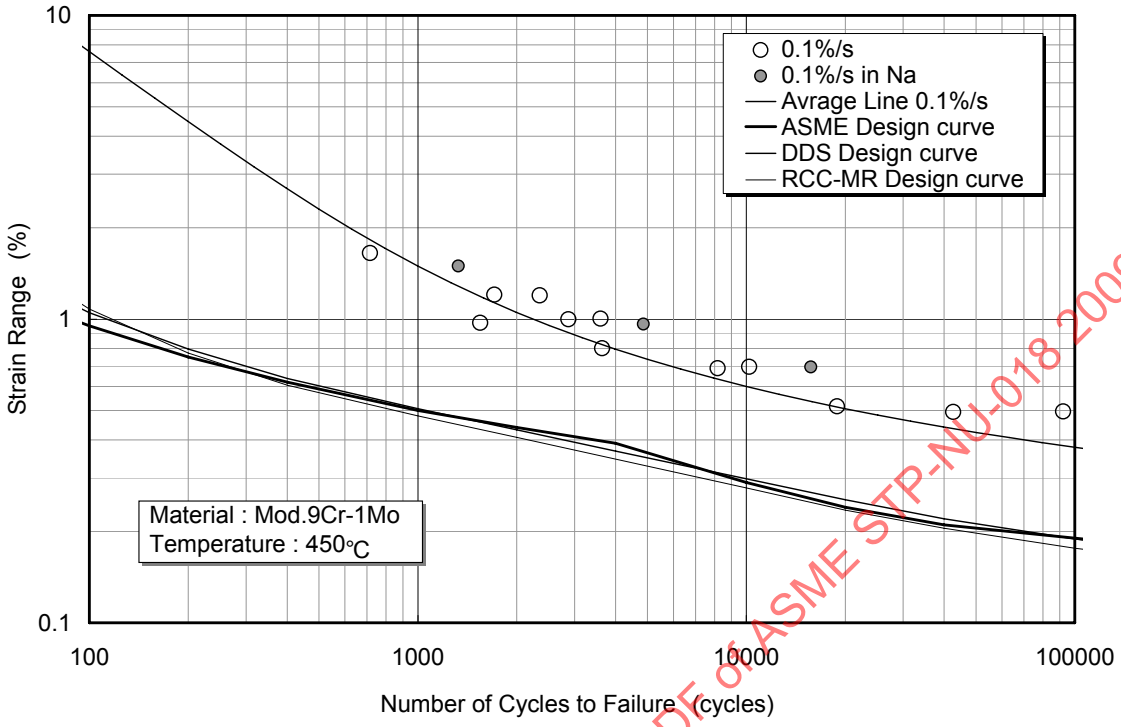


**Figure 3 - Fatigue Life: Average Curves and Experimental Values at 450˚C**

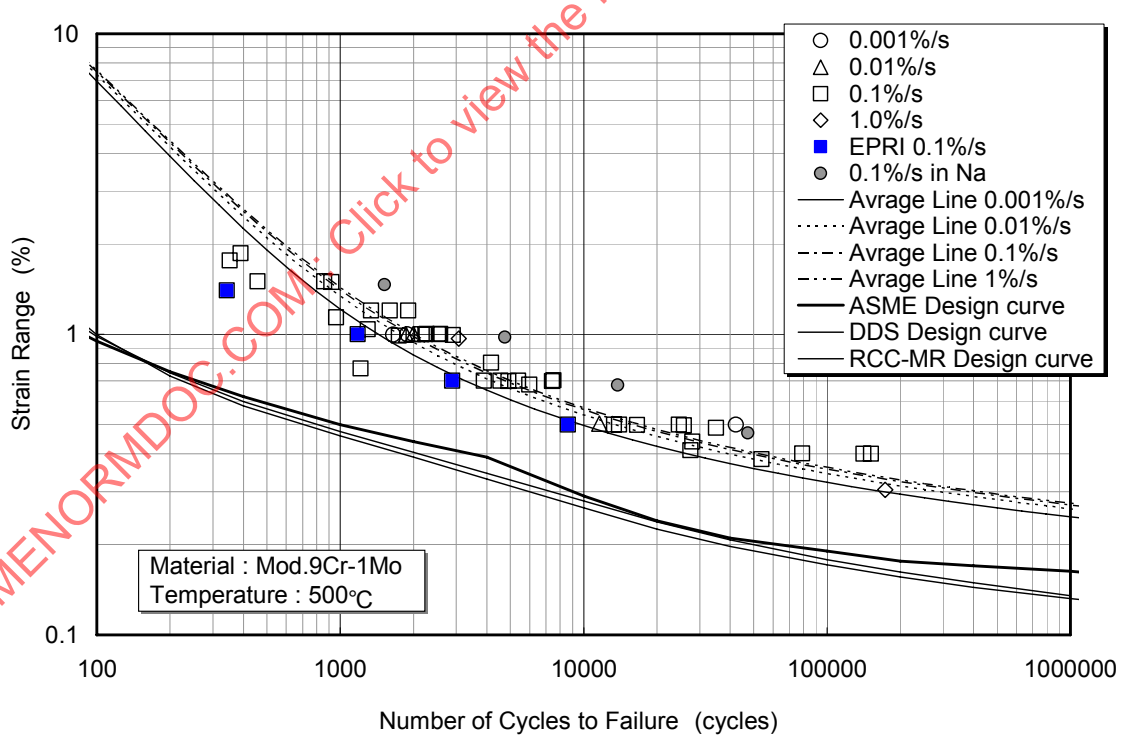


**Figure 4 - Fatigue Life: Average Curves and Experimental Values at 500˚C**

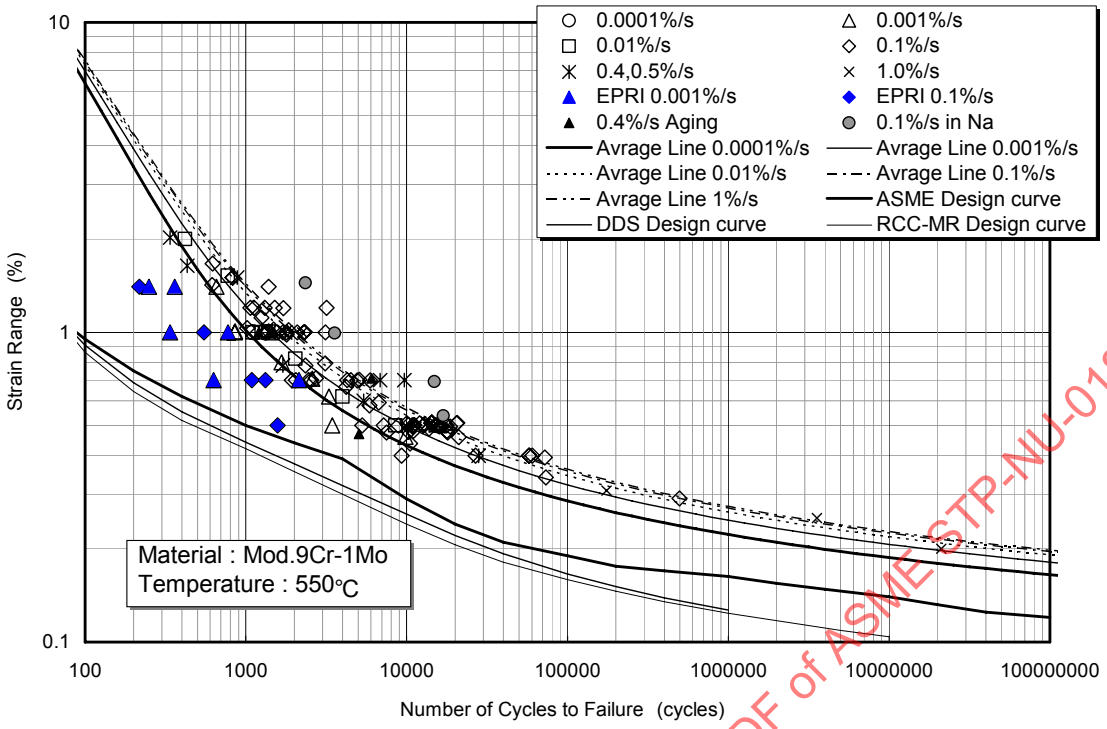


**Figure 5 - Fatigue Life: Average Curves and Experimental Values at 550˚C**

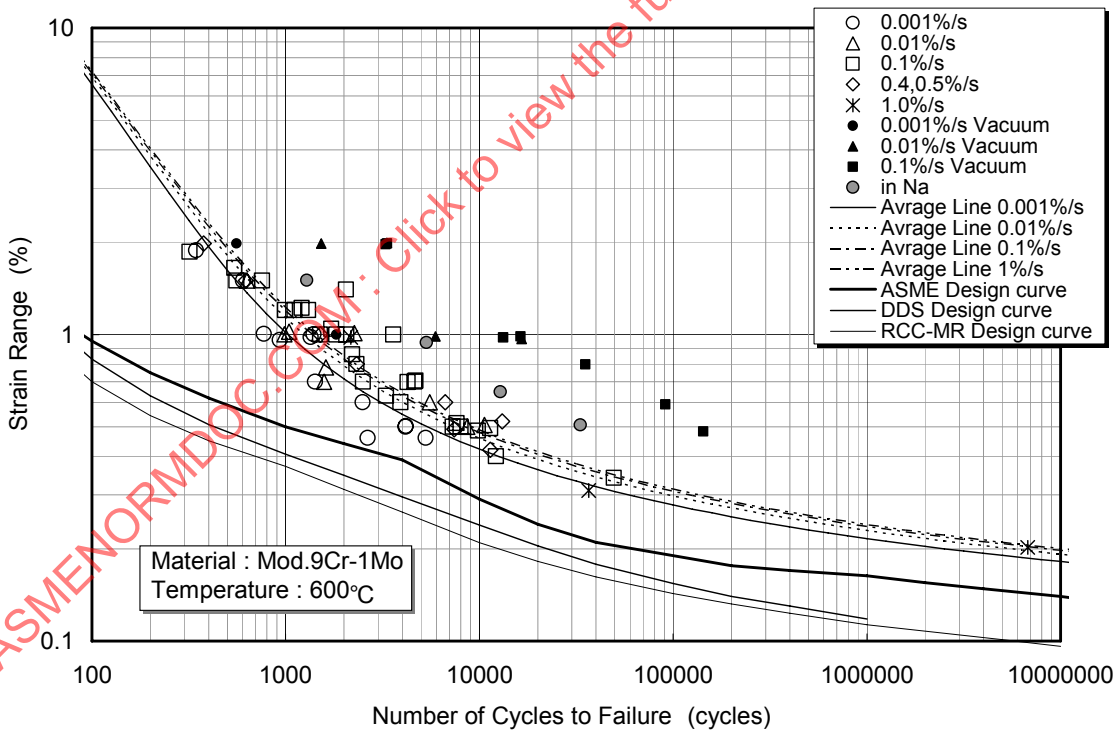


**Figure 6 - Fatigue Life: Average Curves and Experimental Values at 600˚C**

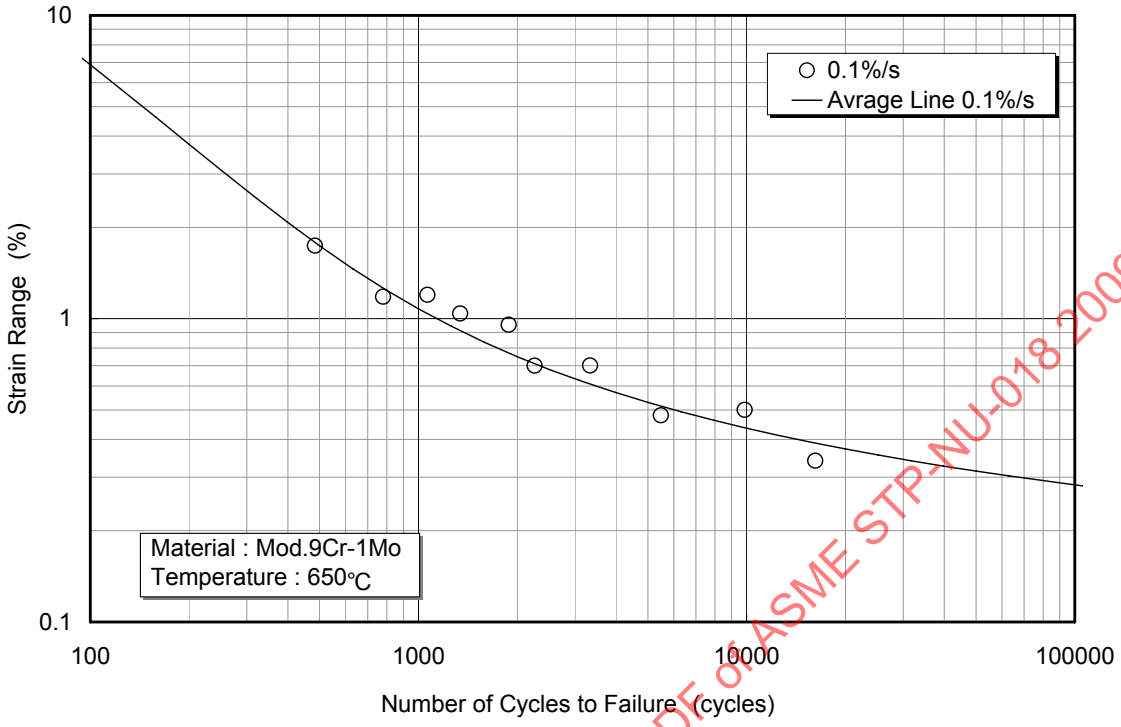


**Figure 7 - Fatigue Life: Average Curves and Experimental Values at 650˚C**

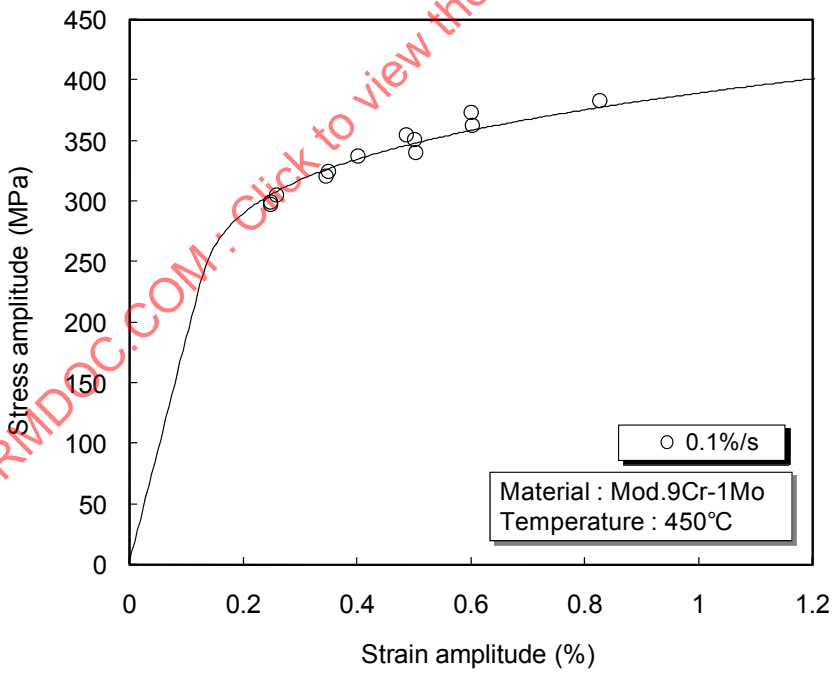


**Figure 8 - Cyclic Stress-Strain Curve: Average Curve and Experimental Values at 450˚C**

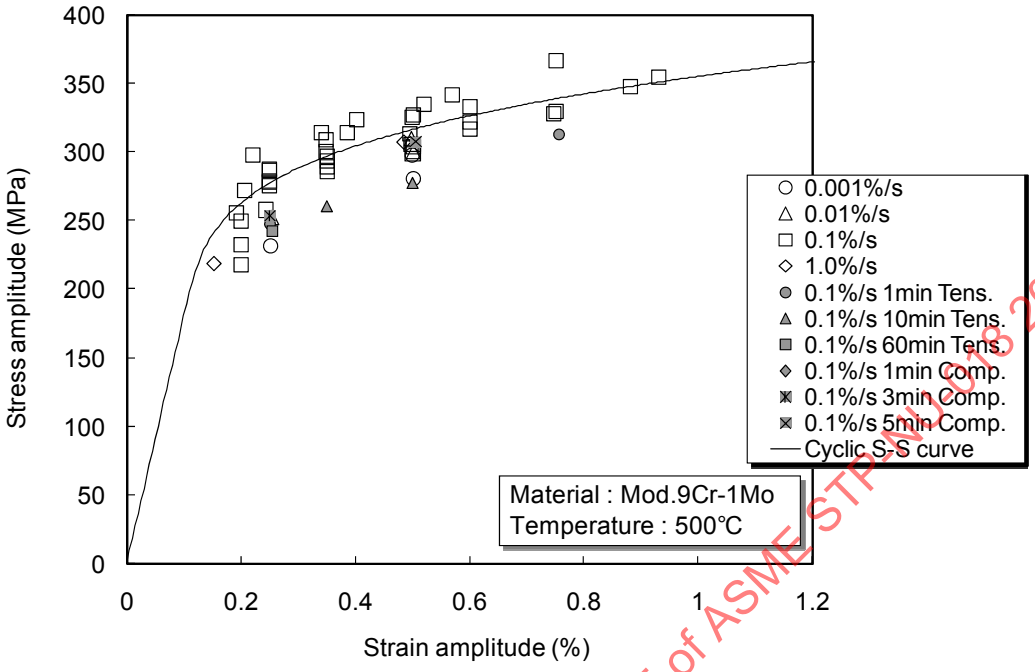


**Figure 9 - Cyclic Stress-Strain Curve: Average Curve and Experimental Values at 500˚C**

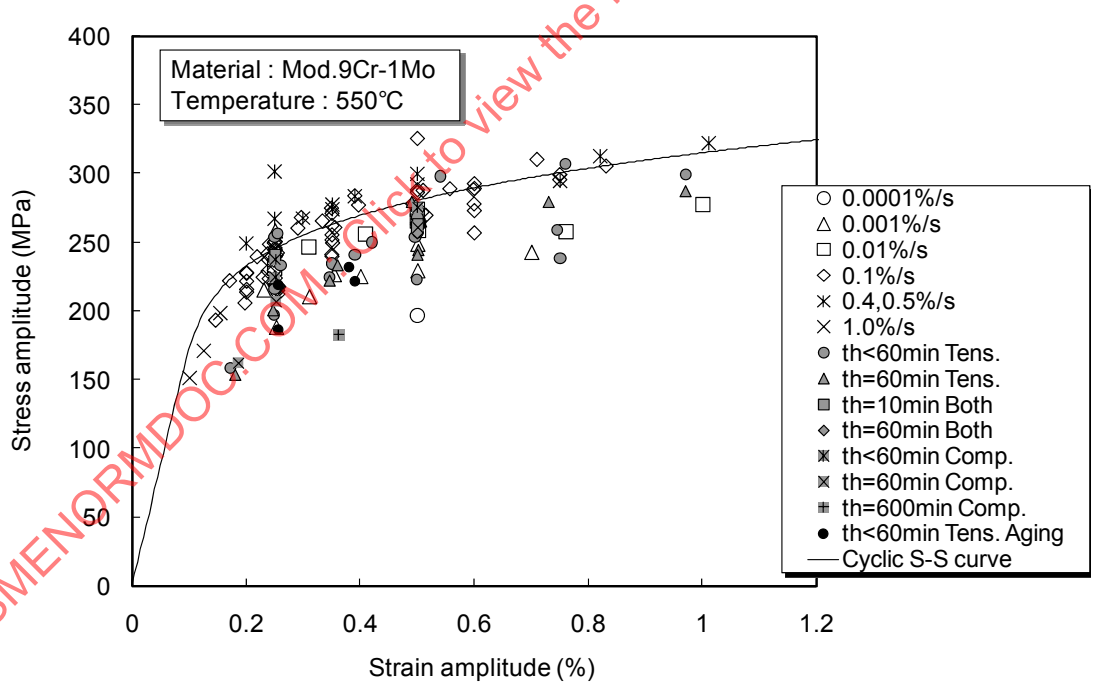


**Figure 10 - Cyclic Stress-Strain Curve: Average Curve and Experimental Values at 550˚C**

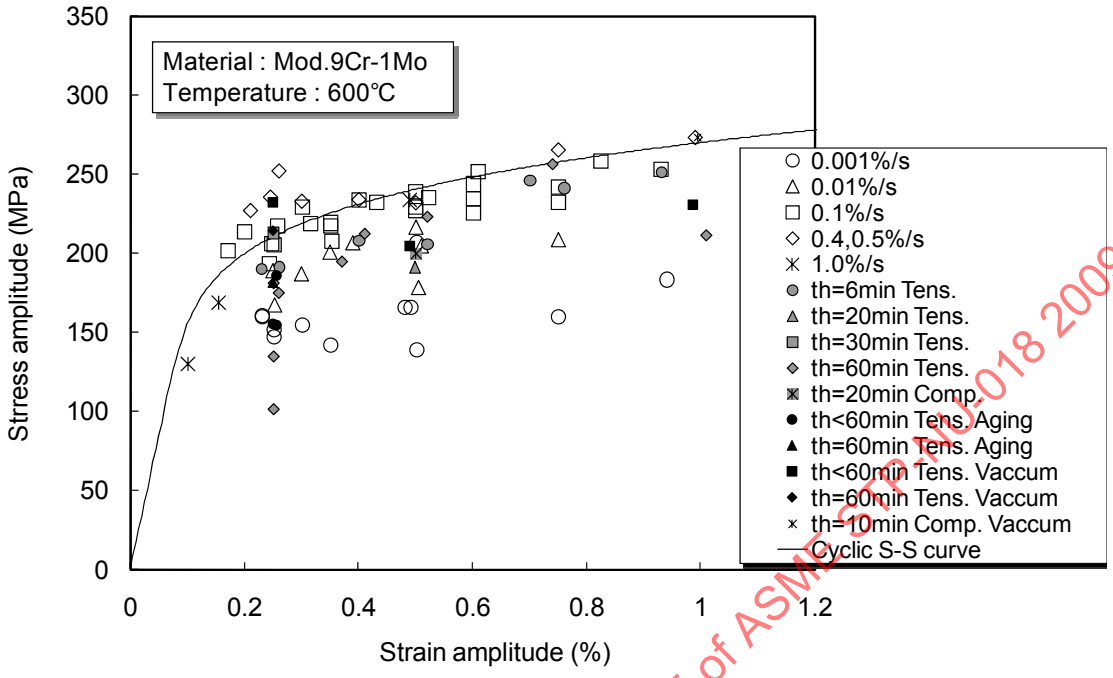


**Figure 11 - Cyclic Stress-Strain Curve: Average Curve and Experimental Values at 600˚C**

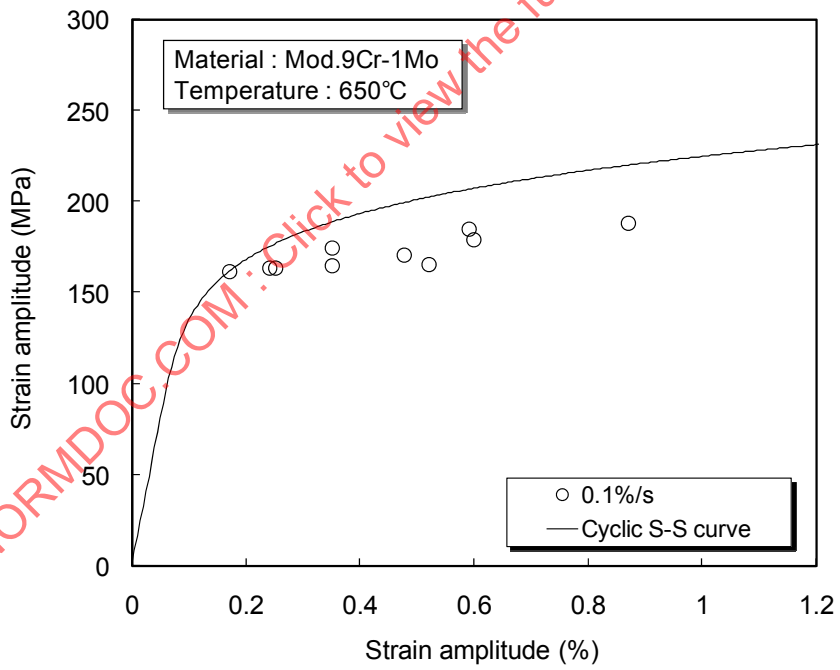


**Figure 12 - Cyclic Stress-Strain Curve: Average Curve and Experimental Values at 650˚C**

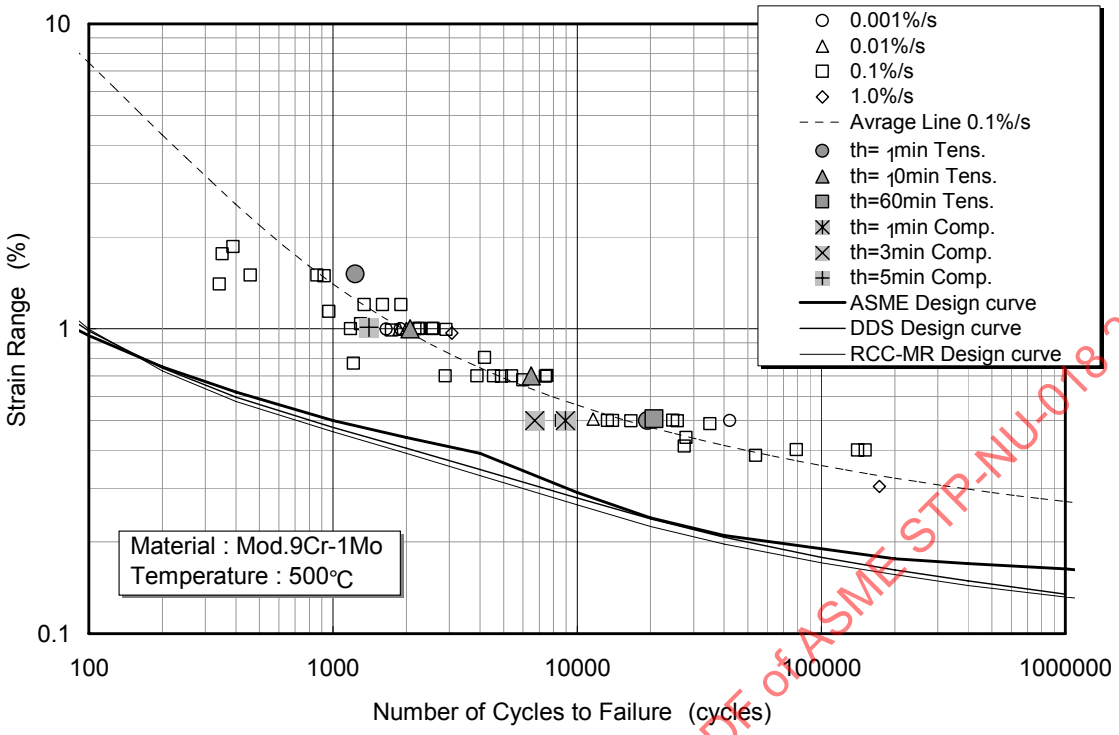


**Figure 13 - Creep-Fatigue Life: Average Curves and Experimental Values at 500˚C**

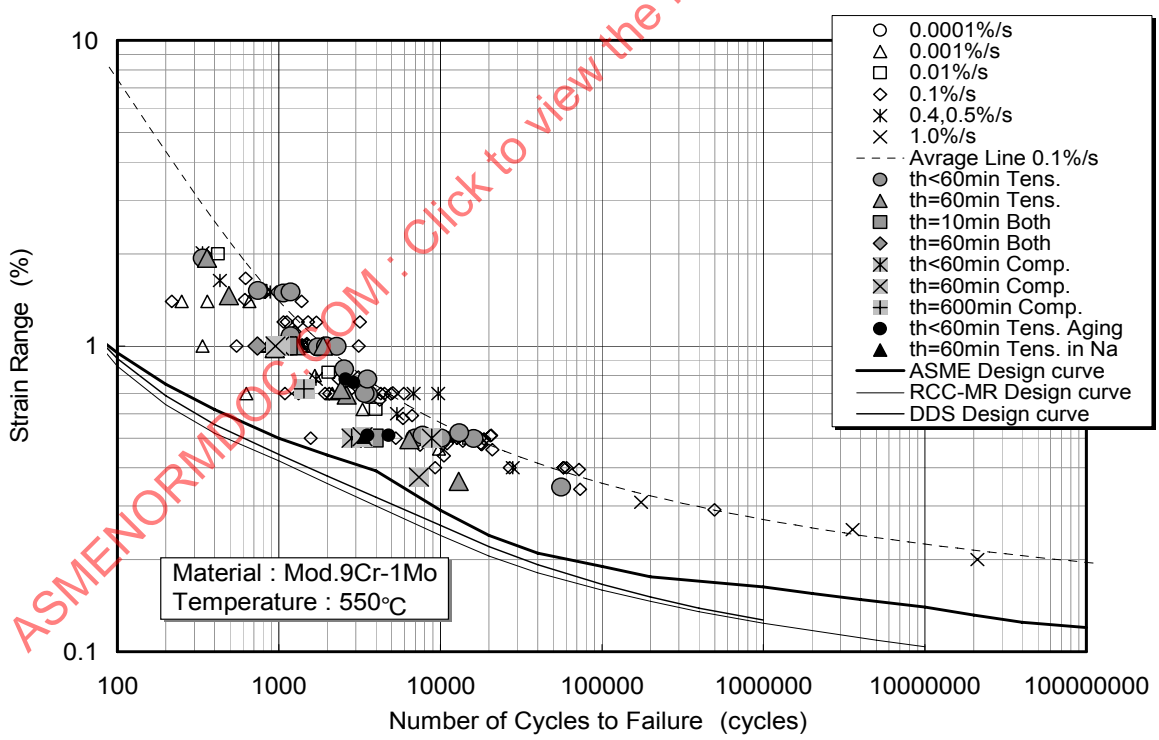


**Figure 14 - Creep-Fatigue Life: Average Curves and Experimental Values at 550˚C**

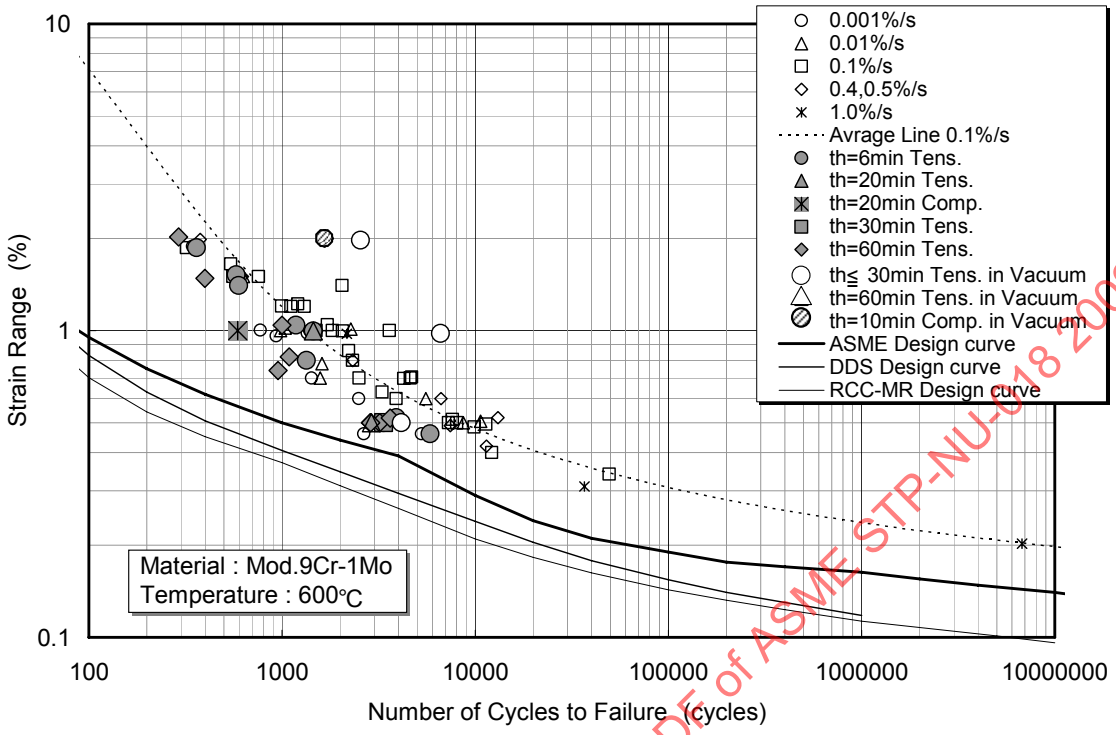


**Figure 15 - Creep-Fatigue Life: Average Curves and Experimental Values at 600˚C**

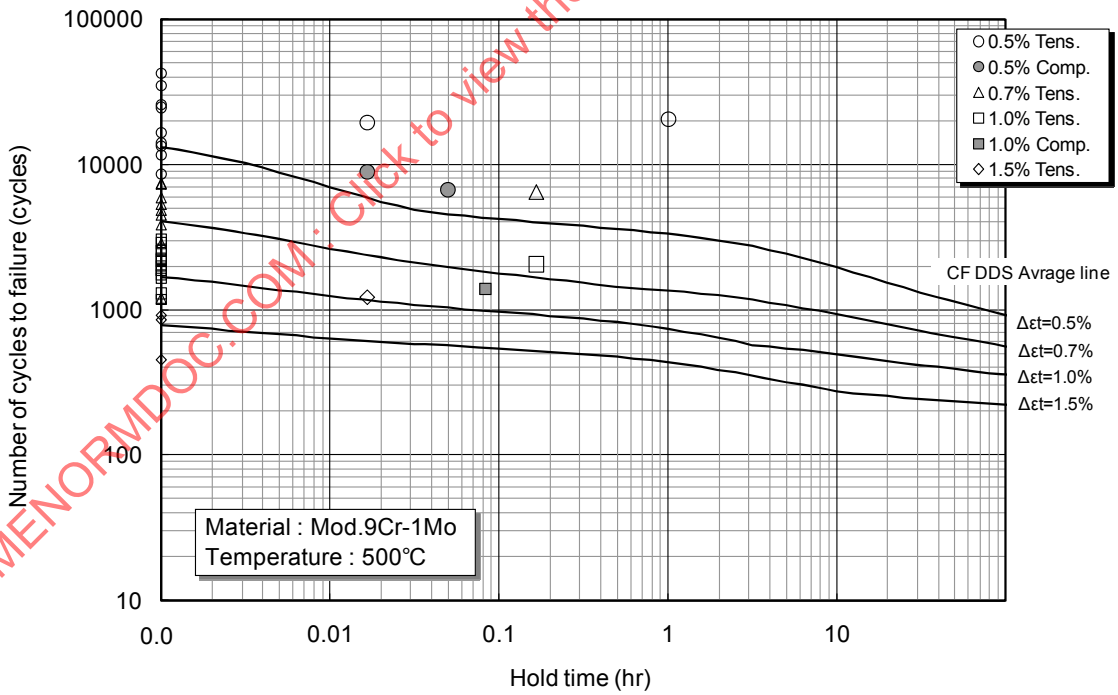


**Figure 16 - Creep-Fatigue Life: Average Curves and Experimental Values at 500˚C**

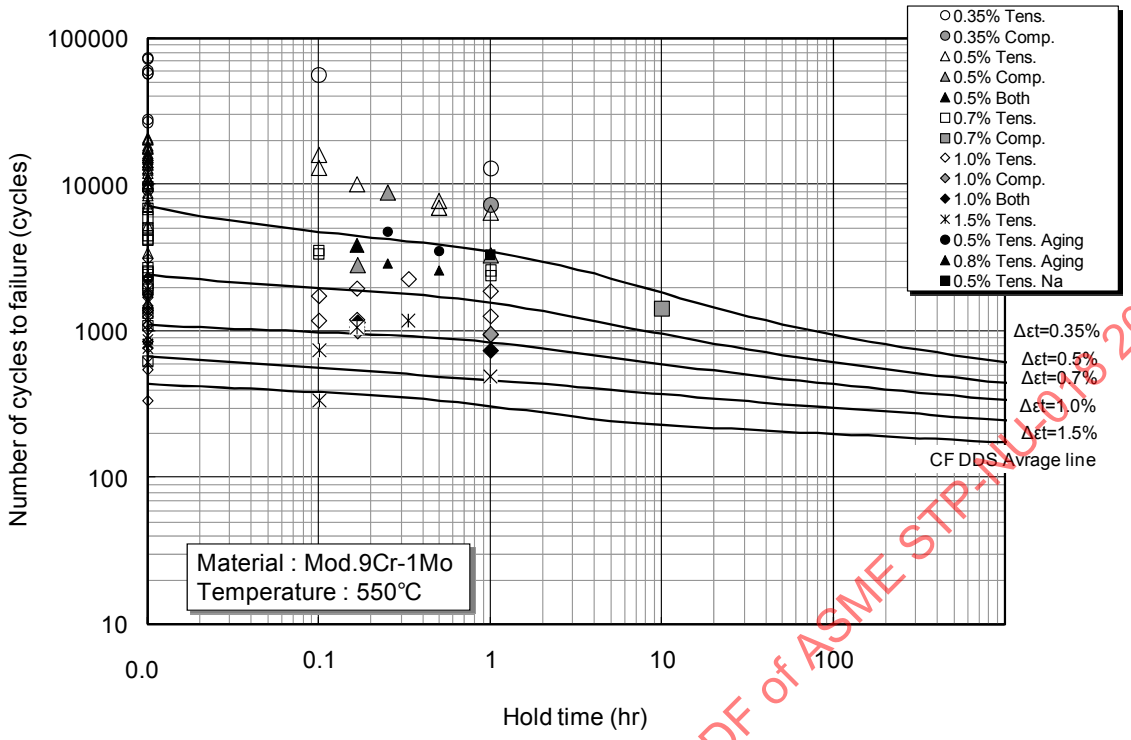


**Figure 17 - Creep-Fatigue Life: Average Curves and Experimental Values at 550˚C**

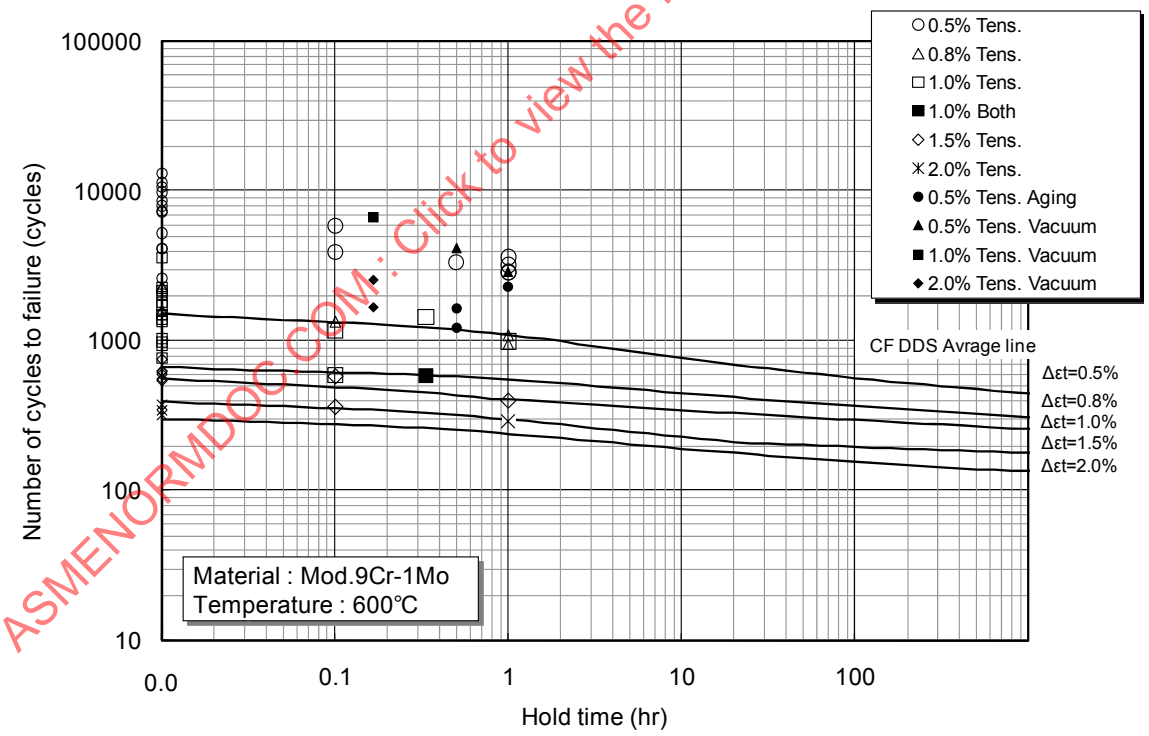


**Figure 18 - Creep-Fatigue Life: Average Curves and Experimental Values at 600˚C**

# 2 CREEP-FATIGUE EVALUATION METHOD

## 2.1 Procedures of ASME-NH, DDS and RCC-MR

Procedures for creep-fatigue evaluation methods in ASME-NH, RCC-MR and DDS (See Reference) are summarized. DDS is the draft design standard for Japanese demonstration fast breeder reactor developed by electric utilities. In DDS, a creep-fatigue evaluation procedure for Modified 9Cr-1Mo steel was developed to apply the material to steam generators (Asada et. al., 1991a, Asada et. al., 1991b). The creep-fatigue evaluation procedure in DDS (Asada et. al., 1993, Taguchi et. al., 1993, Taguchi et. al., 1995) is basically the same as that determined in the Elevated Temperature Structural Design Guide for the Prototype Reactor "Monju."

### 2.1.1 ASME-NH

#### 2.1.1.1 Fatigue Damage

Creep-fatigue damage evaluation procedure described in Nonmandatory Appendix T is summarized here. Fatigue damage is calculated by equation:

$$D_f = \sum_{j=1}^{P} \left( \frac{n}{N_d} \right)_j$$

where:

$D_f$: fatigue damage

$(n)_j$: number of applied repetitions of cycle type, $j$

$(N_d)_j$: number of design allowable cycles for cycle type, $j$, determined from one of the design fatigue curves corresponding to the maximum metal temperature occurring during the cycle. The design fatigue curves were determined from completely reversed loading conditions at strain rates greater than, or equal to, those noted on the curves.

Strain range that is used to calculate design fatigue life is obtained by the following equation:

$$\varepsilon_t = K_v \Delta\varepsilon_{\text{mod}} + K\Delta\varepsilon_c$$

$K_v$: the multiaxial plasticity and Poisson ratio adjustment factor

$\Delta\varepsilon_c$: the creep strain increment

$K$: local geometric concentration factor

$\Delta\varepsilon_{\text{mod}}$: the modified maximum equivalent strain range

$\Delta\varepsilon_{\text{mod}}$: is calculated using the procedure specified in any one of (a), (b) or (c) described below.

*(a)* The modified maximum equivalent strain range is calculated as:

$$\Delta\varepsilon_{\text{mod}} = \left( \frac{S^*}{\bar{S}} \right) K^2 \Delta\varepsilon_{\max}$$

where,

$K$: either the equivalent stress concentration factor, as determined by test or analysis, or, the maximum value of the theoretical elastic stress concentration factor in any direction for the

local area under consideration. The equivalent stress concentration factor is defined as the effective (von Mises) primary plus secondary plus peak stress. Note that fatigue strength reduction factors developed from low temperature continuous cycling fatigue tests may not be acceptable for defining K when creep effects are not negligible.

$S^*$: the stress indicator determined by entering the stress-strain curve of Fig. T-1432-1 at a strain range of $\Delta\varepsilon_{\max}$

$\bar{S}$ : the stress indicator determined by entering the stress-strain curve of Fig. T-1432-1 at a strain range of $K\Delta\varepsilon_{\max}$

$\Delta\varepsilon_{\max}$ : the maximum equivalent strain range as determined in T-1432 (a).

*(b)* The modified maximum equivalent strain range is calculated as:

$$\Delta\varepsilon_{\text{mod}} = \frac{K^2 S^* \Delta\varepsilon_{\max}}{\Delta\sigma_{\text{mod}}}$$

where,

$\Delta\sigma_{\text{mod}}$ : the range of effective stress that corresponds to the strain range, $\Delta\varepsilon_{\text{mod}}$, in the composite stress-strain curve of Fig. T-1432-1.

*(c)* The modified maximum equivalent strain range is calculated as:

$$\Delta\varepsilon_{\text{mod}} = K_e K \Delta\varepsilon_{\max}$$

$$K_e = 1 \quad if \quad K\Delta\varepsilon_{\max} \le 3\bar{S}_m / E$$

$$K_e = K\Delta\varepsilon_{\max} E / 3\bar{S}_m \quad for \quad K\Delta\varepsilon_{\max} \ge 3\bar{S}_m E$$

$$3\bar{S}_m = 1.5S_m + S_{rH}$$

$$\bar{S} = \sigma_S\left(K\Delta\varepsilon_{\max}\right)$$

A schematic illustration of procedures (a) and (b) are shown in Figure 19. Procedure (c) is employed to calculate modified maximum strain range most conservatively.

### 2.1.1.2 Creep Damage

Creep damage $D_c$ is calculated by the following equation.

$$D_c = \sum_k \left(\frac{\Delta t}{T_d}\right)_k$$

$$\sigma_j = \frac{S_{rj}}{K'}$$

$(T_d)_k$: allowable time duration determined from stress-to-rupture curves for a given stress and the maximum temperature at the point of interest and occurring during the time interval, *k*. For elastic analysis, the appropriate stress measure is defined in T-1433.

$(\Delta t)_k$: duration of the time interval, *k*

$S_{rj}$: the expected minimum stress-to-rupture strength given in Tables I-14.6 during the time interval, $j$.

$K'$: the factor determined in Table T-1411-1.

$T_d$ is calculated based on minimum stress-to-rupture curve from applied stress divided by the factor K'. K' is determined as shown in Table 3. The initial stress of relaxation is calculated from $\varepsilon_t$. Stress relaxation behavior is calculated from isochronous stress-strain curves as shown in Figure 20. The initial stress of stress and strain of relaxation are determined by the following equations:

$$S_i = \Delta\sigma_{\text{mod}} - S_{rH}$$

$$\varepsilon_t = \Delta\varepsilon_{\text{mod}} - S_{rH} / E$$

As shown in Figure 21, creep damage per one cycle is calculated as a summation of damage corresponding from peak stress to the relaxation strength associated with the hot extreme $S_{LB}$, and damage corresponding to the stress level of $S_{LB}$. $S_{LB}$ is calculated from the following equation, where Z is a factor to take ratcheting into account. In this investigation, Z was set to zero, because all the data collected and used for the evaluation of creep-fatigue evaluation procedure were obtained under strain controlled condition which corresponds to Z=0.

$$S_{LB}=1.25\sigma_c$$

$$\sigma_c = Z \cdot S_y$$

#### 2.1.1.3 Damage Envelope

The intersection of a damage envelope of creep-fatigue criteria for Grade 91 is ($D_f$, $D_c$) = (0.1, 0.01) as shown in T-1420-2 (Figure 27). The intersection point is most restrictive compared to other materials such as 304 stainless steel, 316 stainless steel and 2 1/4 Cr-1Mo steel.

### 2.1.2 DDS

#### 2.1.2.1 Fatigue Damage $D_f$

Fatigue damage is calculated from the following equation.

$$D_f = \sum_i \frac{n_i}{N_{di}}$$

$n_i$: number of applied repetition of cycle type, j

$N_{dt}$: number of design allowable cycles for cycle type, $j$, determined from one of the design fatigue curves corresponding to the maximum metal temperature occurring during the cycle.

Strain range is calculated from the following equation. The first term is calculated as shown in Figure 22.

$$\varepsilon_t = K''_\varepsilon \varepsilon_0 + K_L \varepsilon_c$$

$\varepsilon_0$: elastically calculated peak strain range including peak strain

$\varepsilon_c$: equivalent creep strain induced in an interested cycle by long term stress controlled loading

$K_\varepsilon$": elastically calculated stress concentration factor corresponding to peak strain range $\varepsilon_0$

$K_L$: stress concentration factor corresponding to long term stress controlled loading

Strain range $\varepsilon_0$ can be calculated by the following equation:

$\varepsilon_0 = S_p E$

where, $S_p$ is determined based on the stresses at two extreme points 1 and 2. $K_\varepsilon$" can be calculated by the following equation when a hold time at elevated temperature is introduced in a cycle:

$$K''_\varepsilon = 1 + (q_p - 1)\{1 - 3\overline{S_m} / (E\varepsilon_0)\}$$

$$3\overline{S_m} = S_{rH} + 1.5S_{mc}$$

$$q_P = K \cdot q_n$$

where,

$S_{rH}$: stress value determined based on the elevated temperature service time and the history of metal temperature of an interested point

$S_{mc}$: stress determined for temperature $T_c$

$q_p$: elastic follow-up parameter for peak stress

K: stress concentration factor corresponding to primary plus secondary stress

$q_n$: elastic follow-up parameter for primary plus secondary stress

### 2.1.2.2 Creep damage $D_c$

Creep damage is calculated from the following equation:

$$D_C = D_{CR} + D_{CN}$$

$$D_{CR} = D_0^* + \sum n_k D_k^*$$

$$D^*_k = 2\int_0^{t_k} \frac{dt}{td(T_k, \sigma_k)} - \frac{2t_k}{td(T_k, S_g)}$$

where,

$D_{CN}$: creep damage factor induced by steady stress

$D^*_0$, $D^*_k$: stress relaxation damage factor determined corresponding to strain range that determines strain cycle $k$, metal temperature history at an interested point, stress level $S_g$ and elastic follow-up parameter $q_p$.

$td(T_1, \sigma_1)$: allowable hold time determined from creep rupture curve or design stress

$td(T_1, S_g)$: allowable hold time determined from creep rupture curve or design stress $S_g$

The initial stress of stress relaxation is obtained from the cyclic stress-strain curve in the case of austenitic stainless steels, and from the monotonic stress-strain curve in the case of ferritic steels, in order to account for cyclic hardening and cyclic softening, respectively. Schematic illustration is shown in Figure 23.

*(a)* Austenitic stainless steels (304, 316 and 316FR)

$D_0^*$ : $S_i = 1.5S_m$

$$D^* : \text{Min}\left(S_i = \frac{1}{2}\Delta\sigma_R(\varepsilon_t)\ ,\ E\varepsilon_t - \left(3\overline{S_m} - S_{rH}\right)\right)$$

*(b)* Ferritic steels (2 1/4Cr-1Mo, Mod.9Cr-1Mo)

$D_0^*$ : $S_i = < P_L + P_b + Q >$

$D^*$ : Min( $S_i = S\left(\frac{1}{2}\varepsilon_t\right)$ , $E\varepsilon_t - \left(3\overline{S_m} - S_{rH}\right)$)

where,

$\Delta\sigma_R\left(\varepsilon_t\right)$: stress range determined from the cyclic stress-strain curve

$S_i = S\left(\frac{1}{2}\varepsilon_t\right)$: stress obtained by entering the strain amplitude to elastic-plastic stress-strain curve

Stress relaxation behavior is estimated by creep strain law and the strain hardening rule. A factor that represents the scatter of creep strain curve is taken into account ( $\alpha_R = 3$ ).

$$S(T,t) = \sigma_i + \int_0^t \dot{\sigma}_c dt$$

$$\dot{\sigma}_c = -E\dot{\varepsilon}_c / q_c$$

$$q_c = 3 \cdot K$$

$\dot{\varepsilon}_c$: creep strain rate

$E$: elastic modulus

$q_c$: elastic follow-up parameter

$K$: stress concentration factor

The method of creep damage calculation is schematically illustrated in Figure 24. Creep damage corresponding to a stress level Sg is always accounted for. A safety factor of 20 is incorporated.

$$t_R = 2t^* / D_{CN}$$

$t^*$: service time at elevated temperature

$D_{CN}$: creep damage factor due to steadily imposed stress

If long-term stress is low, $D_{CN} = 0.3$

If creep damage is not significant, $D_{CN} = 0.1$

### 2.1.2.3 Damage Envelope

The intersection of a damage envelope of creep-fatigue criteria for Grade 91 is ($D_f$, $D_c$) = (0.3, 0.3) as shown in Figure 27. The intersection point is the same as other materials such as 304 stainless steel, 316 stainless steel, 321 stainless steel and 2 1/4 Cr-1Mo steel.

### 2.1.3 RCC-MR

#### 2.1.3.1 Fatigue damage

Fatigue damage is calculated by the following equation:

$$D_f = \sum_i \frac{n_i}{N_{di}}$$

Strain range is determined by the following equation, as schematically shown in Figure 25.

$$\overline{\Delta\varepsilon} = \overline{\Delta\varepsilon}_{\text{el+pl}} + \overline{\Delta\varepsilon}_{\text{cr}}$$

$$\overline{\Delta\varepsilon}_{\text{el+pl}} = \overline{\Delta\varepsilon}_1 + \overline{\Delta\varepsilon}_2 + \overline{\Delta\varepsilon}_3 + \overline{\Delta\varepsilon}_4$$

$\overline{\Delta\varepsilon}_1$: strain range obtained from elastic analysis

$\overline{\Delta\varepsilon}_2$: increment of plastic strain corresponding to initial stress range, equals to $\overline{\Delta\left[P_m + 0.67\left(P_b + P_L - P_m\right)\right]}$ see Figure 25

$\overline{\Delta\varepsilon}_3$: see Figure 25

$\overline{\Delta\varepsilon}_4$: plastic strain range to account for multiaxial stress state

$$\overline{\Delta\varepsilon}_4 = \left(K_v - 1\right) \times \overline{\Delta\varepsilon}_1$$

$\overline{\Delta\varepsilon}_{\text{cr}}$: creep strain range

#### 2.1.3.2 Creep Damage

Creep damage is calculated by the following equation. $T_d$ is calculated by entering an equivalent stress divided by 0.9 to the design creep rupture curve.

$$D_C = \sum_k \frac{\Delta t_k}{T_{dk}}$$

$$\sigma_j = \frac{Sr_j}{0.9}$$

Stress relaxation behavior is estimated by the creep strain law and the strain hardening rule. The initial stress is calculated as shown in Figure 76. If symmetrization effects are to be taken into account, $\Delta\overline{\sigma}^*$ is replaced by $K_s\Delta\overline{\sigma}^*$.

$$S(T,t) = \overline{\sigma_k} + \int_0^t \dot{\sigma}_c dt$$

$$\overline{\sigma_k} = K_s\Delta\overline{\sigma}^*$$

$$\dot{\sigma}_c = -E\dot{\varepsilon}_c / q_c$$

where,

$q_c$: elastic follow-up parameter, =3

$\dot{\varepsilon}_c$: creep strain rate

E: elastic modulus

Ks: symmetrization effects factor

$\overline{\Delta\varepsilon_{cr}}$ can be calculated as follows:

$$\overline{\Delta\varepsilon_{cr}} = \left(\overline{\sigma}_k - S\left(T, t_H\right)\right)/E$$

where $t_H$ is strain hold time.

#### 2.1.3.3 Damage Envelope

The intersection of a damage envelope of creep-fatigue criteria for Grade 91 is ($D_f$, $D_c$) = (0.3, 0.3) as shown in Figure 27, which is the same as the other materials in the code.

## 2.2 Comparison of the Procedures

The differences between ASME-NH, DDS and RCC-MR are described focusing on the method of determination of strain range, initial stress of stress relaxation, stress relaxation behavior and formulation of creep damage.

### 2.2.1 Determination of Strain Range

ASME-NH determines strain range for fatigue damage calculation by a monotonic stress-strain curve, stress concentration factor, elastically calculated strain range, using the Neuber's rule for both austenitic stainless steels which cyclically harden and ferritic steels which cyclically soften. If elastically calculated stress is the same, the procedure gives a larger strain range for austenitic steels than ferritic steels because monotonic stress-strain curves are softer for austenitic steels. The linear extension of the zero isochronous stress-strain curve by $S_{rh}$ as shown in Figure 19 has not been taken into account in Section 2.3 but has been taken into account in Section 2.4.

RCC-MR uses elastically calculated stress range and cyclic stress strain curves based on the Neuber's rule. Since the cyclic stress-strain curve of austenitic steel is harder than that of ferritic steels, a larger strain range is predicted for ferritic steels than for austenitic steels, whose tendency is the opposite of ASME-NH.

DDS determines a strain range applying an elastically calculated stress range that includes peak stress to a perfect elastic-plastic stress strain curve with a yield stress of $3\overline{S}_m$ using an elastic follow-up factor.

### 2.2.2 Initial Stress of Stress Relaxation

ASME-NH determines the initial stress of relaxation as an intersection of a stress-strain curve and a locus obtained from the Neuber's rule. As a stress-strain curve, an isochronous curve is used and as a strain range is entered into the curve, calculated initial stress becomes large.

RCC-MR is basically the same as ASME-NH, however, as a stress-strain curve, cyclic stress-strain curves that are obtained at the mid-life cycle are used.

DDS uses monotonic stress-strain curves for cyclically softening material such as Grade 91. Elastically calculated stress is entered in to the monotonic stress-strain curve, and the point and perfect elastic-plastic stress-strain curve are connected by a slope corresponding to the elastic follow-up factor.

### 2.2.3 Estimation of Stress Relaxation Behavior

ASME-NH uses isochronous stress-strain curves to estimate stress relaxation behavior.[1] Although this method does not take elastic follow-up into account, it takes into account multiaxial effects on stress relaxation. The initial stress is multiplied by the K' factor. The value of the factor is 0.67 but revision of the value to 0.9 is in progress.

RCC-MR uses creep strain curves and the strain hardening law. RCC-MR adopts the same kind of factor as K' in ASME-NH, and the value is 0.9.

DDS is the same as RCC-MR. The creep strain curves determined in DDS is derived as a function of creep stress-to-rupture. There is no factor corresponding to the K' factor in ASME-NH.

### 2.2.4 Formulation of Creep Damage

ASME-NH formulates creep damage as a time fraction of creep rupture time that corresponds to the stress level at a point of interest. Stress relaxation curve is only considered above $S_{LB}$ level.

DDS adopts a similar approach. Creep damage is formulated as a time fraction of creep rupture time that corresponds to the stress level at a point of interest. The stress relaxation curve is only considered above $S_g$ level. Creep damage corresponding to $S_g$ level, which is 0.3 and denoted as $D_{c1}$, is always taken into account.

The approach in RCC-MR is basically the same.

## 2.3 Creep-Fatigue Evaluation Without Safety Margins

In evaluating creep-fatigue evaluation procedures, it is very useful to apply them to experimental results. In this case, it is useful to remove safety margins from every step of the procedures. Therefore, the procedures of ASME-NH, RCC-MR and DDS were applied to the collected data described in chapter 1 without safety factors. This evaluation focuses on the following key points.

*(a)* Determination of the initial stress of stress relaxation

*(b)* Description of stress relaxation behavior during strain hold period

*(c)* Creep-fatigue damage diagram

### 2.3.1 Conditions of Evaluation

In order to capture the characteristics of existing procedures, creep-fatigue evaluation was performed without applying safety margins determined in the procedures. Basic conditions of this evaluation are described below.

The strain ranges in the experiments were used for evaluation. Stress concentration coefficients were not considered because all the tests were performed using smooth bar specimens.

The initial stress of stress relaxation was basically calculated based on the strain range using stress-strain curves that are specified in each procedure. No multiplication factors considered as safety margins such as those determined in ASME-NH (K') were taken into account. As for stress-strain relationship, monotonic stress strain relationship was used for ASME-NH and DDS, while cyclic stress-strain curves were used for RCC-MR, as determined in each procedure. For comparison, the monotonic stress-strain curve was also used with RCC-MR, as the cyclic stress-strain curve was used with DDS.

[1] Although use of the isochronous stress-strain curves to calculate $S_{rh}$ is described in ASME-NH, it is also permissible to use a value calculated similarly to the methods employed in the DDS and RCC-MR.

Stress relaxation behavior was estimated using the isochronous stress-strain curves for ASME-NH, and the strain hardening law for RCC-MR and DDS. Elastic follow-up factor during strain hold period was set to 1, because the tests were performed under strain controlled conditions.

Average creep rupture curves and fatigue life curves were used for creep-fatigue damage evaluation. For compressive hold tests, the same procedure for tensile hold tests were applied (Both tensile hold tests and compressive hold tests were evaluated in the same manner).

For fatigue life curves, in addition to the average trend which was obtained by removing safety factors from the design curve, curves with 1/10 of average fatigue life were also used to take into account of crack initiation.

### 2.3.2 Description of Stress Relaxation Behavior

Description of stress relaxation behavior may affect the estimation of creep damage significantly. Therefore, in this section, monotonic stress relaxation behaviors and stress relaxation behaviors during creep-fatigue tests were examined and compared with predictions by the procedures of ASME-NH, RCC-MR and DDS. For stress relaxation during creep-fatigue tests, relaxation behaviors at the first cycle and the mid-life were examined.

Figure 28 to Figure 34 show monotonic stress relaxation behavior along with the predictions by ASME-NH, RCC-MR and DDS. In the prediction, initial stresses obtained experimentally were used to predict relaxation behaviors. ASME-NH procedure generally predicts higher stress compared to the experimental results. On the other hand, RCC-MR and DDS procedures generally predict stresses closer to experimental results. Overall, all procedures tend to predict higher stresses then experiments during stress relaxation.

Figure 35 to Figure 40 show stress relaxation during creep-fatigue tests along with the predictions by ASME-NH, RCC-MR and DDS. For each creep-fatigue test, relaxation behavior at the first cycle and the mid-life are examined. Generally, ASME-NH gives the highest stress but other two procedures also give higher stress than observed. However, it is to be noted that at lower strain range, i.e., if the initial stress is low, all three procedures tend to give lower stress than actually observed.

Figure 41 shows the evolution of creep damage corresponding to Figure 32. Creep damage was calculated according to the DDS procedure. Vertical axis indicates the ratio of creep damage to creep damage at 2000 hr. at an arbitrary time. It can be seen that more than 70% of the damage has been accumulated in the first 500 hours.

### 2.3.3 Creep-Fatigue Damage Evaluation and Life Prediction

#### 2.3.3.1 Creep-Fatigue Damage Evaluation

In this section, creep-fatigue damage is evaluated. For strain range, experimental value was used. Fatigue damage per cycle, $d_f$, is calculated using an average fatigue life curve. Creep damage per cycle, $d_c$, was calculated according to the method determined in ASME-NH, RCC-MR and DDS. Total fatigue damage, $D_f$, and creep damage, $D_c$, were obtained by multiplying $d_f$ and $d_c$ by number of cycles to failure, Nf.

Figure 42 and Figure 43 show creep-fatigue damage calculated according to ASME-NH, using monotonic stress-strain curves. Figure 42 is the result when stress amplitude was used for determining the initial stress. Figure 43 is the result when stress range was used for determining the initial stress. In both cases, creep damage is calculated very conservatively, comparing to the damage envelope of which intersection is (0.1, 0.01). It is understood that this conservatism is caused by the description of stress relaxation by isochronous stress-strain curves, in that the same initial stress as used in Figure 44 and Figure 45, which will be described later, was used.

Figure 44 and Figure 45 show creep-fatigue damage calculated according to DDS, using monotonic stress-strain curves and cyclic stress-strain curves. When monotonic stress-strain curves were used, creep damage is calculated somewhat conservatively, comparing to damage envelope of which intersection is (0.3, 0.3). When cyclic stress-strain curves were used, calculated creep damage is plotted approximately on the damage envelope.

Figure 46 shows creep-fatigue damage calculated according to RCC-MR, using cyclic stress strain curves. Creep damage is plotted approximately on the damage envelope of which intersection is (0.3, 0.3). The difference of calculated creep damage between Figure 45and Figure 46 (DDS and RCC-MR) is caused by the difference of creep rupture curves determined in each procedure.

#### 2.3.3.2 Life Prediction

Creep-fatigue life prediction was performed based on the creep-fatigue damage evaluation described above. The trends in creep-fatigue life prediction coincide with these in creep-fatigue damage evaluation. ASME-NH procedure gives the most conservative results as shown in Figure 47 to Figure 48. The degree of conservatism is up to 100 times in life when stress range is used for the estimation of initial stress, and 50 times when stress amplitude is used. Figure 49 shows the result when damage envelope was replaced by the one used in DDS and RCC-MR of which intersection point is (0.3, 0.3). Somewhat less conservative results were obtained but the difference is not significant.

Figure 50 shows creep-fatigue life predicted by RCC-MR. Predicted life scatters around the observed life without any significant conservatism.

Figure 51 and Figure 52 show creep-fatigue life predicted by DDS. When monotonic stress-strain curves were used, somewhat conservative result was obtained. The conservatism tended to be larger in long term region. When cyclic stress-strain curves were used, the degree of conservatism reduced, yet maintaining the tendency that the conservatism becomes larger in long term region.

#### 2.3.3.3 Applicability of Linear Damage Summation Rule

*(a)* Creep-Fatigue Damage Evaluation

In the above evaluation, stress relaxation behavior during strain hold was estimated either by isochronous stress-strain curves (ASME-NH) or creep strain equation and strain hardening law (RCC-MR and DDS). Here, experimentally obtained stress relaxation curves were used for creep-fatigue damage calculation and creep-fatigue life prediction. This is to examine the applicability of linear damage summation rule that are commonly employed in the three procedures to the evaluation of creep-fatigue damage.

Figure 53 shows the results using experimentally obtained stress relaxation curves at the first cycle and the mid-life cycle of creep-fatigue loading.[2] When the stress relaxation curve at the first cycle was used, results became very conservative. If the stress relaxation curves at the mid-life were used, creep-fatigue damage was plotted approximately on the damage envelope of which intersection of (0.3, 0.3). This shows the applicability of the linear damage summation rule to the creep-fatigue damage evaluation of Grade 91 steels. However, if the same data and calculation results are plotted in a normal scale, the figure looks very different and one will have an impression that creep-fatigue damage is evaluated too much unconservatively. Which type of the figures is to be used depends on how it is used. When it is used for creep-fatigue life prediction, observed life and predicted life are normally plotted in logarithmic scale. Therefore,

[2] An "experimentally obtained stress relaxation curve" means a curve corresponding to a specific test piece obtained by a creep-fatigue experiment.

adequacy of damage envelope should also be discussed based on figures drawn using logarithmic scale.

*(b)* Creep-Fatigue Life Prediction

Creep-fatigue life was predicted using the experimentally obtained stress relaxation curves at the first cycle and at the mid-life cycle with damage envelopes with intersection point of (0.1, 0.01) and (0.3, 0.3), as shown in Figure 54. When the stress relaxation curve of the first cycle was used with a damage envelope of which intersection is (0.1, 0.01), very conservative results were obtained, in which predicted life was about an order of magnitude shorter than actual life. When the stress relaxation curves at the mid-life cycle were used, predicted life becomes closer to actual life with conservatism retained somewhat.

When a damage envelope of which intersection point of (0.3, 0.3) is used, the degree of conservatism becomes smaller to some extent. The results corresponding to the first cycle stress relaxation curves are not much different from those obtained with a damage envelope of which intersection is (0.1, 0.01), while obvious improvement is observed when the results obtained from the mid-life cycle with the envelope with (0.3, 0.3). In this case, experimentally obtained creep-fatigue life was predicted fairly well, as shown in Figure 55.

In the calculation of creep-fatigue life prediction in Figure 54 and Figure 55, creep rupture curves determined in the DDS were used. Because creep rupture curves are different in RCC-MR, the same calculation as Figure 55 was performed using the curves determined in RCC-MR. The result is shown in Figure 56, which is almost identical to Figure 55 (See Appendix B for comparison of creep rupture curves between DDS and RCC-MR).

### 2.3.4 Discussions

#### 2.3.4.1 Estimation of Initial Stress of Relaxation

*(a)* Stress-strain curve for estimation of initial stress of relaxation

In ASME-NH and DDS, monotonic stress-strain curves are used for the estimation of the initial stress of stress relaxation. This is to reserve margins in the estimation of initial stress, because Grade 91 steel cyclically softens. However, RCC-MR uses cyclic stress-strain curves. Even if we use cyclic stress-strain curves, if they are obtained from fatigue tests of which strain rate is 0.01%/s for example, possibly there still remains conservatism. It is because the steel not only cyclically softens but also softens further due to the introduction of strain hold time and aging, as shown in Figure 57. In the practical application, strain hold time is long and corresponding softening is considered to occur. Therefore, if sufficient cyclic loading is expected in the application, from the viewpoint of creep-fatigue evaluation, there is a possibility to adopt cyclic stress-strain curves for the estimation of initial stress without losing conservatism necessary in creep-fatigue life evaluation. For the effect of aging on stress-strain relationship, also see Figure 76 and Figure 77.

*(b)* Description of stress relaxation behavior

ASME-NH uses isochronous stress-strain curves for description of stress relaxation behavior while RCC-MR and DDS use creep strain curves and strain hardening law. Generally, both methods predicted higher stresses than actually observed, except for stress relaxation in a low strain range creep-fatigue tests. Of the two methods, ASME-NH procedure predicted even higher stresses. For the purpose of reproducing stress relaxation curves, adopting the method used in RCC-MR and DDS can be an option.

*(c)* Creep damage estimation

All the procedures investigated in this study use creep rupture curve obtained by creep tests with as-received material. There may be a possibility that the creep strength of cyclically softened material is degraded by softening. If so, this should be taken into account. However, one can also consider that this effect, if it exists, is already taken into account in a creep-fatigue damage envelope, which normally takes into account creep-fatigue interaction by setting intersection point to (0.3, 0.3) or (0.1, 0.01), which can be (0.5, 0.5) if no interaction is assumed.

*(d)* Creep-fatigue damage envelope

ASME-NH uses (0.1, 0.01) as an intersection point while RCC-MR and DDS uses (0.3, 0.3). Creep-fatigue damage evaluation based on experimentally obtained stress relaxation curves revealed that the ASME-NH envelope is conservative, as shown in Figure 53 (Because plots in Figure 53 were obtained using average properties, plots should be expected to scatter around the envelope, not totally outside of the envelope). On the other hand, an intersection point of (0.3, 0.3) seems to be reasonable as shown in the same figure.

Another point to be noted regarding damage envelopes is that the difference of envelope is most pronounced when fatigue damage and creep damage occur at a comparable magnitude. If creep damage is far dominant, which is expected in certain applications, evaluation points are plotted on the upper left part of the envelope where creep damage is close to 1 and fatigue damage is not much larger than zero. In this region, the effect of intersection point is small. In the discussion of an intersection point, the ratio of fatigue damage and creep damage of interest should be made clear.

*(e)* Safety margins

Safety margins in creep-fatigue evaluation can be maintained in the steps of evaluation investigated above. ASME-NH procedure seems to have margins at every step of evaluation, i.e., strain range, initial stress of relaxation, description of stress relaxation curve during strain hold and damage envelope for creep-fatigue interaction. This is made clear based on the evaluation of creep-fatigue tests using average trends, and the margins can be considered as of unintended nature. In the application of the procedure, in addition to those intended safety margins unitended margins are incorporated and the degree of conservatism can be even larger. This point is discussed in the next chapter.

*(f)* Miscellaneous: Fatigue damage corresponding to crack initiation

Fatigue damage is calculated based on experimentally obtained fatigue curves. The definition of fatigue life is a cycle that corresponds to 25% drop of peak tensile stress during fatigue tests. This is considered to correspond to a situation where a visible crack has been initiated and propagated to cover approximately 25% of the cross section of the specimen. However, some consider that fatigue life used in creep-fatigue damage evaluation should be defined based on the initiation of a crack whose size is something equivalent to grain size. Therefore, in this study, creep-fatigue damage evaluation and life prediction was also performed assuming “fatigue life corresponding to crack initiation” is 1/10 of normally used fatigue life. The results are shown in Figure 58 to Figure 60. As a result, fatigue damage becomes 10 times larger than “normal fatigue damage.” Correspondence between observed and predicted creep-fatigue life was improved, but the difference is not significant.

## 2.4 Creep-Fatigue Evaluation According to Code Procedures

### 2.4.1 Purpose

In the previous chapter, to capture the characteristics of ASME-NH, RCC-MR and DDS, creep-fatigue evaluation without safety or design factors that are particular to each procedure was performed and conservatism adherent to each procedure was clarified. In this chapter, based on the knowledge thus obtained, creep-fatigue evaluation according to each procedure, including factors of various kinds, was performed.

### 2.4.2 Conditions for Evaluation

Considering creep-fatigue loadings in power plants, strain range is low and hold period is long, and creep damage is dominant. Therefore, in this section, creep damage was calculated according to the three procedures and compared. The conditions for evaluation are shown in Table 5.

Creep damage was calculated for various elastically calculated stress ranges. Parameters used in the calculation are summarized in Table 6. Since misprints were found with $S_r$ values of ASME-NH, $S_r$ values of DDS were used for the evaluation of ASME-NH. If necessary material properties were not determined explicitly in a procedure, those described in DDS were used.

Moreover, the creep fatigue damage evaluation with the design base was performed based on the strain range and the failure life obtained by experiments. In this case, strain range was assumed to be already known, an initial stress was calculated from the stress-strain relation, and damage was calculated assuming all creep damage. The stress concentration coefficient provided in ASME-NH was assumed to be one. The procedures in the three codes are schematically shown in Figure 61 to Figure 63.

### 2.4.3 Discussions

Figure 64 shows creep damage evaluated according to the three procedures. Generally, ASME-NH gives the highest value, and DDS and RCC-MR follow. In the region corresponding to the stress level of around 400MPa, ASME gives a prediction 10 times more conservative than that of DDS. For components in which stress concentration is significant, the difference may enlarge because ASME-NH uses Neuber's rule. Figure 65 shows the result of creep-fatigue damage evaluated based on the procedures determined in ASME-NH, RCC-MR and DDS. In the evaluation of Figure 65, safety factors/margins were included. Creep damage calculated according to ASME-NH, RCC-MR and DDS procedures scatter around $10^4$, 10 and $10^2$, respectively. The strain ranges of creep-fatigue tests correspond to 400 to 600 MPa, where the differences among the three procedures are pronounced. RCC-MR gives smallest values because it adopts cyclic stress-strain curves for the estimation of the initial stress of relaxation and it estimates stress relaxation behavior less conservatively compared to other two methods. In Figure 66, the margin compared to the creep fatigue damage envelope is shown. The margins calculated this way are approximately 10 to $10^2$ for RCC-MR, $10^2$ to $10^3$ for DDS and $10^3$ to $10^4$ for NH.

Although the difference between the three methods is pronounced in the region where experimental results are available, it is understood from Figure 64 that the difference may not be so large in the region where actual design is performed. It is to be noted that the observations obtained in a relatively high stress region where experimental results are available are not necessarily applicable to a low stress region where most of the actual components are operated.

## 2.5 Other Factors to be Considered

### 2.5.1 Environmental Effects on Tensile and Compressive Hold Tests

Figure 67 compares the creep-fatigue life under tensile hold conditions and compressive hold conditions in an air environment. In a temperature range of 500 to 600˚C and a hold time range of 1 to 60 minutes, compressive hold tests showed shorter creep-fatigue life than tensile hold tests under all conditions. In a sodium environment, a test has been performed at 550˚C with a strain range of 0.5% and a hold time of 60 minutes as shown in Figure 68. In this case, a compressive hold test showed a longer life. In a vacuum environment, a test has been performed at 600˚C with a strain range of 2% and a hold time of 10 minutes as shown in Figure 63. In this case, a tensile hold test showed a longer life.

For the life reduction under compressive hold tests of Grade 91 steel, principally two mechanisms have been suggested, one is the effect of oxidation and the other is tensile mean stress developed during cyclic creep-fatigue loading. Figure 70 shows tensile peak stress and compressive peak stress at the mid-life cycle for tensile hold tests, compressive hold tests and tests with both tensile and compressive hold period. It is obviously observed that compressive mean stress develops in tensile hold tests and that tensile mean stress develops in compressive hold tests.

The creep-fatigue test results in air, sodium and vacuum environments can be interpreted as follows. When there is virtually no effect of oxidation, which is the case with sodium and vacuum environments, creep damage and tensile mean stress effect are to be considered. As indicated in Figure 71, when strain range is high and hold time is short, the effect of tensile mean stress is more harmful than creep damage, and a creep-fatigue life of compressive hold tests becomes shorter than that of tensile hold tests. This is basically the same in a sodium environment. However, when a strain range becomes lower and hold time becomes longer, the effect of creep damage can suppress that of a tensile mean stress. Therefore, tensile hold tests can show shorter creep-fatigue life. In an air environment, in addition to the effects of creep damage and tensile mean stress, the effect of oxidation has to be considered (Aoto et. al., 1994). The effect of oxidation can be interpreted as shown in Figure 72 and Figure 73. Oxide layer is formed and develops during a hold time. When the layer is formed during a compressive hold time, it can break during a subsequent tensile deformation. This can accelerate the initiation of cracks, and also the propagation of cracks, once they have been initiated. The oxide layers formed during a tensile hold time will experience compressive loading in the subsequent loading, and no harmful effects such as the one formed in a compressive hold period is expected. The creep-fatigue life in an air environment may be determined by a complicated combination of effects of creep damage, tensile mean stress effect and oxidation. In a short term region, compressive hold tests show shorter creep rupture time due to the effects of tensile mean stress and oxidation which are basically time-independent. On the contrary, in a long term region, creep damage, which is time-dependent, is considered to become dominant.

### 2.5.2 Effect of Thermal Aging

Figure 74 and Figure 75 show creep-fatigue life of aged material. Aged material shows shorter creep-fatigue compared to as-received material and this tendency is more obvious at lower strain ranges (The reason why the tests with 30 minutes hold time showed shorter creep-fatigue life than a test with 60 minutes hold time in Figure 75 is not clear). Figure 76 and Figure 77 show cyclic stress-strain response of aged material. There is possibility that additional softening due to aging exists but a quantitative relationship between aging and additional softening to creep-fatigue is not clear.

Figure 78 shows the tendency of cyclic softening behavior in terms of a ratio of tensile peak stress at mid-life to that of the first cycle. The magnitude of softening becomes larger when strain range becomes larger. It is again observed that the introduction of hold time enhances cyclic softening.

### 2.5.3 Conceptual Investigation of the Relationship between Time Fraction and Ductility Exhaustion Methods

All three creep-fatigue evaluation procedures evaluated so far employ time fraction approach for creep damage evaluation. It would be worthwhile to consider the relationship between time fraction rule and the ductility exhaustion method. Although there are a variety of methods to calculate creep damage according to a "ductility exhaustion" method, what is considered as the simplest formation is examined in this investigation.

Creep damage according to ductility exhaustion method is described as follows (Aoto et. al., 1994):

$$d_c = \int \frac{d\varepsilon_h}{\varepsilon_F} = \frac{\varepsilon_h}{\varepsilon_F}$$

Where,

$d_c$: creep damage per cycle

$\varepsilon_h$ : accumulated creep strain during a hold period

$\varepsilon_F$ : fracture elongation

If we focus on the secondary creep, generally, Monkman-Grant equation holds.

$$\varepsilon_F = \dot{\varepsilon}_m t_R$$

Where,

$\dot{\varepsilon}_m$ : Steady state creep rate

$t_R$: Creep rupture time

From the above equations, we can derive the following:

$$d_c = \int \frac{d\varepsilon_h}{\varepsilon_F} = \int \frac{\dot{\varepsilon}_m dt}{\dot{\varepsilon}_m t_R} = \int \frac{dt}{t_R}$$

This means that when only secondary creep is considered to be responsible for creep damage, time fraction rule and ductility exhaustion method are equivalent.

In order to confirm this assumption, very detailed observation of microstructure focusing on deformation in grain and on grain boundaries will be necessary. From the viewpoint of design standard, the adequacy of the method of creep damage evaluation is only judged in combination with a creep-fatigue interaction damage envelope, in terms of accuracy of life prediction. In that light, making an assumption that steady state creep is solely responsible for creep damage, in other words the use of time fraction rule, can be justified as far as the rule is used with a creep-fatigue interaction envelope whose intersection point is (0.3, 0.3), because Figure 55 gives fairly good prediction of creep-fatigue life.

**Table 3 - Factor K' (TABLE T-1411.1)**

| Material | Elastic analysis[3] | Inelastic analysis |
|---|---|---|
| Austenitic Stainless Steel | 0.9 | 0.67 |
| Ni-Fe-Cr(Alloy 800H) | 0.9 | 0.67 |
| 2 1/4Cr-1Mo | 0.9 | 0.67 |
| 9Cr-1Mo-V | 0.9 | 0.67 |

**Table 4 - Average Material Properties**

| Parameter | ASME-NH | DDS | RCC-MR |
|---|---|---|---|
| Stress-Strain Curves | DDS (Monotonic) | DDS (Monotonic, Cyclic) | RCC-MR (Cyclic) |
| Creep strain curves | DDS | DDS | RCC-MR |
| Fatigue curves | DDS | DDS | DDS |
| Creep rupture curves | DDS | DDS | RCC-MR |
| Estimation of stress relaxation | Isochronous stress-strain curves | Strain hardening rule | Strain hardening rule |
| Stress factor on the initial stress of relaxation | 1 | 1 | 1 |
| Elastic Following-up Coefficient | - | 1 | 1 |



[3] Currently, 0.67 for all materials. Revision to 0.9 is underway in the Code Committee.

**Table 5 - Creep Fatigue Evaluation Conditions on Elastic Design Base**

| Item | Contents |
|---|---|
| Temperature | 550 C |
| Stress concentration factor K | 1 |
| $\Delta\sigma$ | 100~500 MPa |
| Hold time | 1000 hr |
| Number of cycles | 263 cycles (for 30years) |
| Ratcheting creep effects | No effects |
| Symmetrization effects | |

**Table 6 - Material Properties and Design Values**

| Parameter | ASME-NH | DDS | RCC-MR |
|---|---|---|---|
| Stress-Strain Curves | DDS (monotonic) | DDS (monotonic) | RCC-MR (cyclic) |
| Creep | DDS | DDS | RCC-MR |
| The minimum value of creep rupture $S_r$ | DDS | DDS | RCC-MR |
| The allowable strain range | ASME-NH | DDS | RCC-MR |
| Estimation of stress relaxation | Isochronous stress-strain curves | Strain hardening rule | Strain hardening rule |
| Stress factor on creep behavior (relaxation) | 0.9 | 1 | 0.9 |
| Elastic Following-up Coefficient | - | 3 | 3 |
| $S_{rH}$ | DDS | DDS | - |

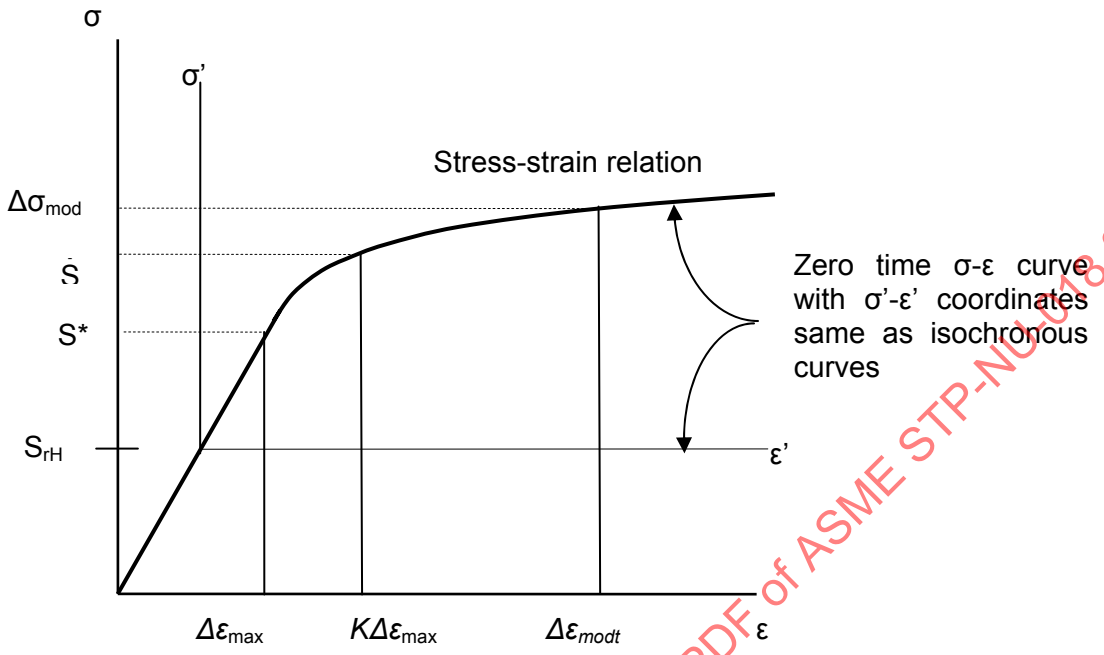


**Figure 19 - Stress-Strain Relationship (ASME-NH)**

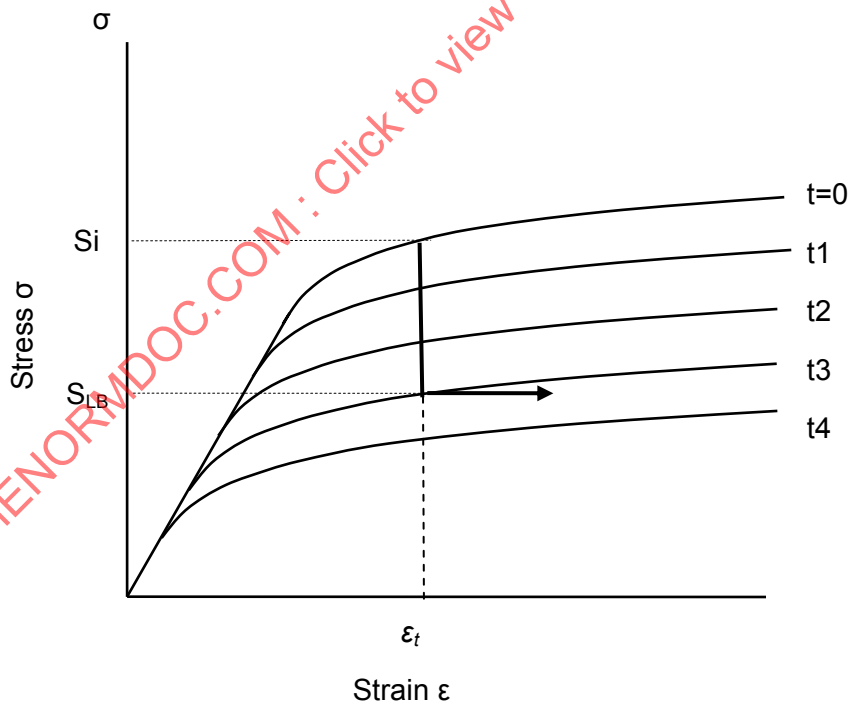


**Figure 20 - Stress Relaxation from Isochronous Stress-Strain Curves (ASME-NH)**

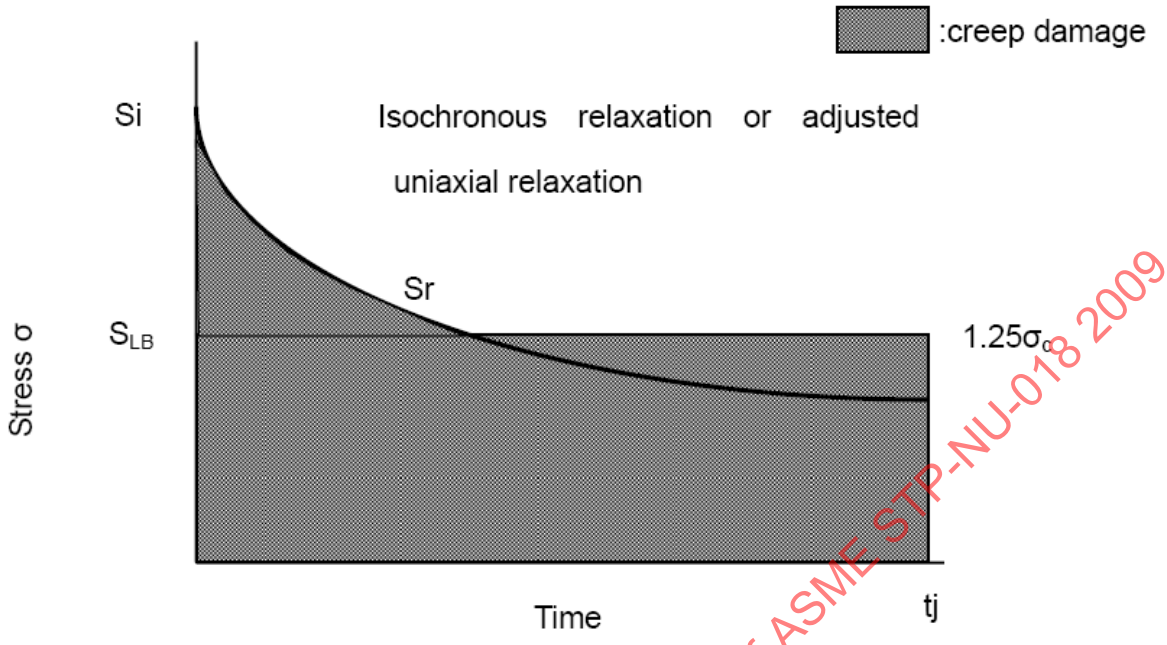


**Figure 21 - Stress-Relaxation Limit for Creep Damage (ASME-NH)**

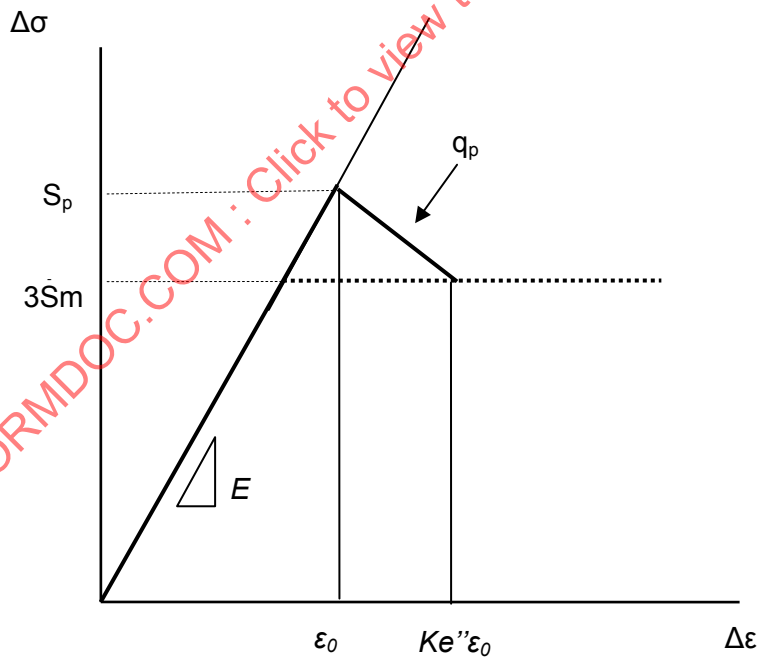


**Figure 22 - Calculation Procedure of $Ke''\varepsilon_0$ (DDS)**

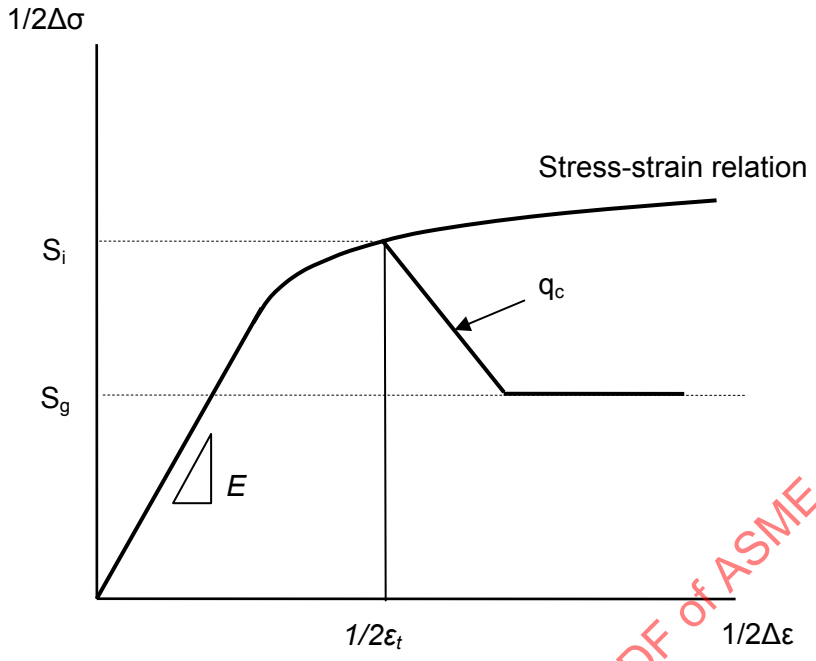


**Figure 23 - Calculation Procedure of Initial Stress and Relaxation Process (DDS)**

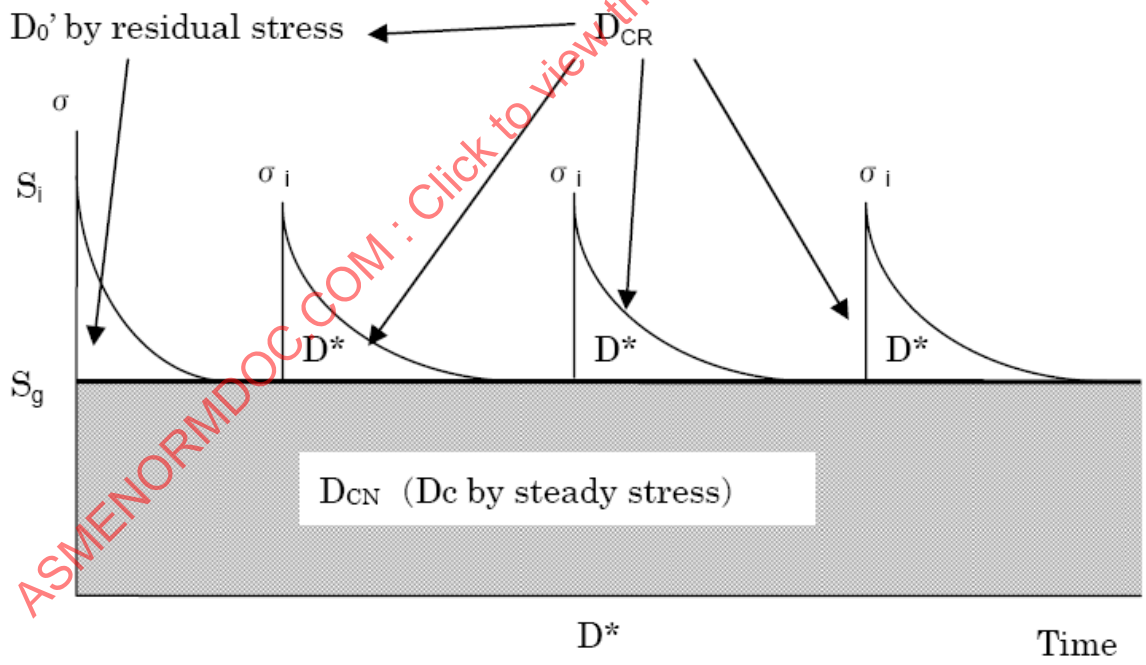


**Figure 24 - Relaxation Behavior and Creep Damage (DDS)**

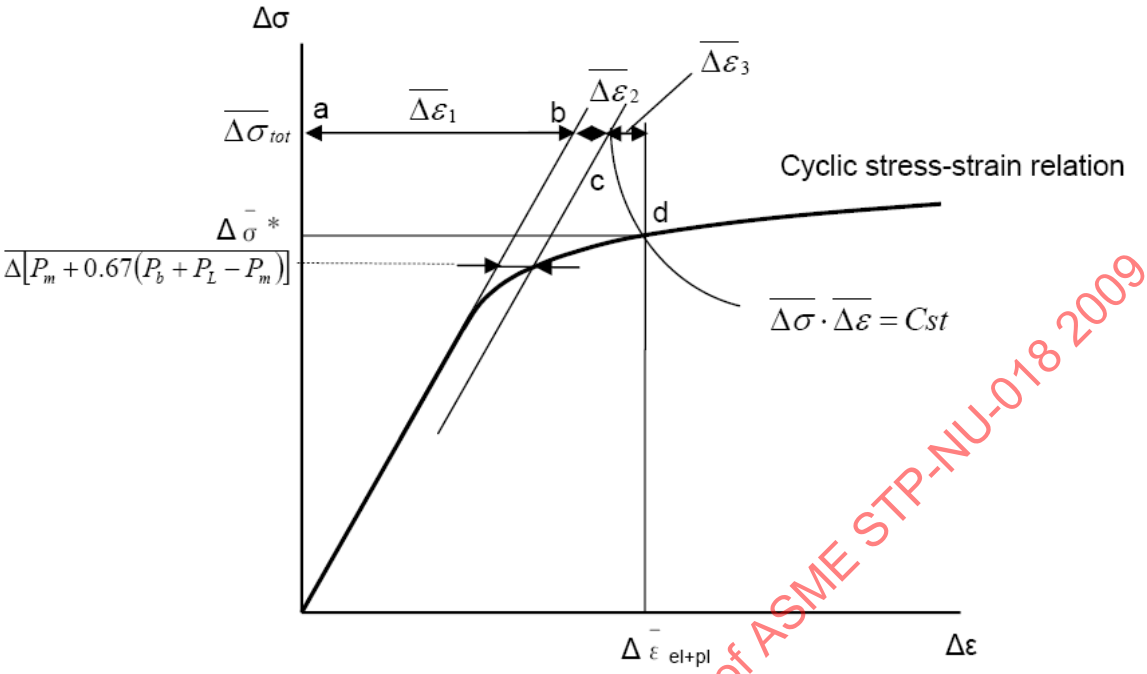


**Figure 25 - Calculation Procedure of Creep Strain Range (RCC-MR)**

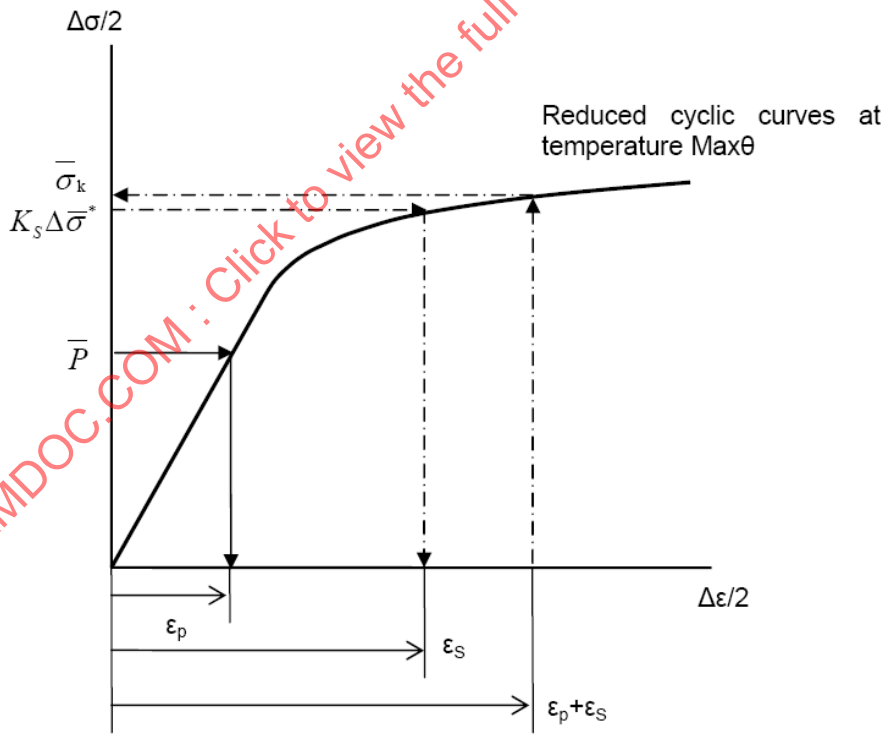


**Figure 26 - Calculation Procedure of $\overline{\Delta\sigma_k}$ (RCC-MR)**

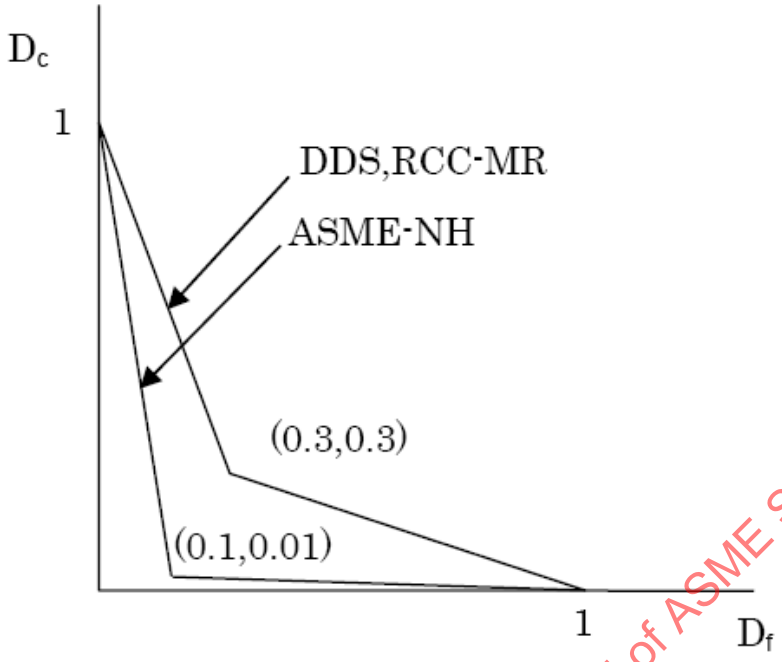


**Figure 27 - Creep-Fatigue Damage Envelopes for Mod. 9Cr-1Mo**

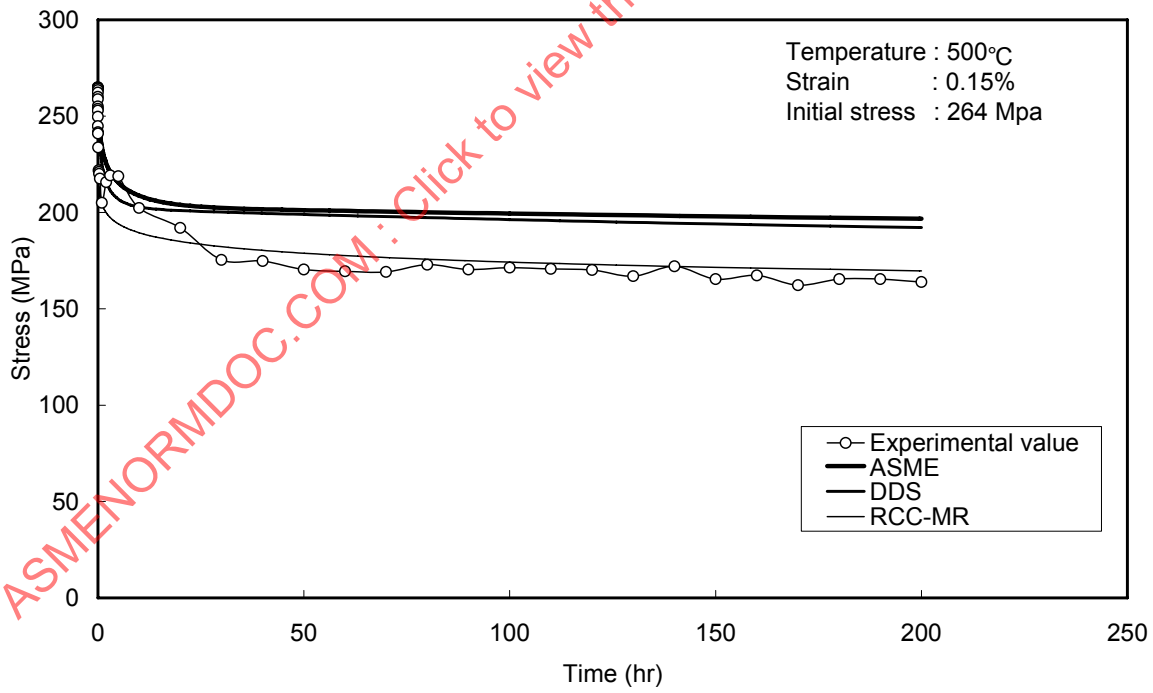


**Figure 28 - Comparison between Experimental and Calculated Values of Static Relaxation Behavior at $\varepsilon_t$ = 0.15%**

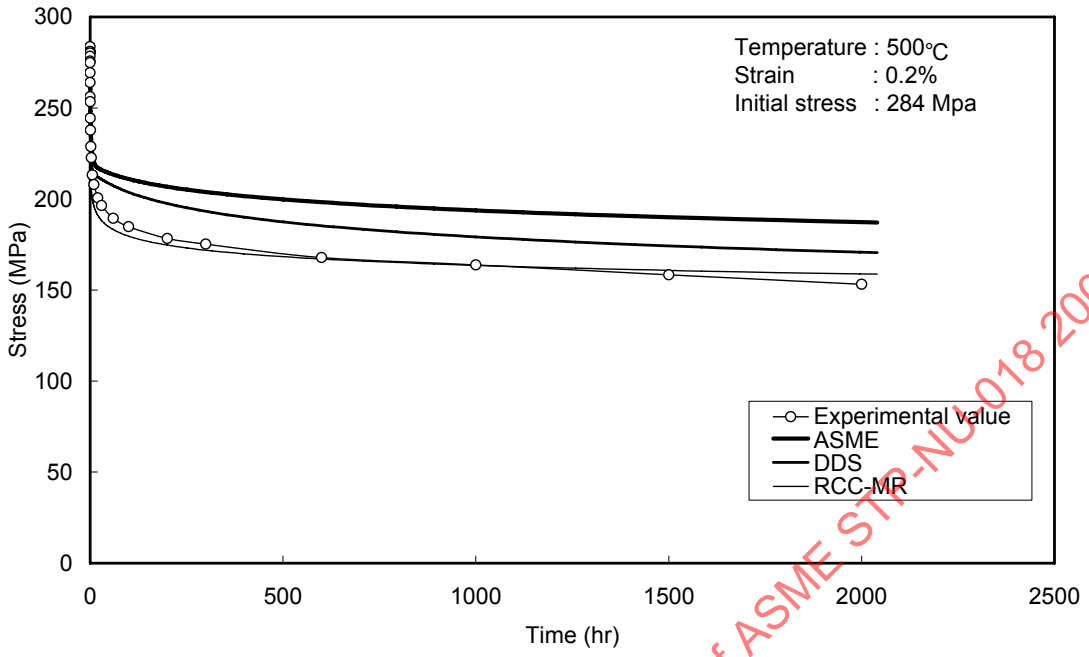


**Figure 29 - Comparison Between Experimental and Calculated Values of Static Relaxation Behavior at $\varepsilon_t$ = 0.2%**

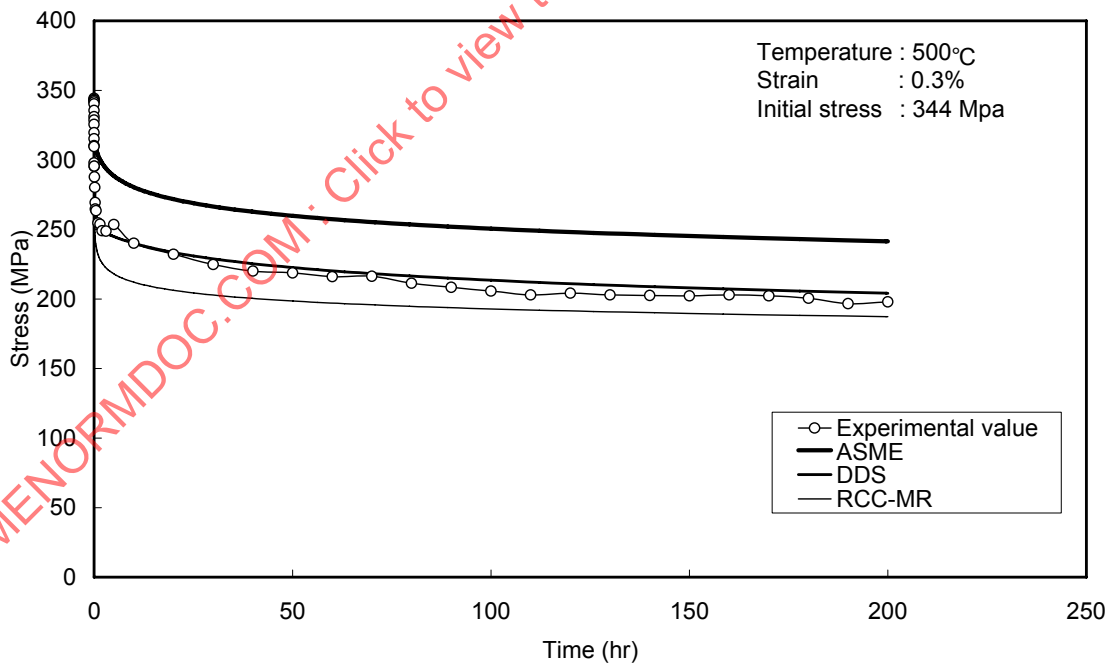


**Figure 30 - Comparison between Experimental and Calculated Values of Static Relaxation Behavior at $\varepsilon_t$ = 0.3%**

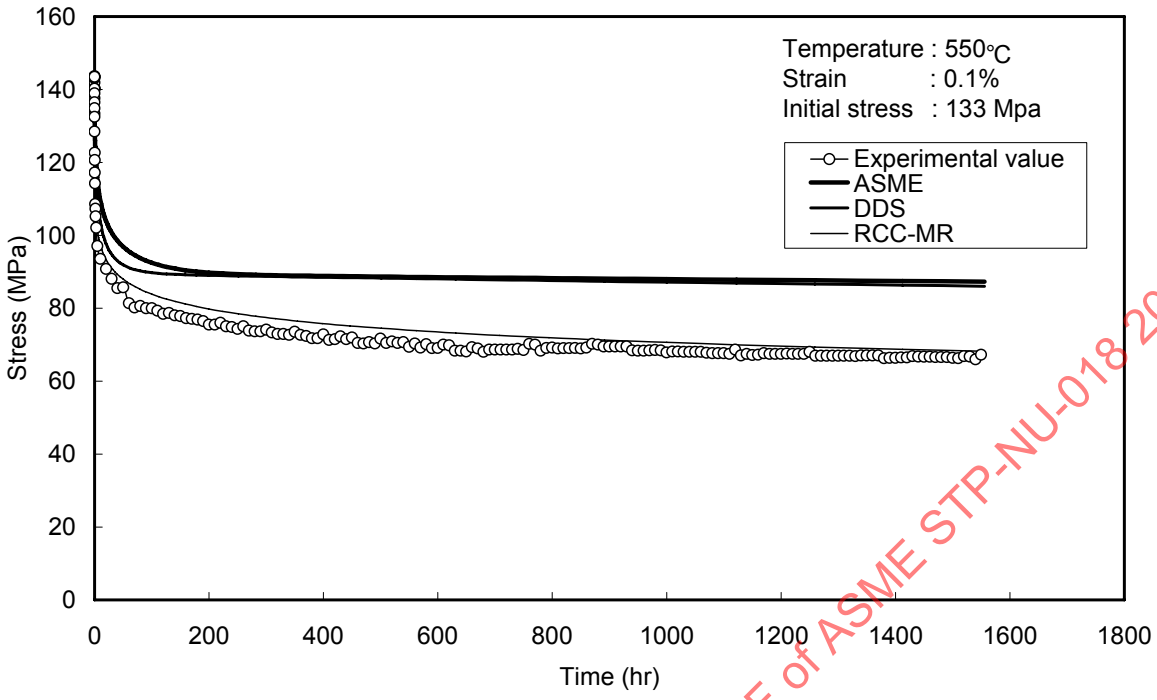


**Figure 31 - Comparison between Experimental and Calculated Values of Static Relaxation Behavior at $\varepsilon_t$ = 0.1%**

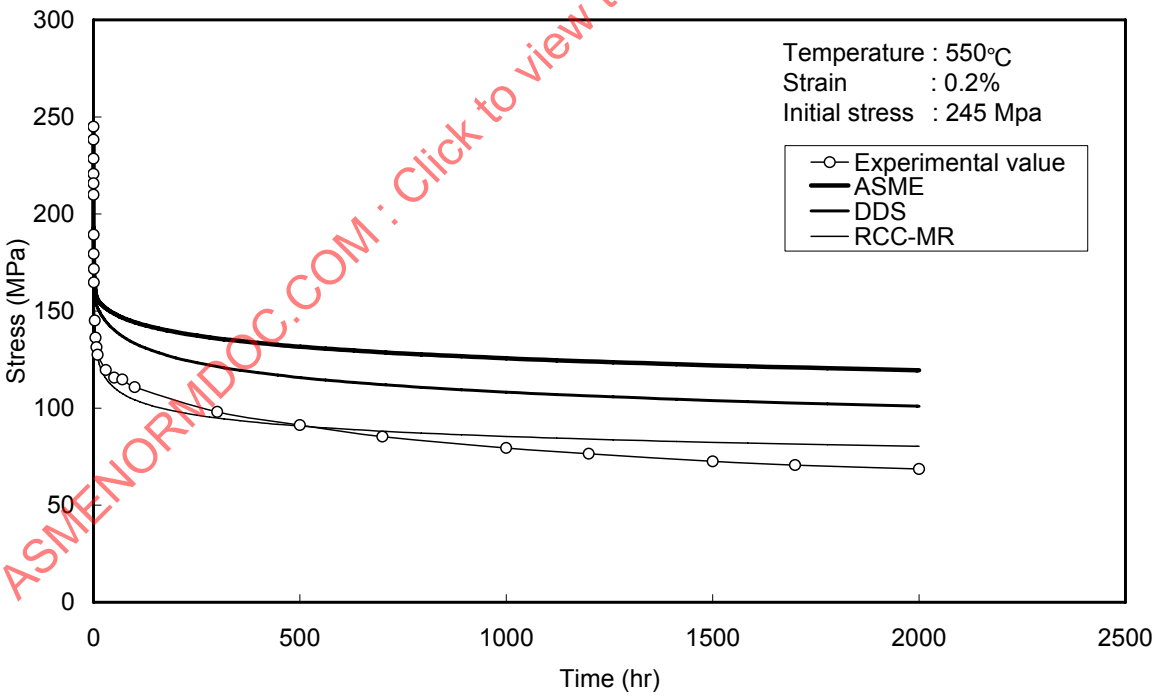


**Figure 32 - Comparison between Experimental and Calculated Values of Static Relaxation Behavior at $\varepsilon_t$ = 0.2%**

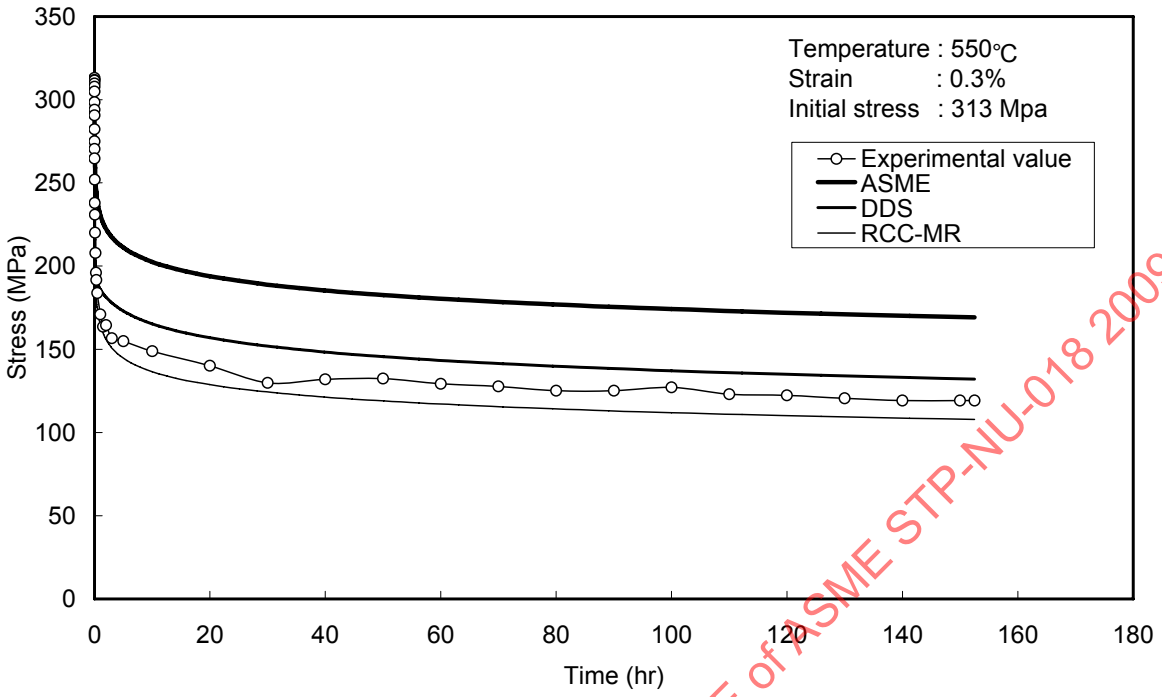


**Figure 33 - Comparison between Experimental and Calculated Values of Static Relaxation Behavior at $\varepsilon_t$ = 0.3%**

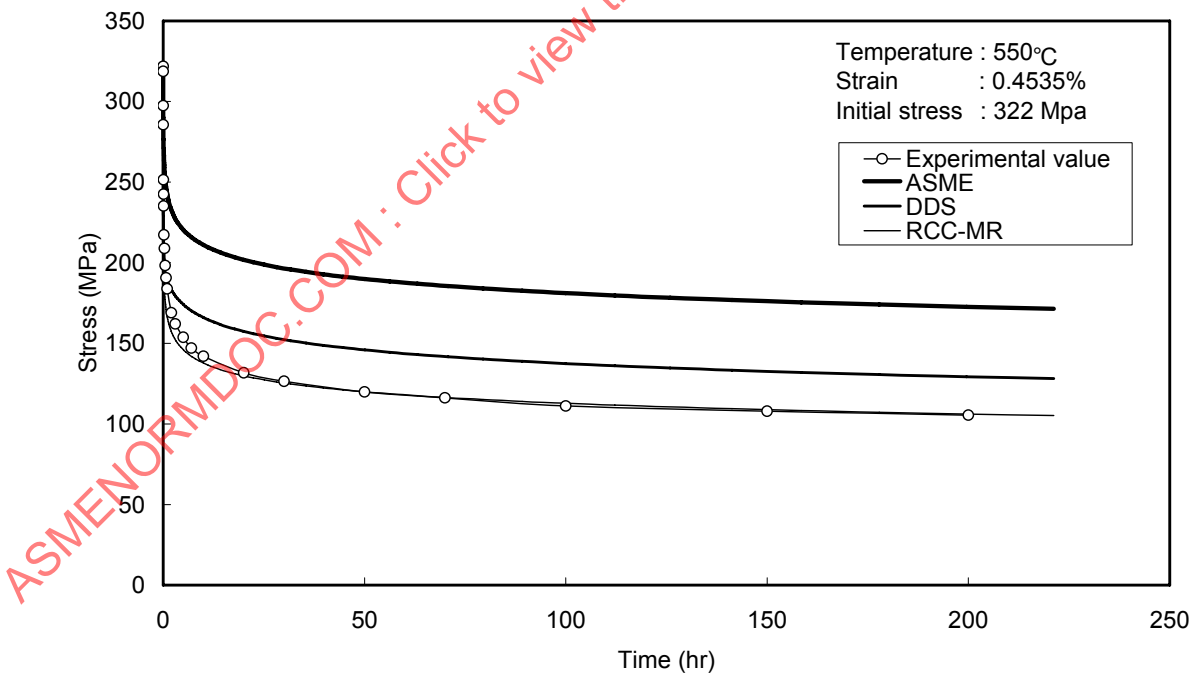


**Figure 34 - Comparison between Experimental and Calculated Values of Static Relaxation Behavior at $\varepsilon_t$ = 0.4535%**

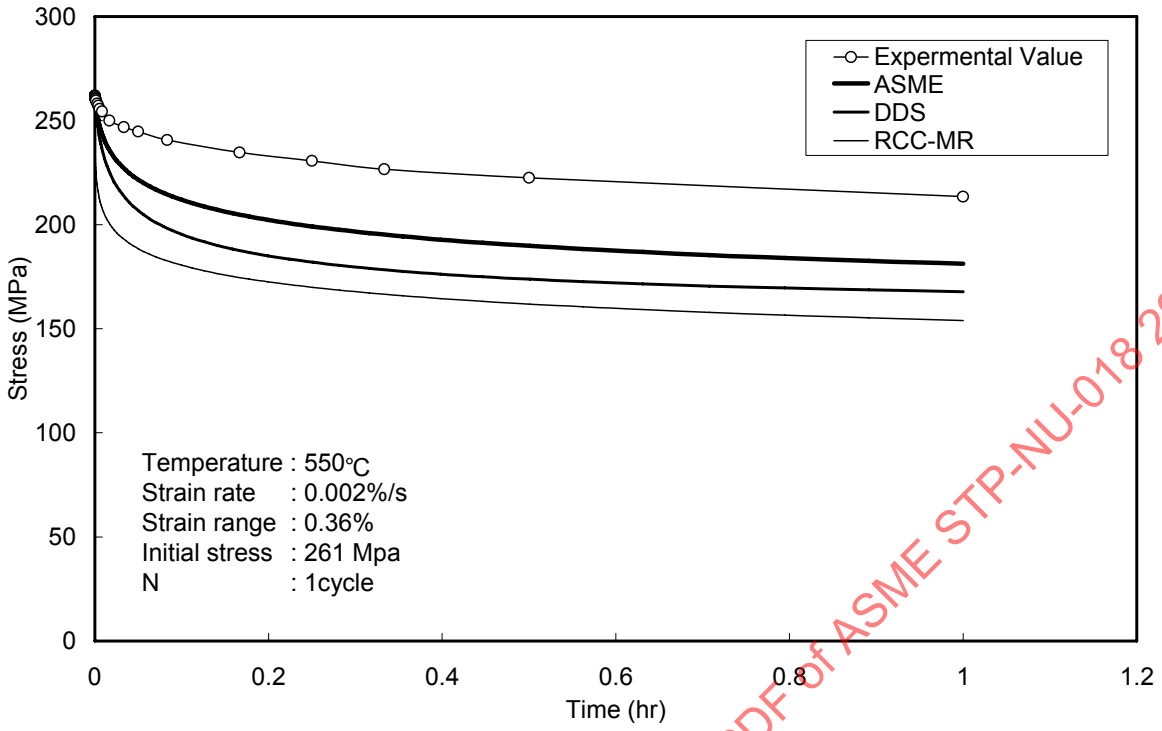


**Figure 35 - Comparison between Experimental and Calculated Values of Cyclic Relaxation Behavior at $\Delta\varepsilon_t$ = 0.36%**

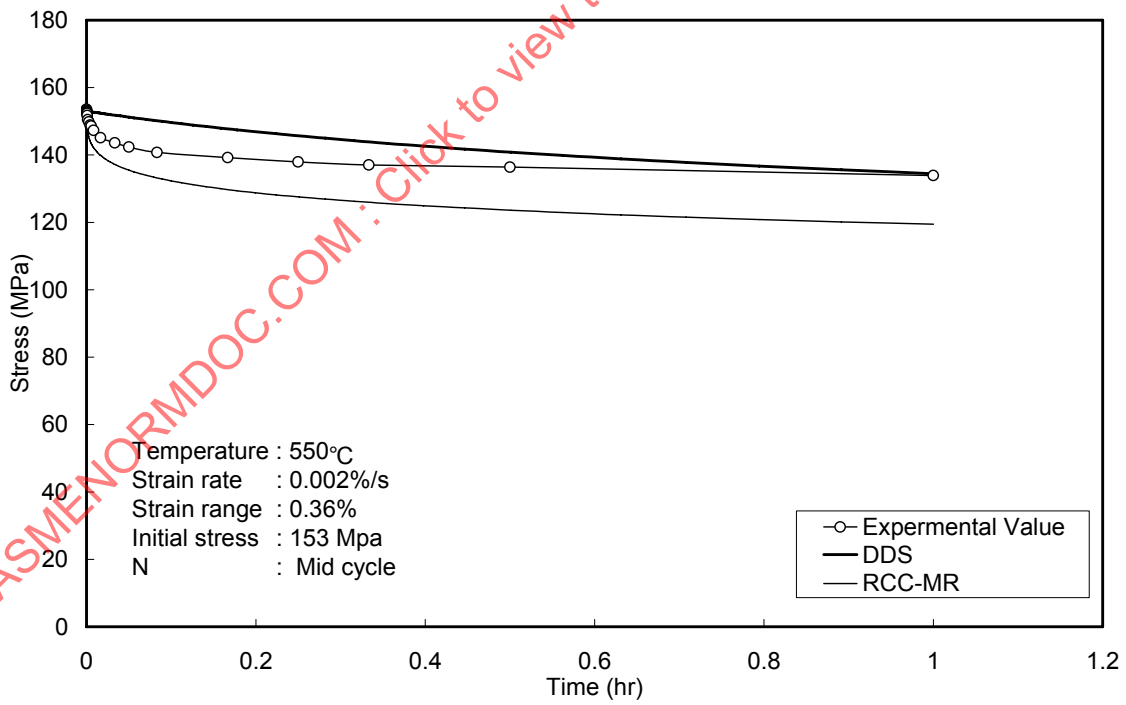


**Figure 36 - Comparison between Experimental and Calculated Values of Cyclic Relaxation Behavior at $\Delta\varepsilon_t$ = 0.36%**

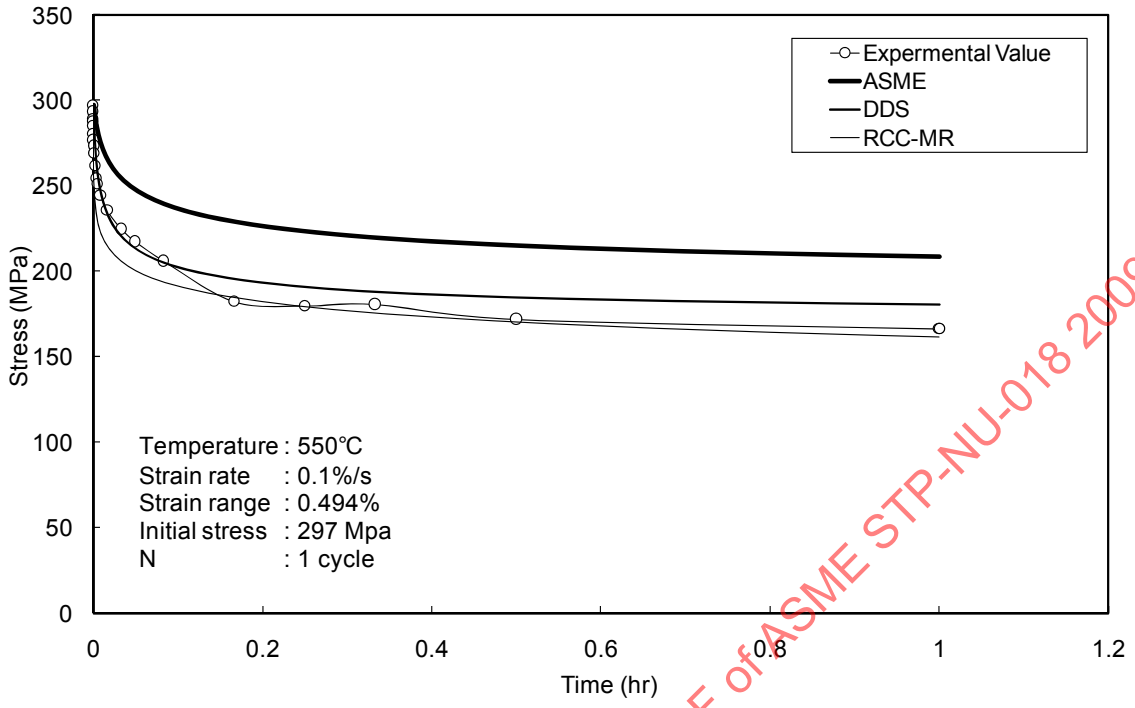


**Figure 37 - Comparison between Experimental and Calculated Values of Cyclic Relaxation Behavior at $\Delta\varepsilon_t$ = 0.494%**

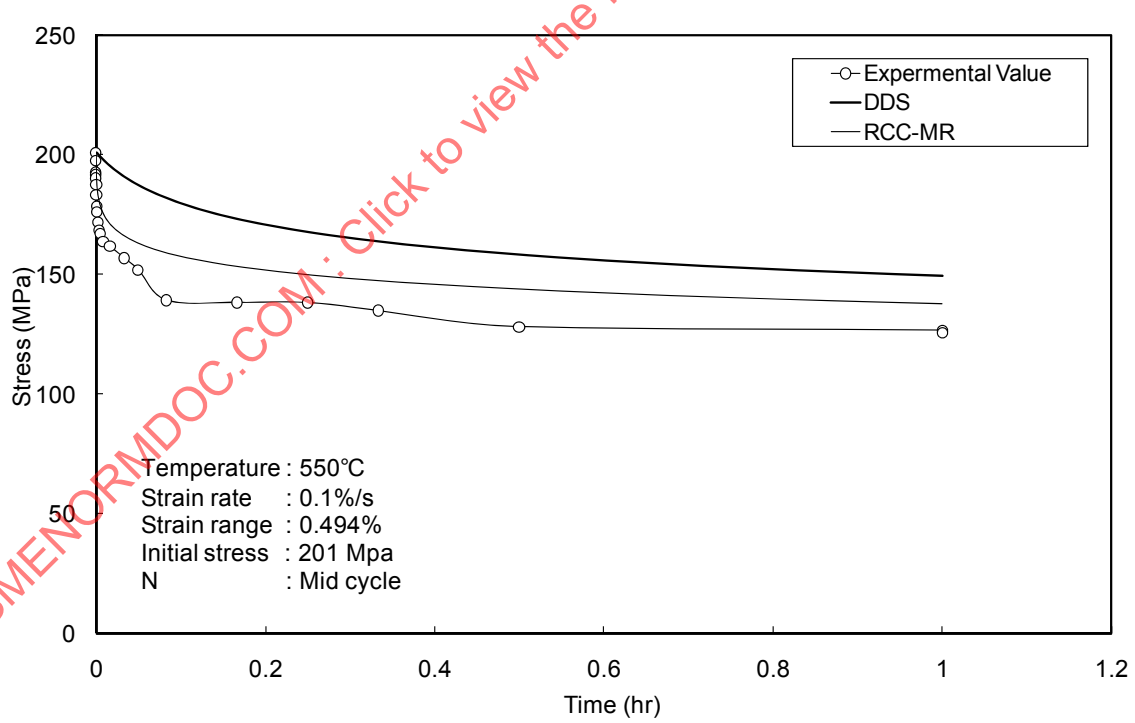


**Figure 38 - Comparison between Experimental and Calculated Values of Cyclic Relaxation Behavior at $\Delta\varepsilon_t$ = 0.494%**

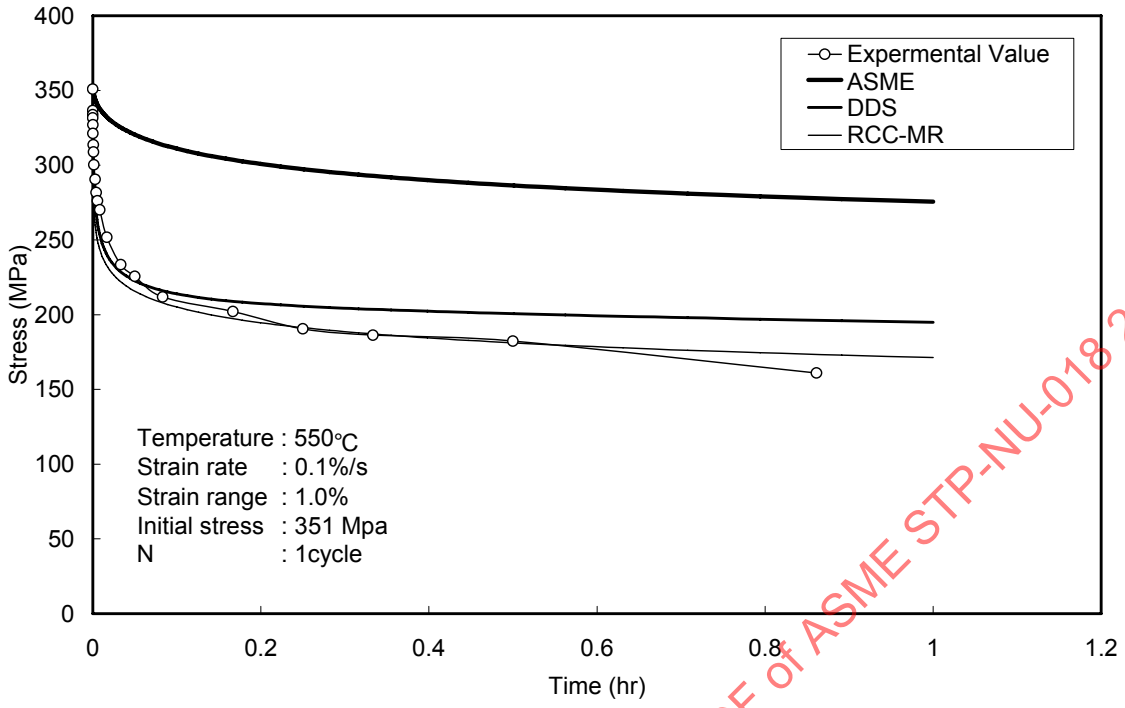


**Figure 39 - Comparison between Experimental and Calculated Values of Cyclic Relaxation Behavior at $\Delta\varepsilon_t = 1.0\%$**

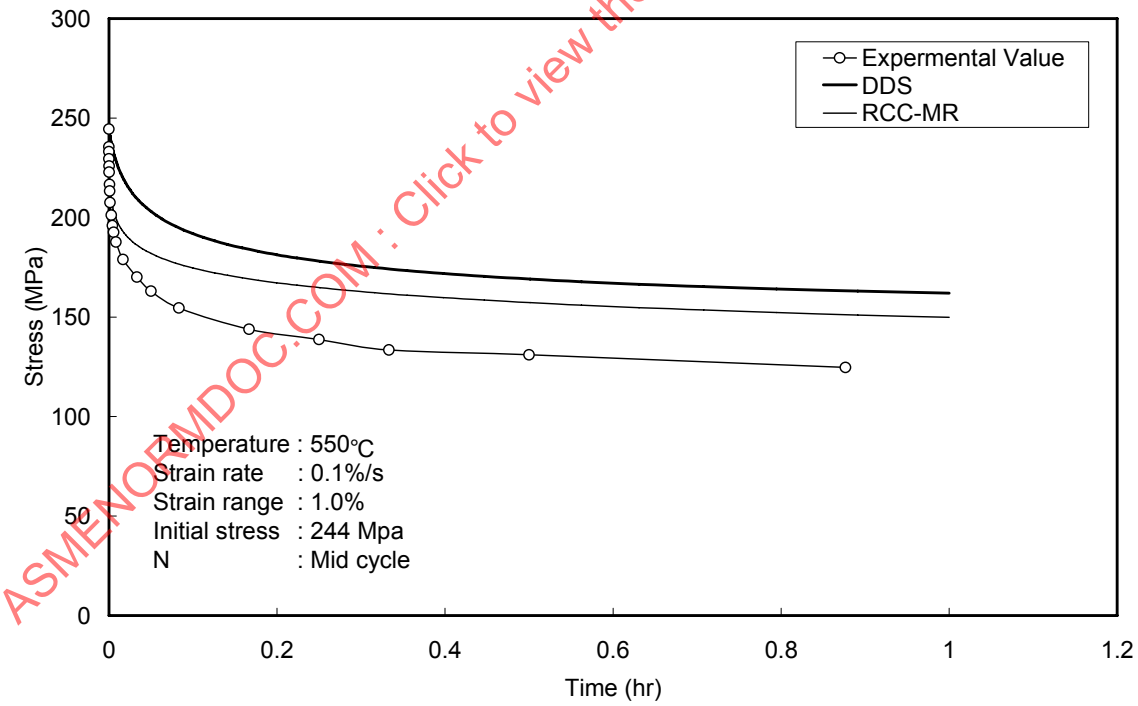


**Figure 40 - Comparison between Experimental and Calculated Values of Cyclic Relaxation Behavior at $\Delta\varepsilon_t = 1.0\%$**

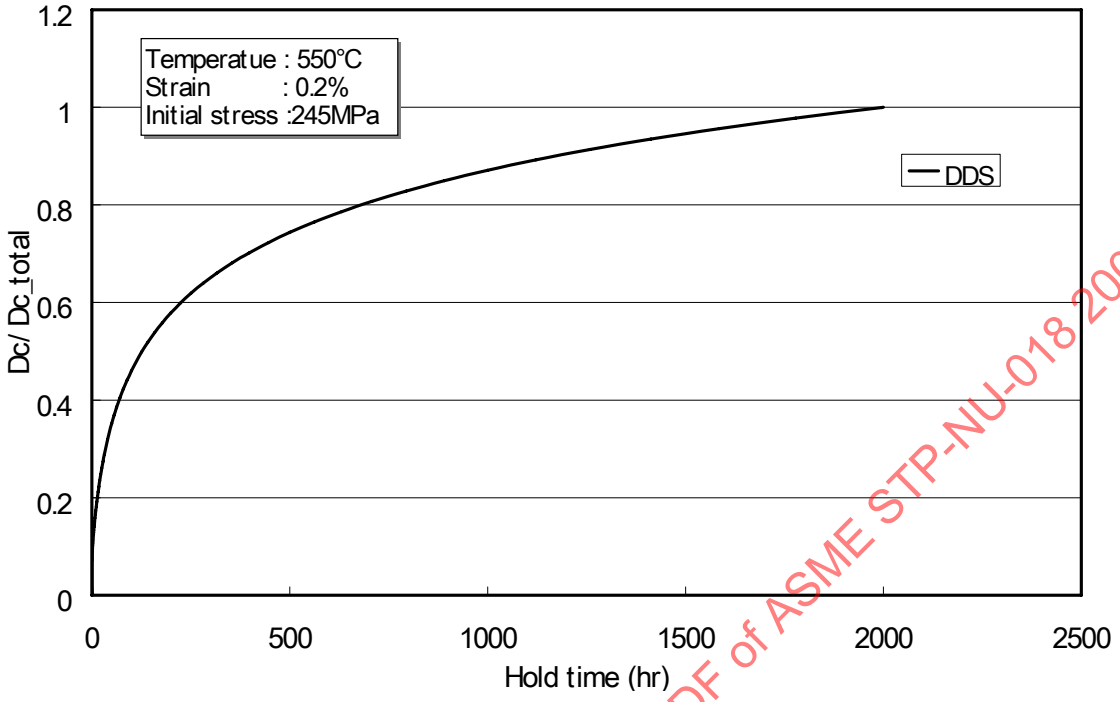


**Figure 41 - Evolution of Creep Damage During Stress Relaxation (DDS)**

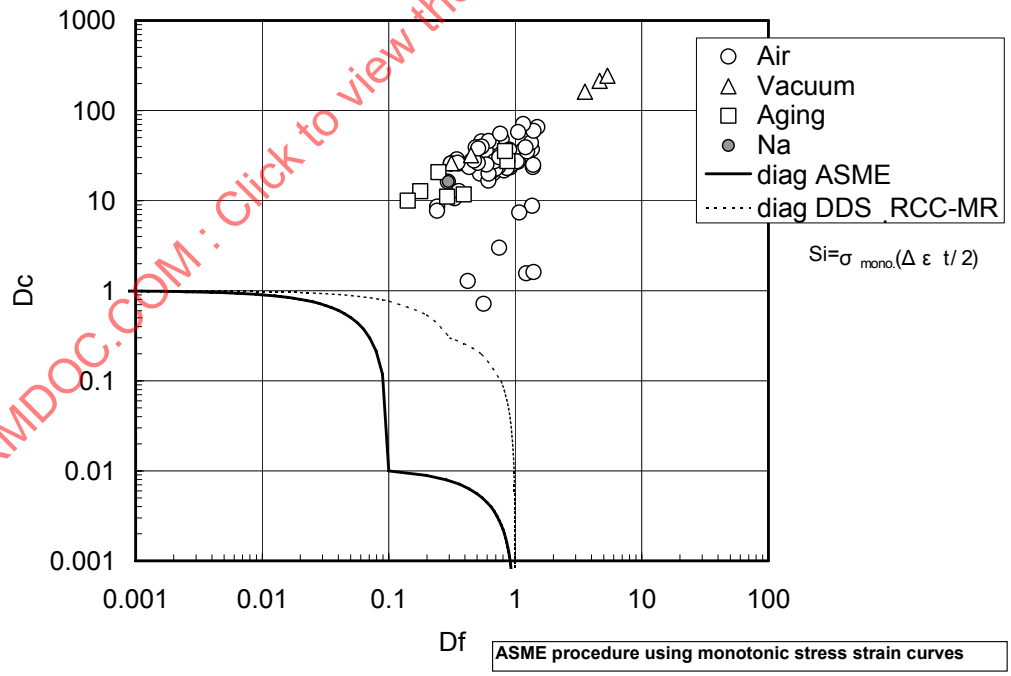


**Figure 42 - Creep-Fatigue Damage Calculated by ASME-NH Procedure Using Monotonic Stress-Strain Curves and Strain Amplitude**

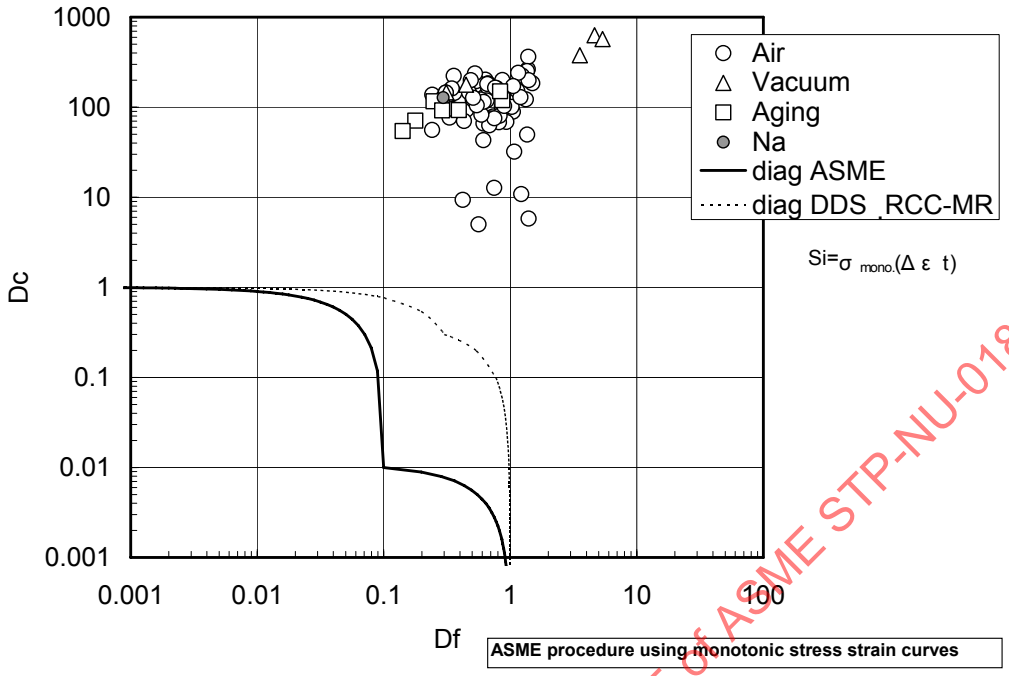


**Figure 43 - Creep-Fatigue Damage Calculated by ASME-NH Procedure Using Monotonic Stress-Strain Curves and Strain Range**

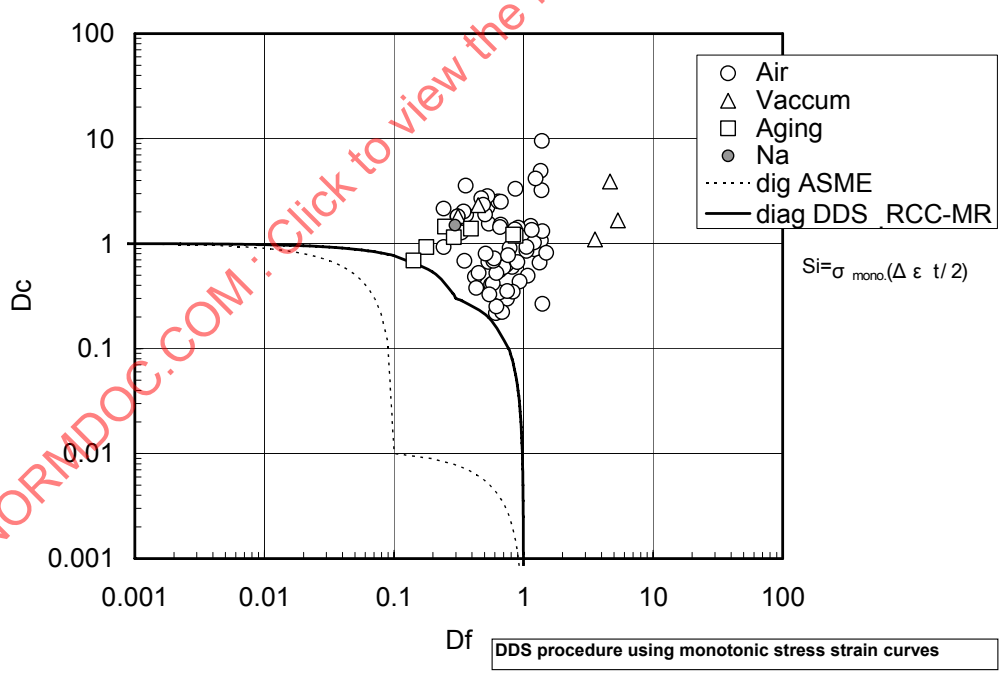


**Figure 44 - Creep-Fatigue Damage Calculated by DDS Procedure Using Monotonic Stress-Strain Curves**

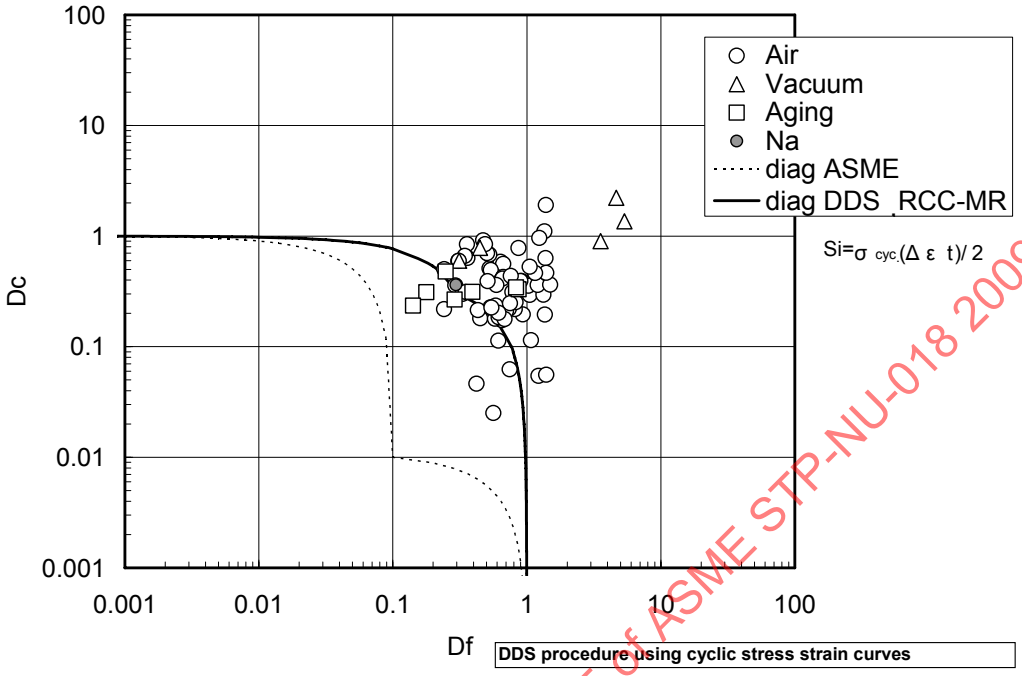


**Figure 45 - Creep-Fatigue Damage Calculated by DDS Procedure Using Cyclic Stress-Strain Curves**

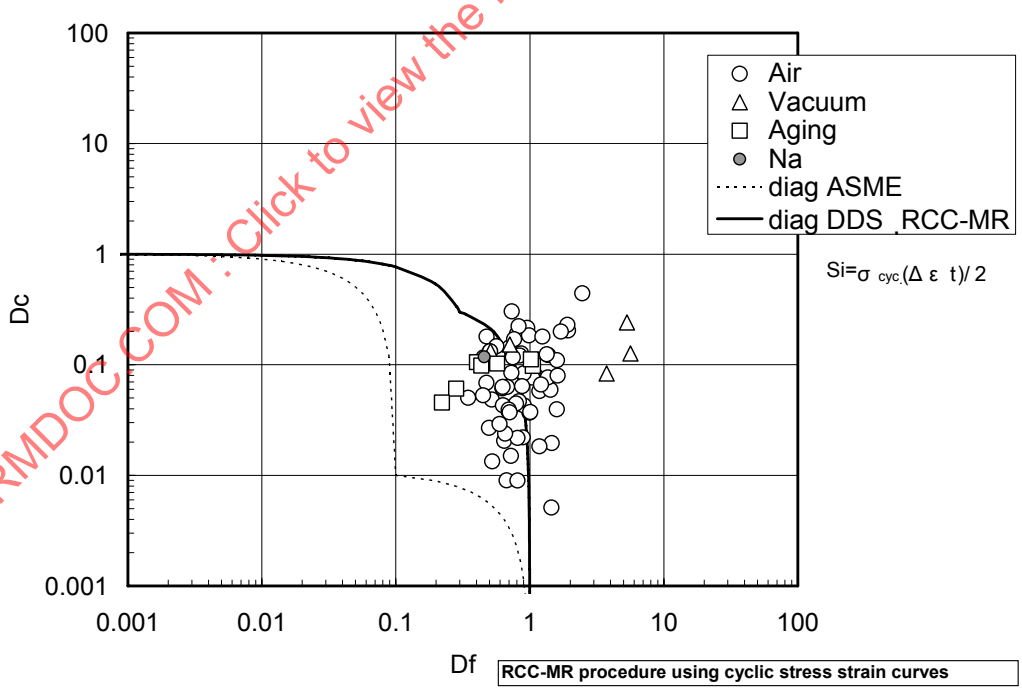


**Figure 46 - Creep-Fatigue Damage Calculated by RCC-MR Procedure Using Cyclic Stress-Strain Curves**

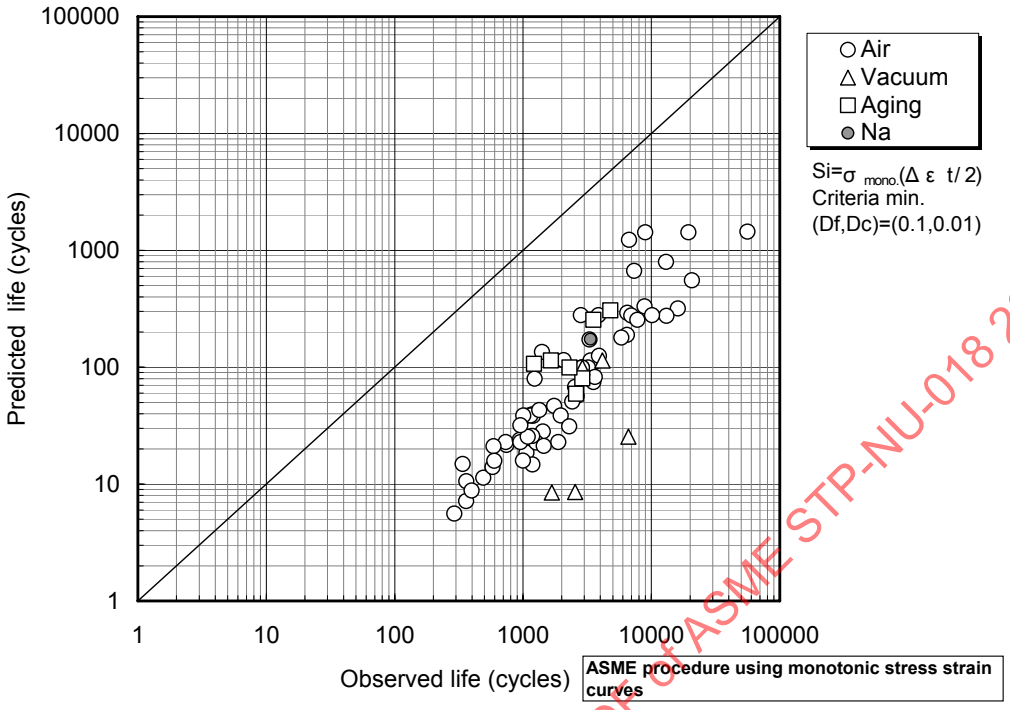


**Figure 47 - Relationship between Observed Life and Predicted Life with ASME-NH Procedure Using Monotonic Stress-Strain Curves and Strain Amplitude**

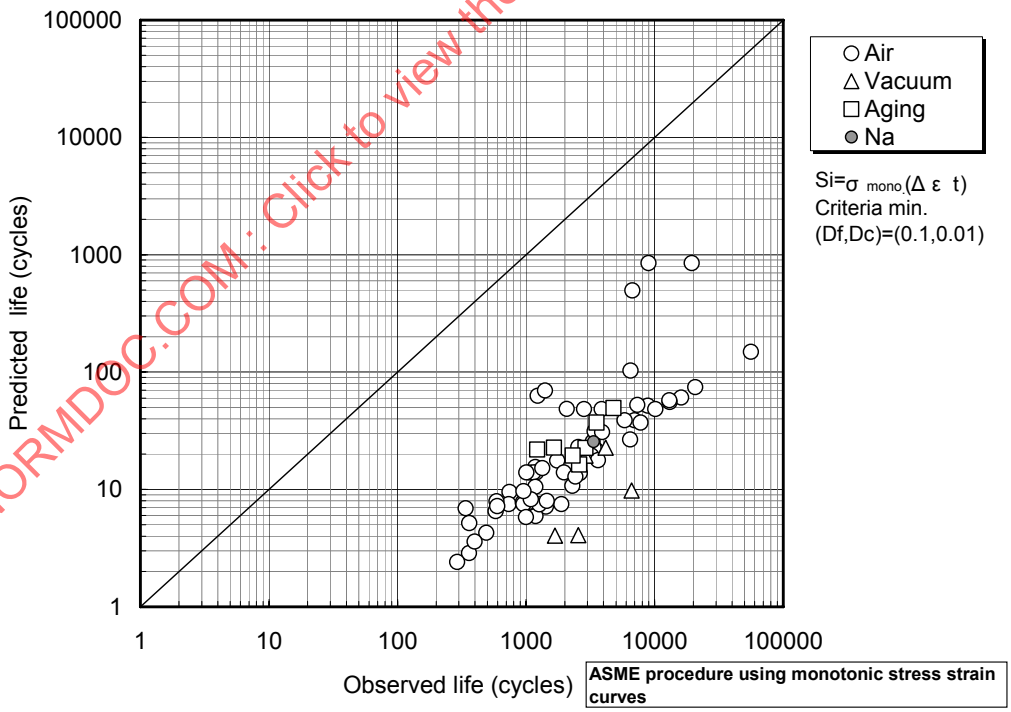


**Figure 48 - Relationship between Observed Life and Predicted Life with ASME-NH Procedure Using Monotonic Stress-Strain Curves and Strain Amplitude**

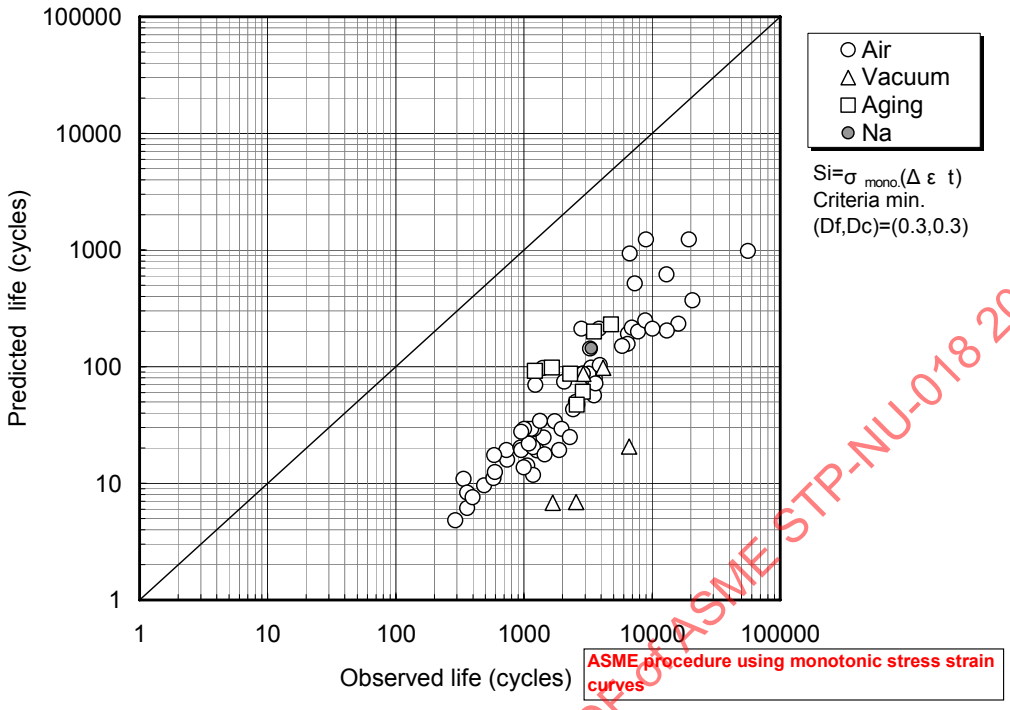


**Figure 49 - Relationship between Observed Life and Predicted Life with ASME-NH Procedure Using Monotonic Stress-Strain Curves with an Interception of (0.3, 0.3)**

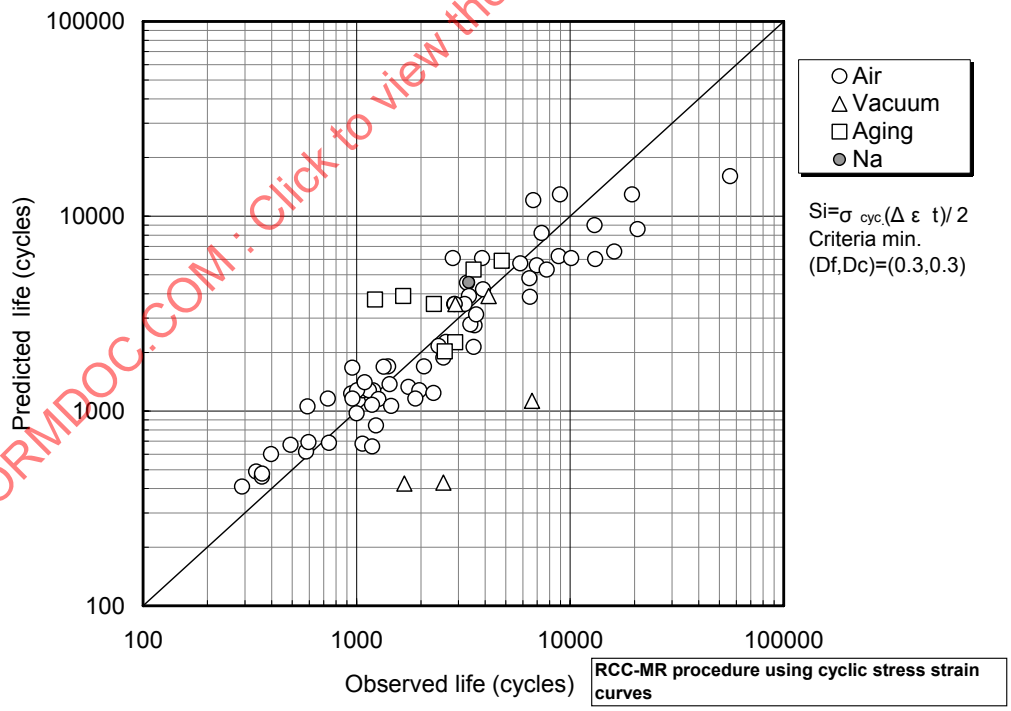


**Figure 50 - Relationship between Observed Life and Predicted Life with RCC-MR Procedure Using Cyclic Stress-Strain Curves**

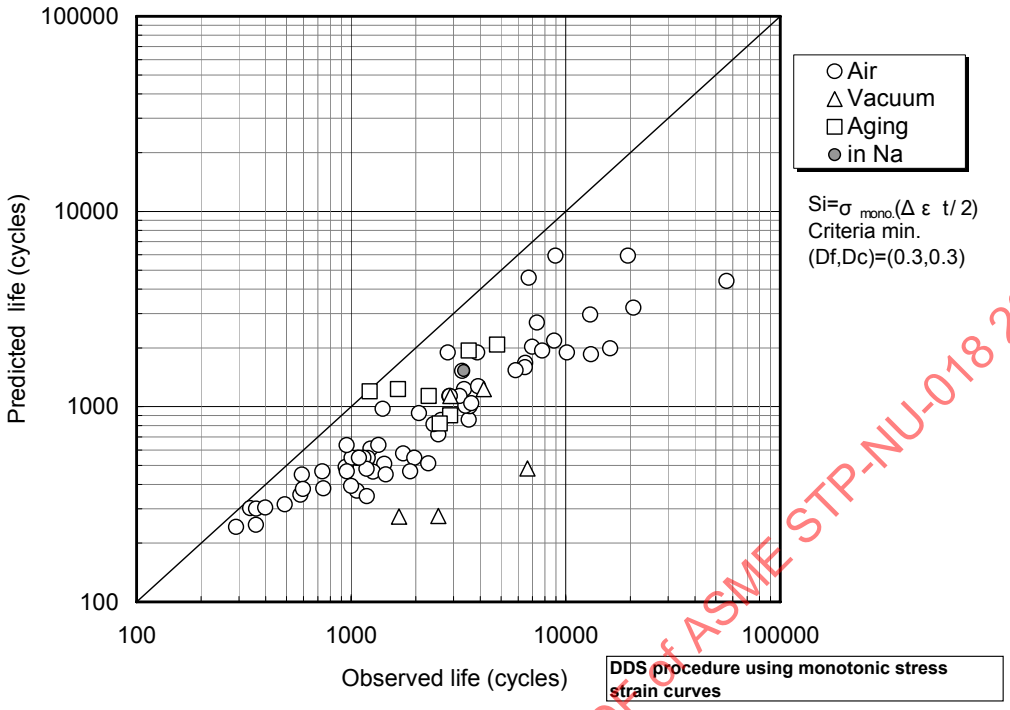


**Figure 51 - Relationship between Observed Life and Predicted Life with DDS Procedure Using Monotonic Stress-Strain Curves**

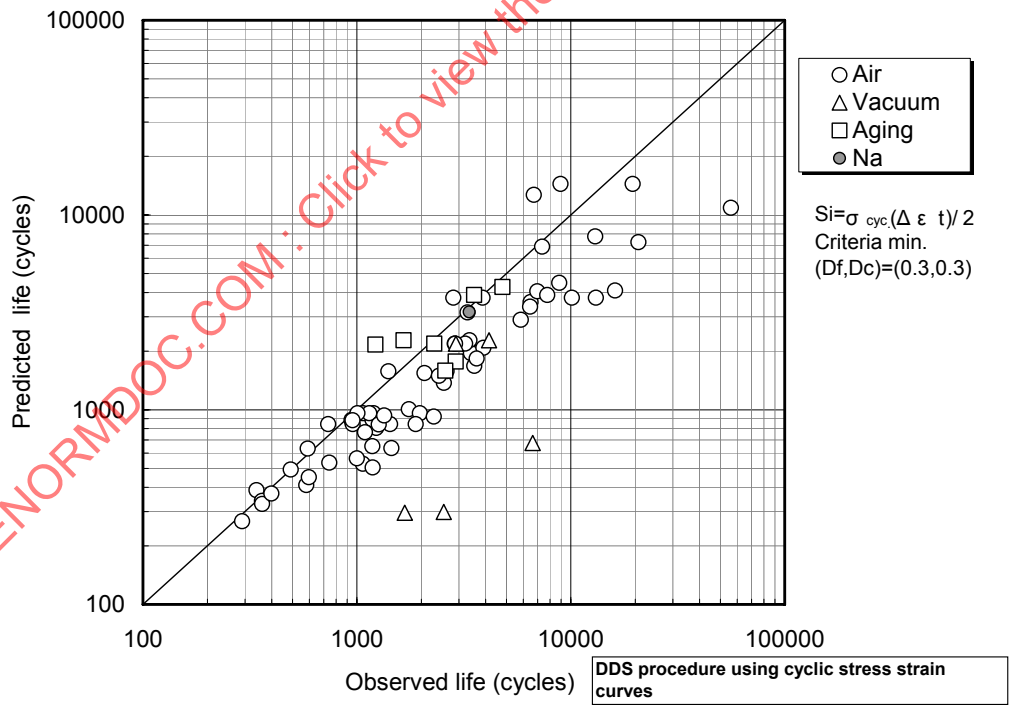


**Figure 52 - Relationship between Observed Life and Predicted Life with DDS Procedure Using Cyclic Stress-Strain Curves**

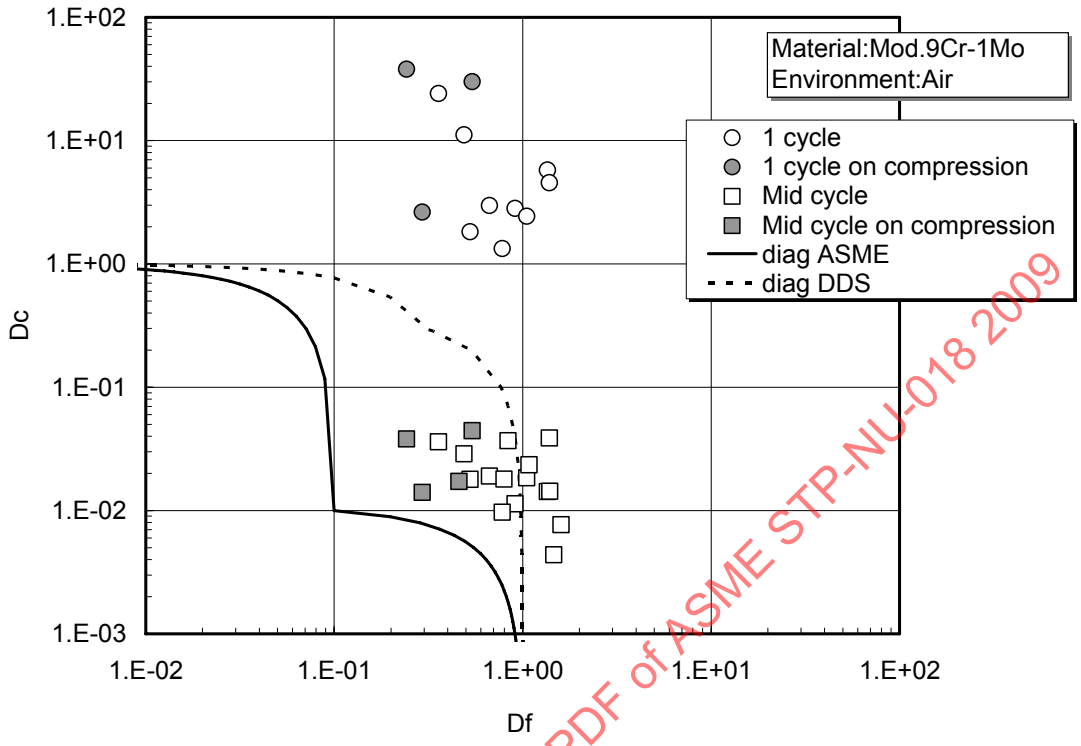


**Figure 53 - Creep-Fatigue Damage Calculated Using Experimentally Obtained Relaxation Curves**

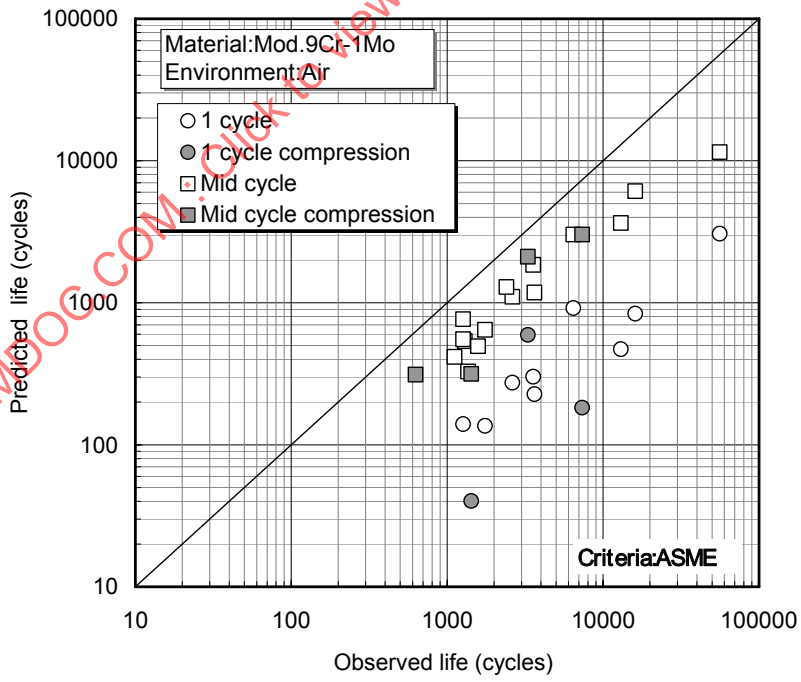


**Figure 54 - Relationship between Observed Life and Predicted Life with ASME-NH Procedure Using Experimentally Obtained Relaxation Curves**

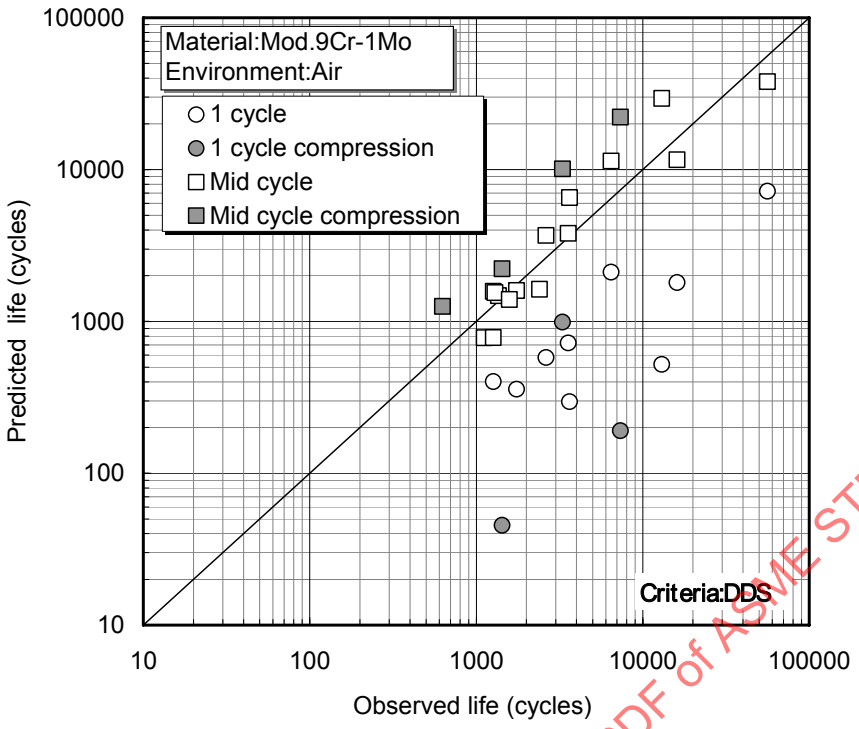


**Figure 55 - Relationship between Observed Life and Predicted Life with DDS Procedure Using Experimentally Obtained Relaxation Curves**

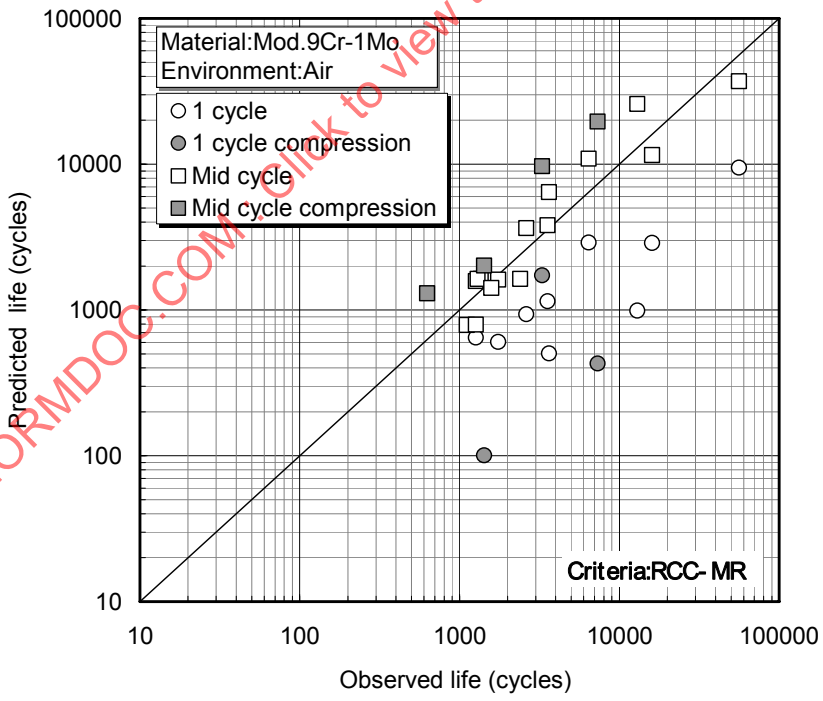


**Figure 56 - Relationship between Observed Life and Predicted Life with RCC-MR Procedure Using Experimentally Obtained Relaxation Curves**

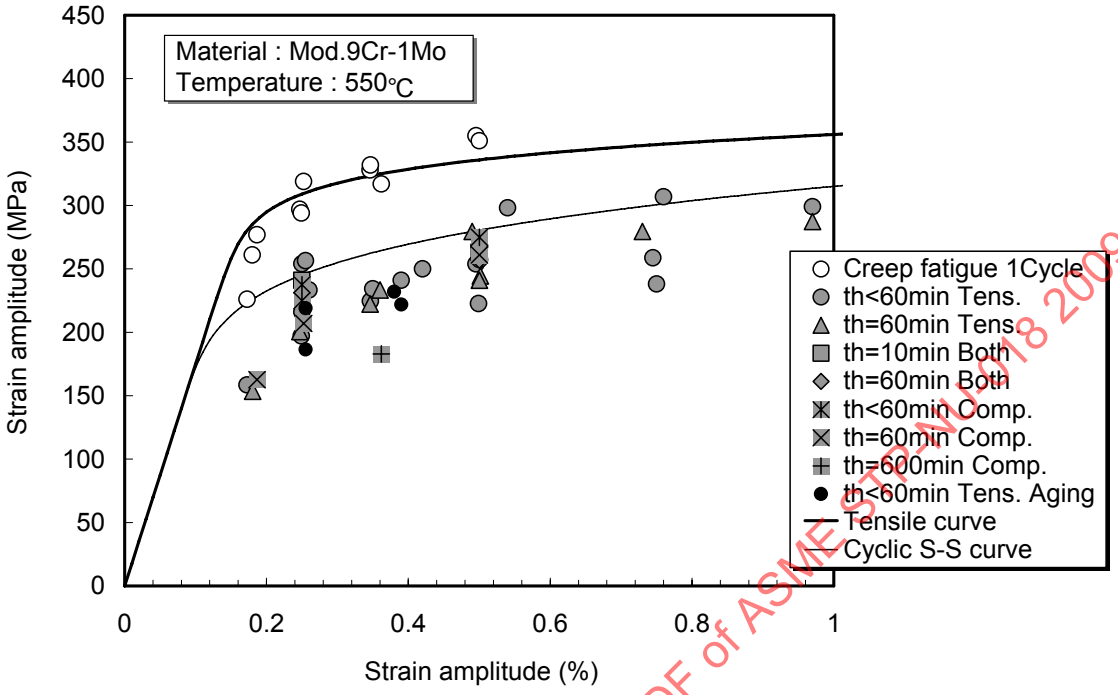


**Figure 57 - Comparison of Monotonic and Cyclic Stress-Strain Curves**

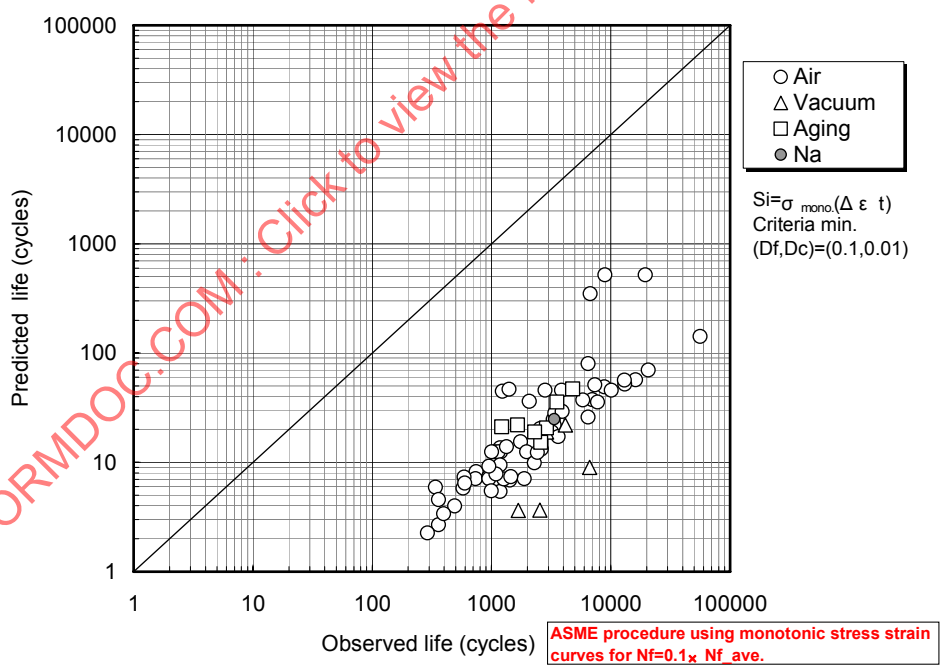


**Figure 58 - Relationship between Observed Life and Predicted Life with ASME-NH Procedure Using Monotonic Stress-Strain Curve (Presumed Fatigue Crack Initiation Life=0.1×$N_f$)**

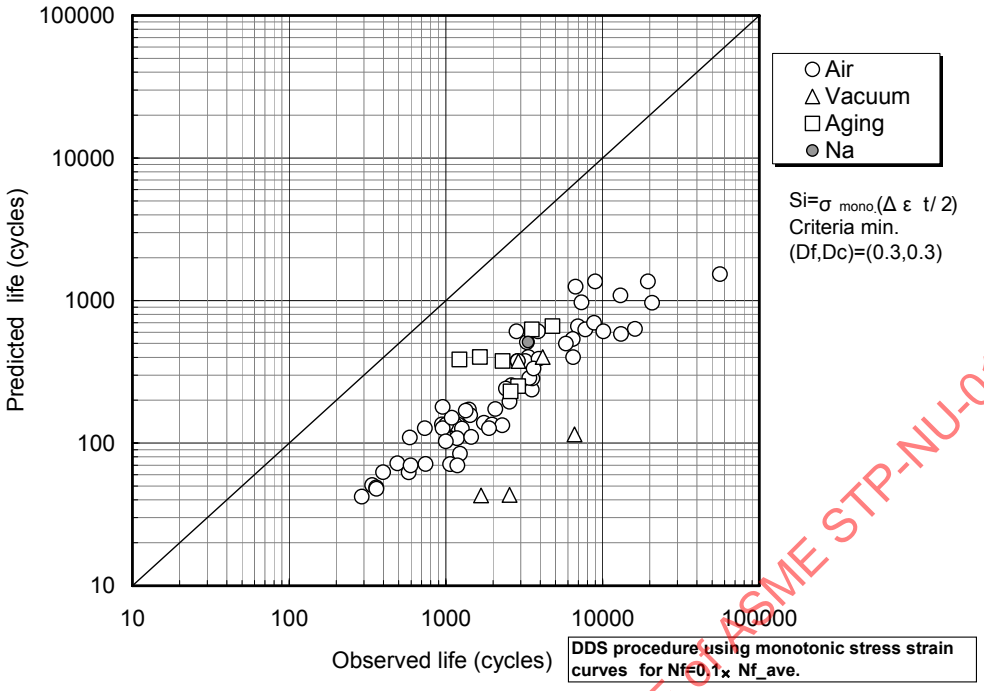


**Figure 59 - Relationship between Observed Life and Predicted Life with DDS Procedure Using Monotonic Stress-Strain Curves (Presumed Fatigue Crack Initiation Life=0.1×$N_f$)**

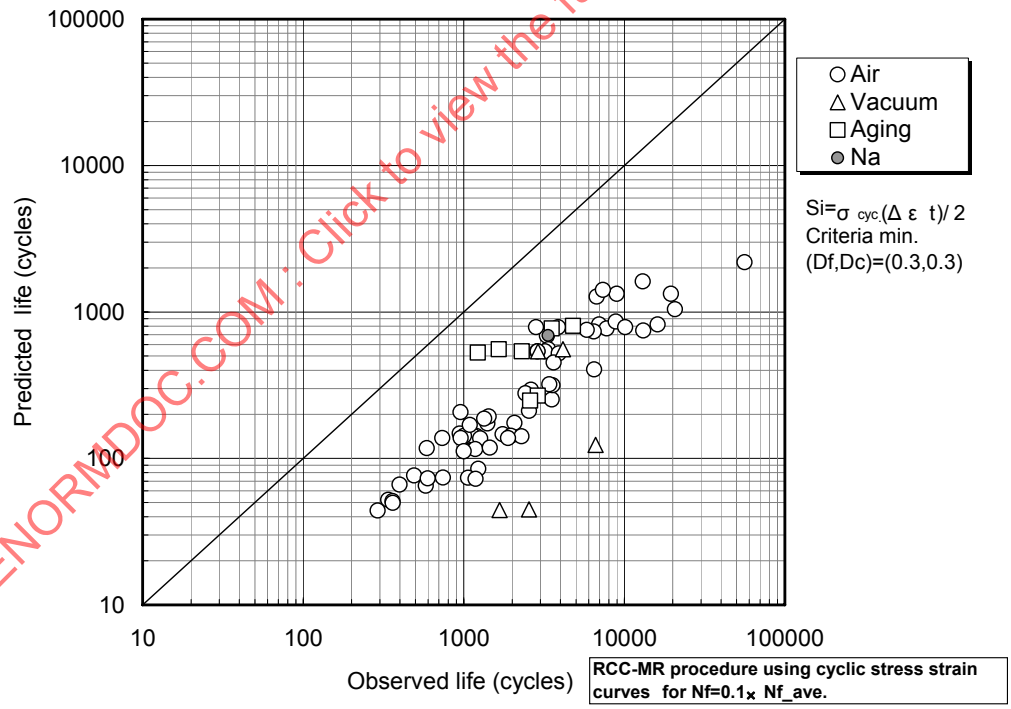


**Figure 60 - Relationship between Observed Life and Predicted Life with RCC-MR Procedure Using Cyclic Stress-Strain Curves (Presumed Fatigue Crack Initiation Life=0.1×$N_f$)**

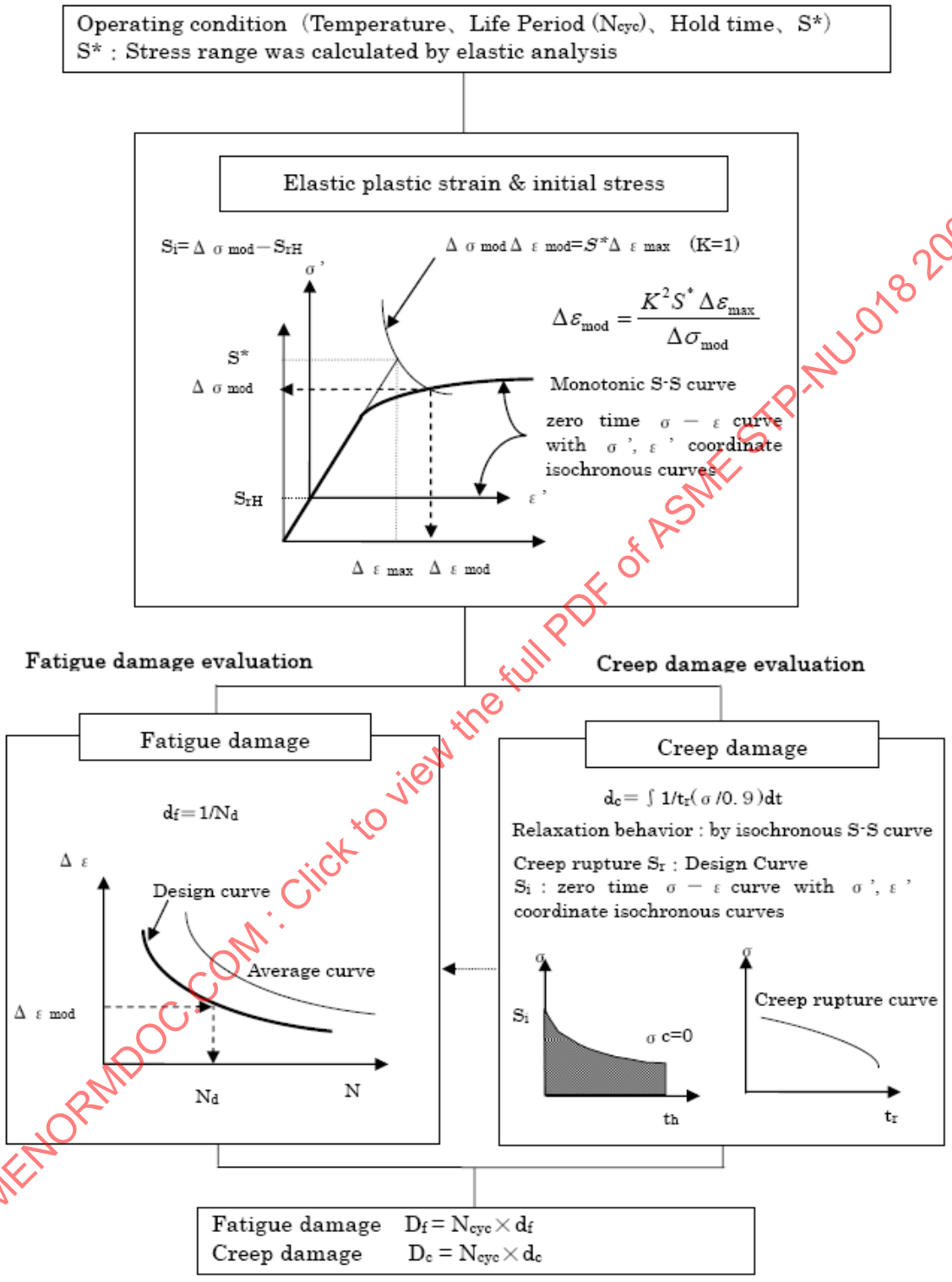




**Figure 61 - Evaluation Flow of Creep-Fatigue Damage by ASME-NH Method**

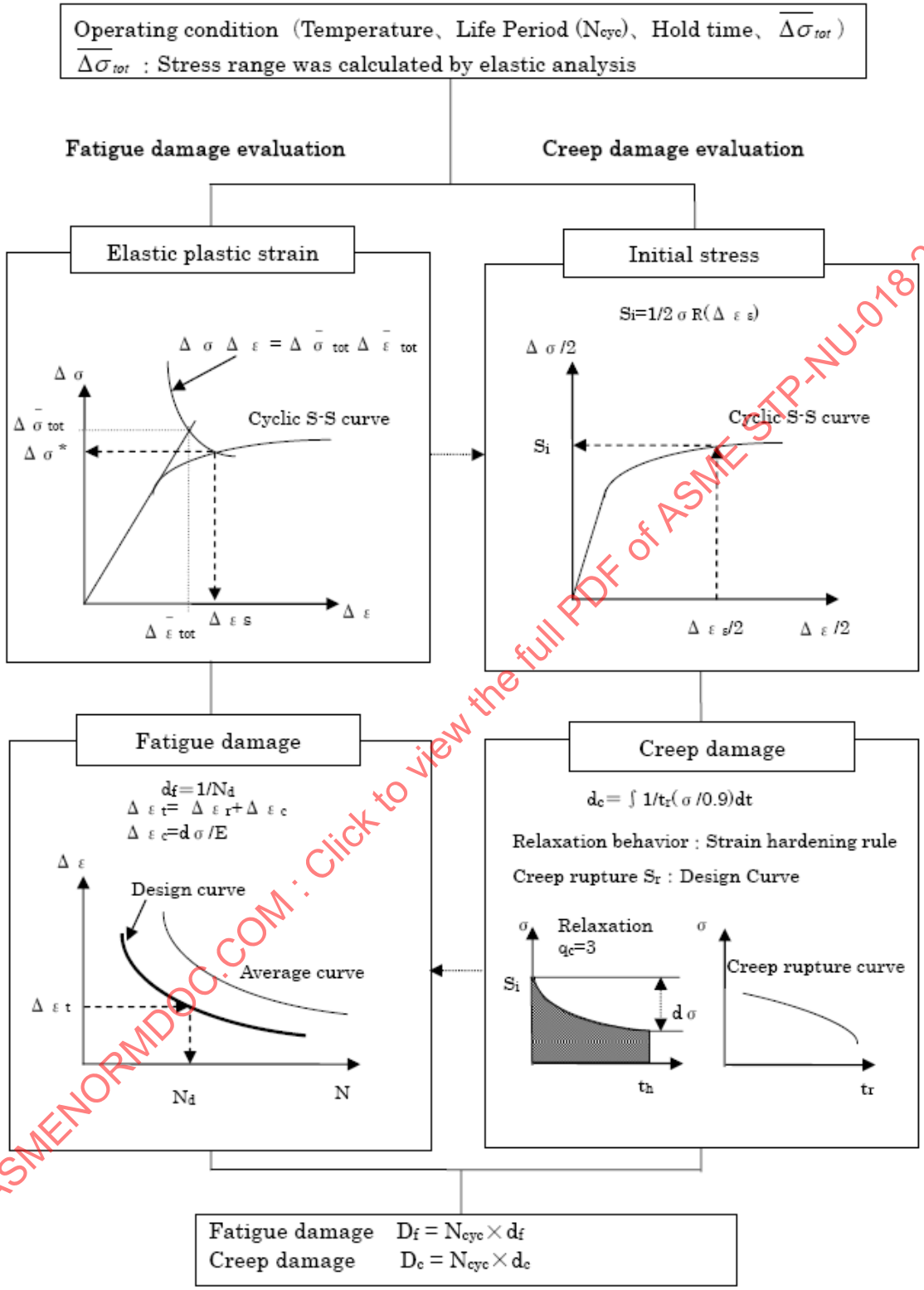




**Figure 62 - Evaluation Flow of Creep-Fatigue Damage by DDS Method**

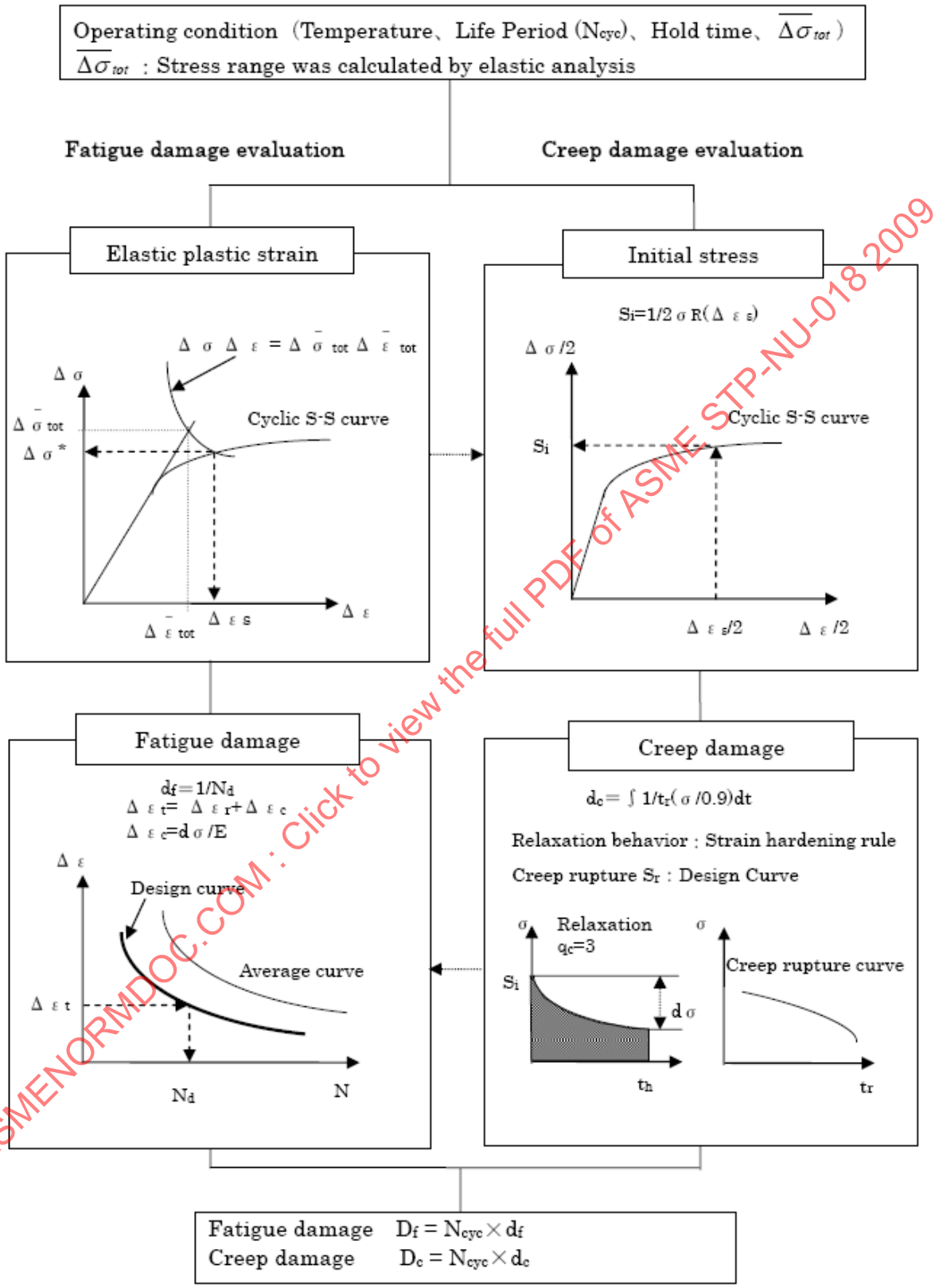




**Figure 63 - Evaluation Flow of Creep-Fatigue Damage by RCC-MR Method**

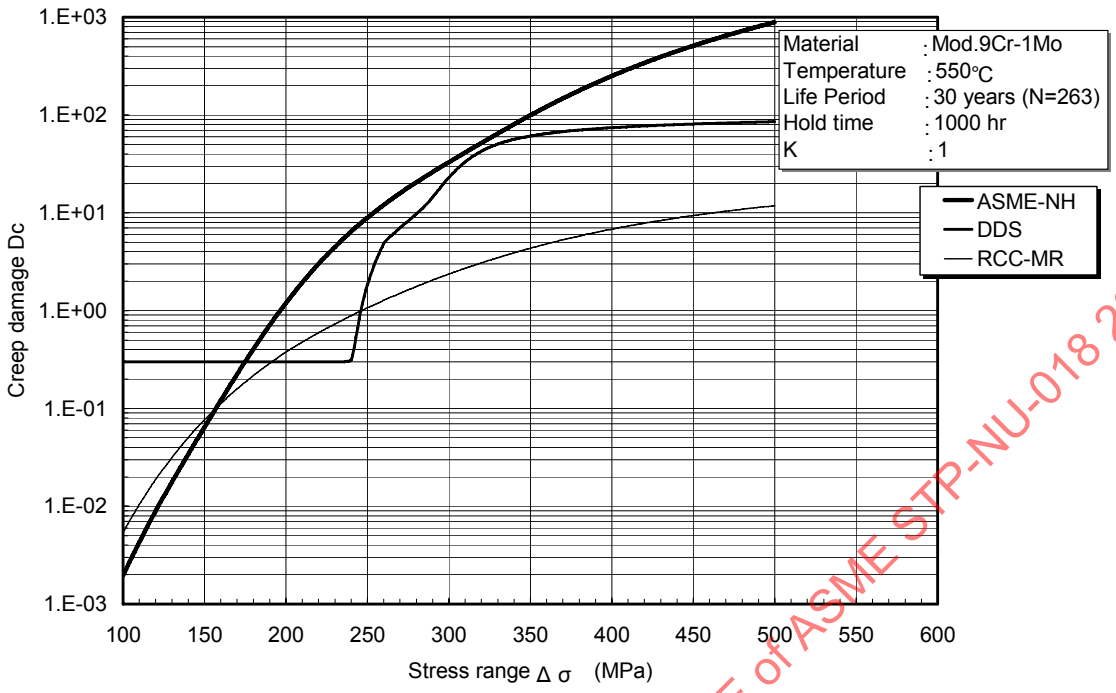


**Figure 64 - Comparison of Creep Damage Evaluation**

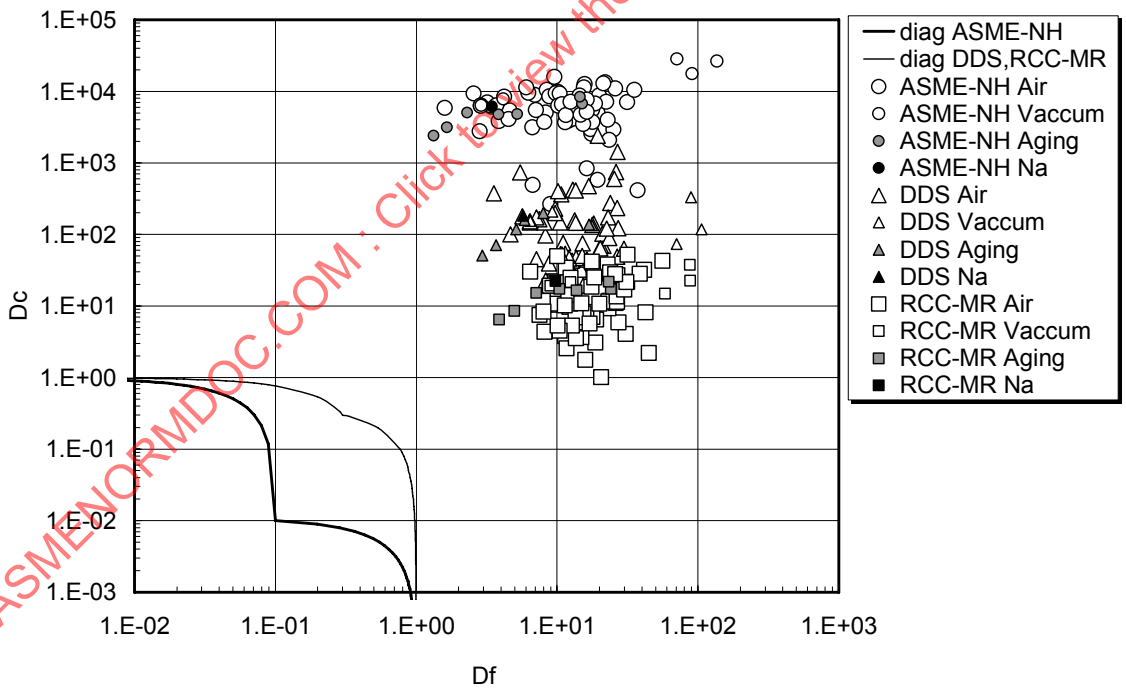


**Figure 65 - Creep-Fatigue Evaluation of Experimental Data by Code Procedure**

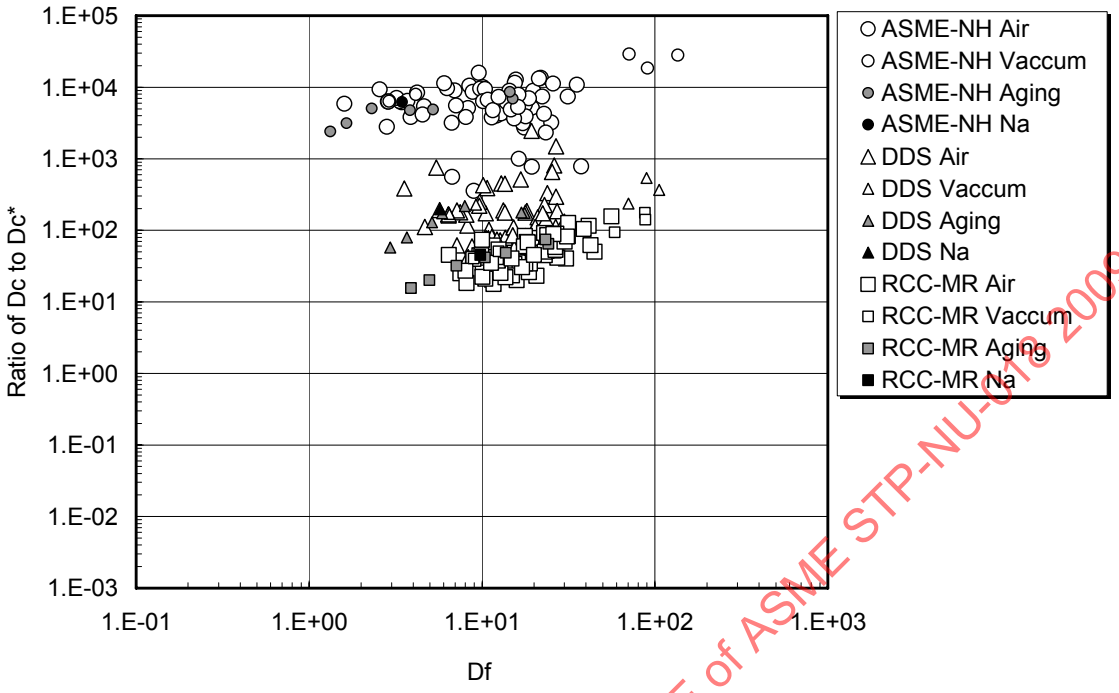


**Figure 66 - Creep-Fatigue Evaluation of Experimental Data by Code Procedure**

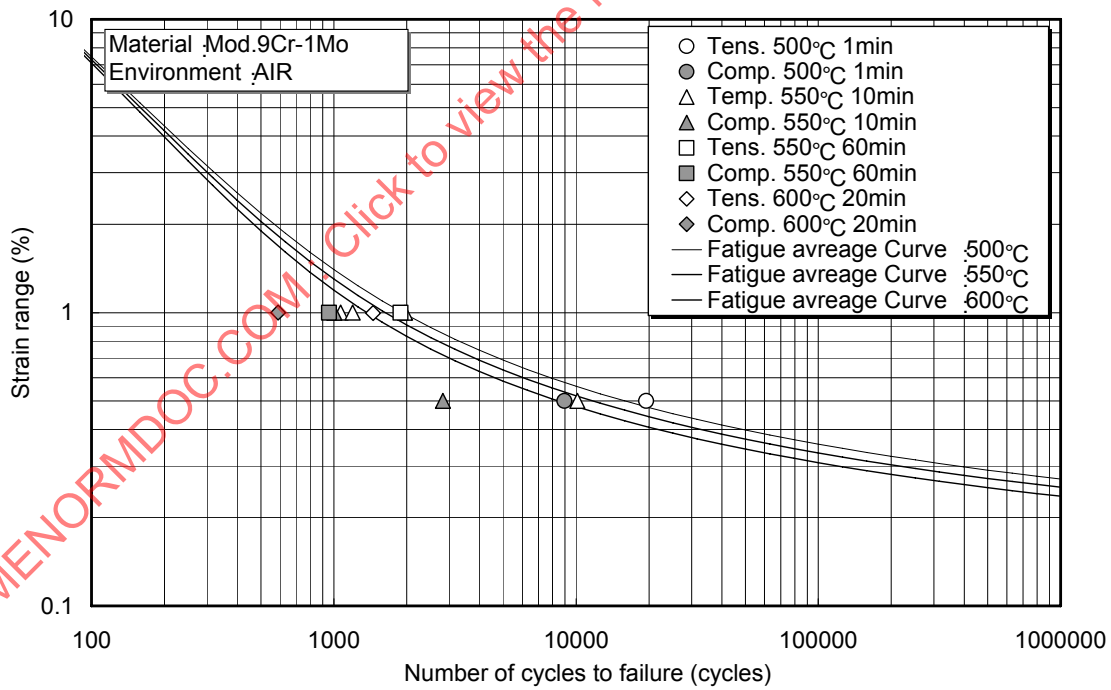


**Figure 67 - Comparison of Creep-Fatigue Life between Tensile Hold Tests and Compressive Hold Tests in Air**

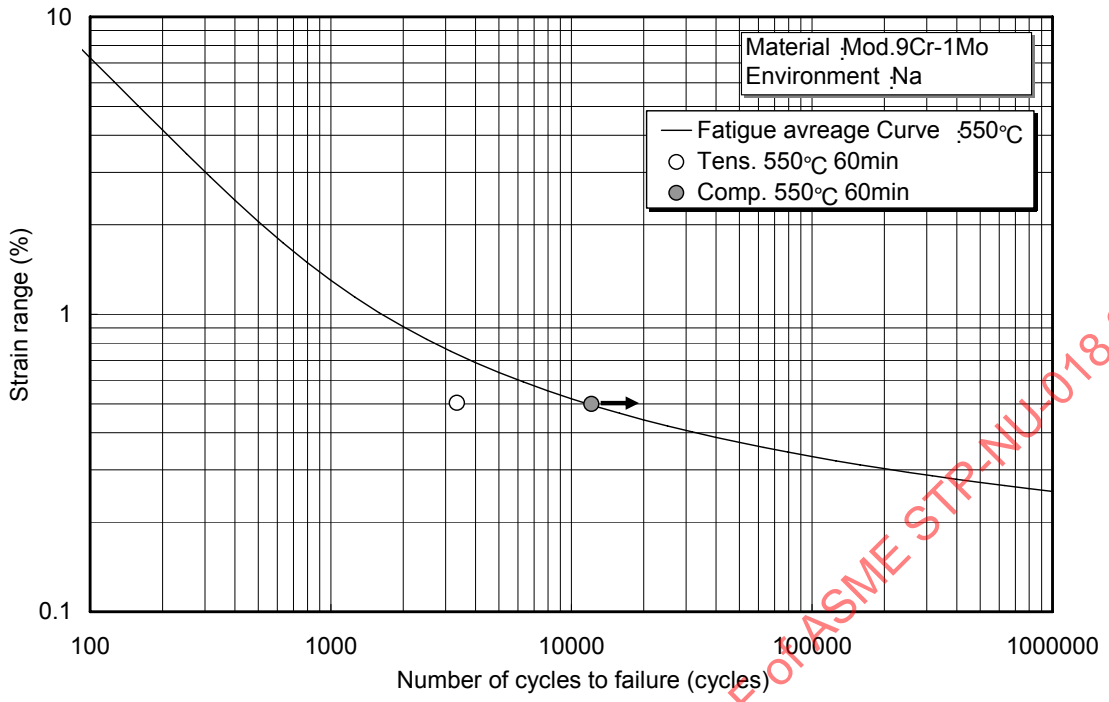


**Figure 68 - Comparison of Creep-Fatigue Life between Tensile Hold Tests and Compressive Hold Tests in Sodium**

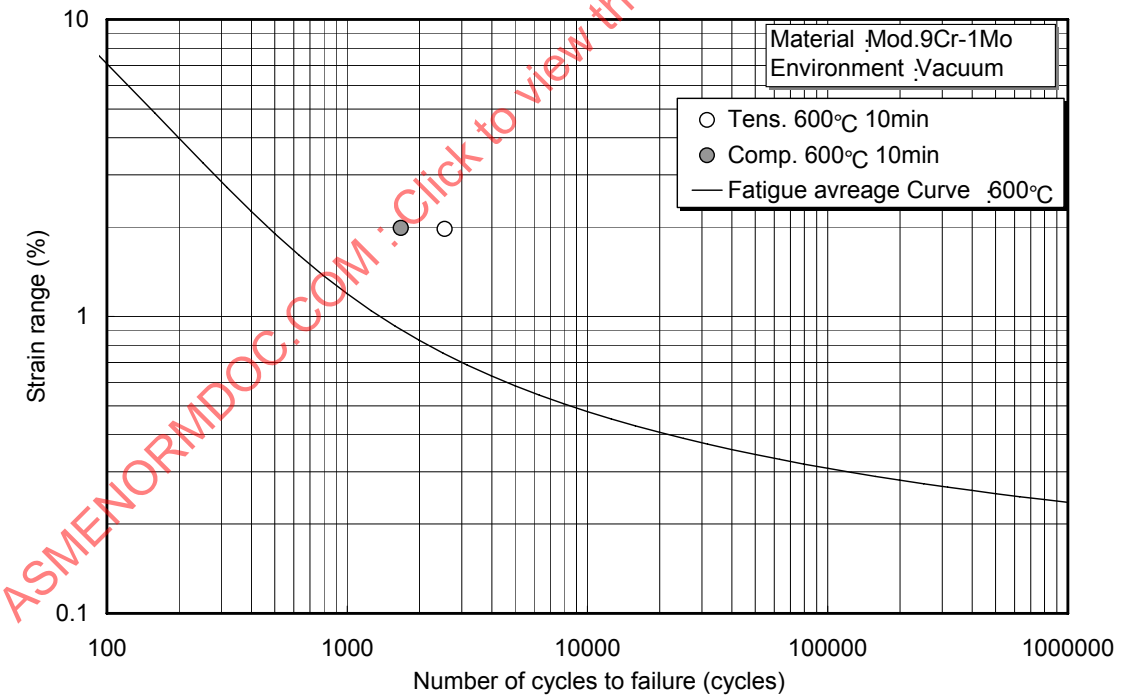


**Figure 69 - Comparison of Creep-Fatigue Life between Tensile Hold Tests and Compressive Hold Tests in Vacuum**

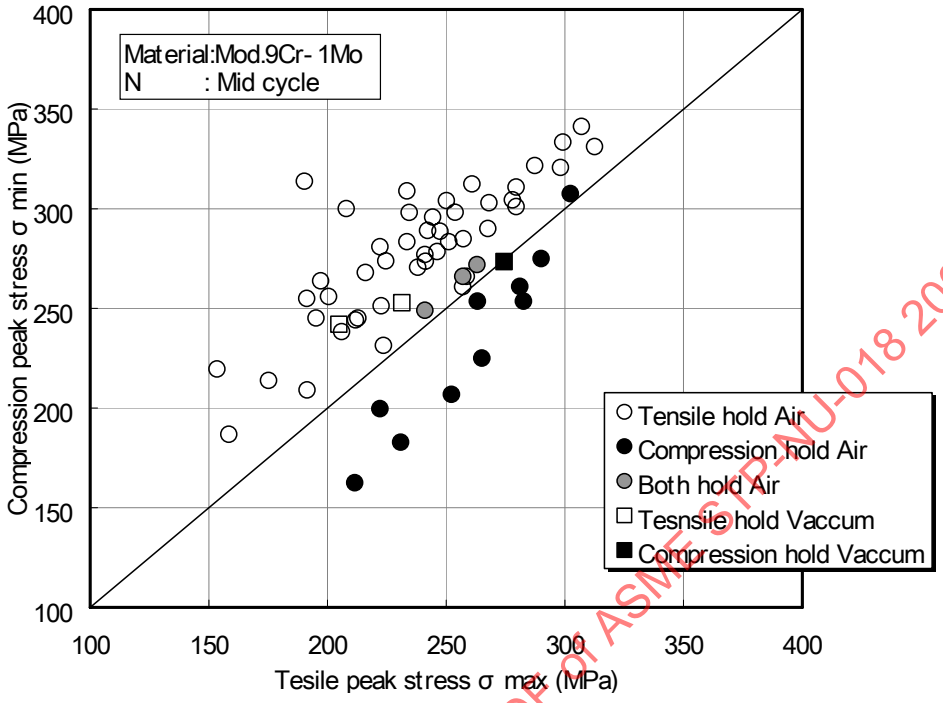


**Figure 70 - Comparison of Tensile and Compressive Peak Stresses**

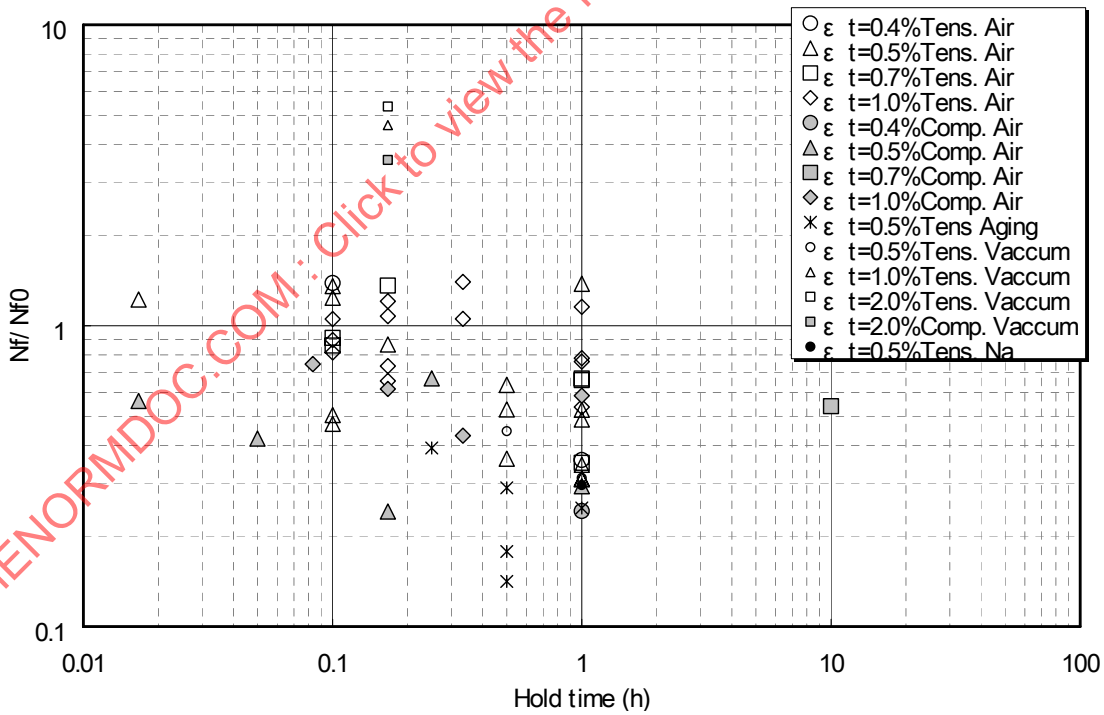


**Figure 71 - Ratio of Creep-Fatigue Life Reduction**

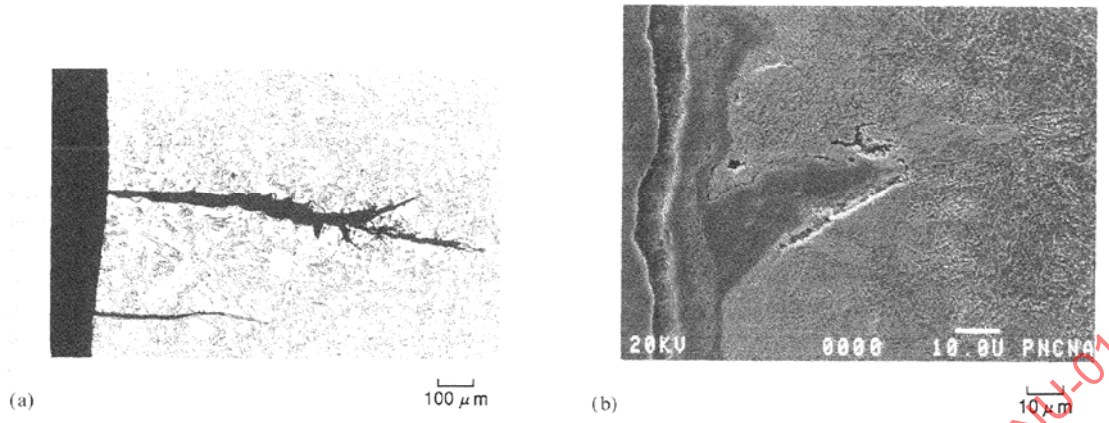


**Figure 72 - Observed Crack Tip Shape**

**(a) Crack Tip Shape Observed in a Compressive Hold Specimen**

**(b) Crack Tip Shape Observed in a Tensile Hold Specimen**

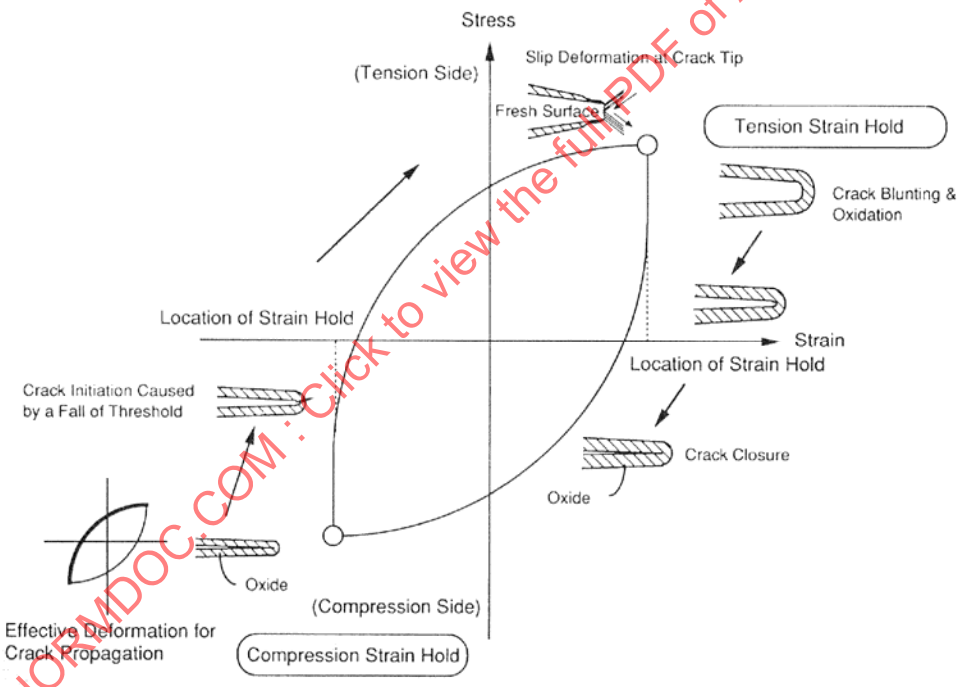


**Figure 73 - Schematic Illustration of Mechanisms that Affect Crack Propagation**

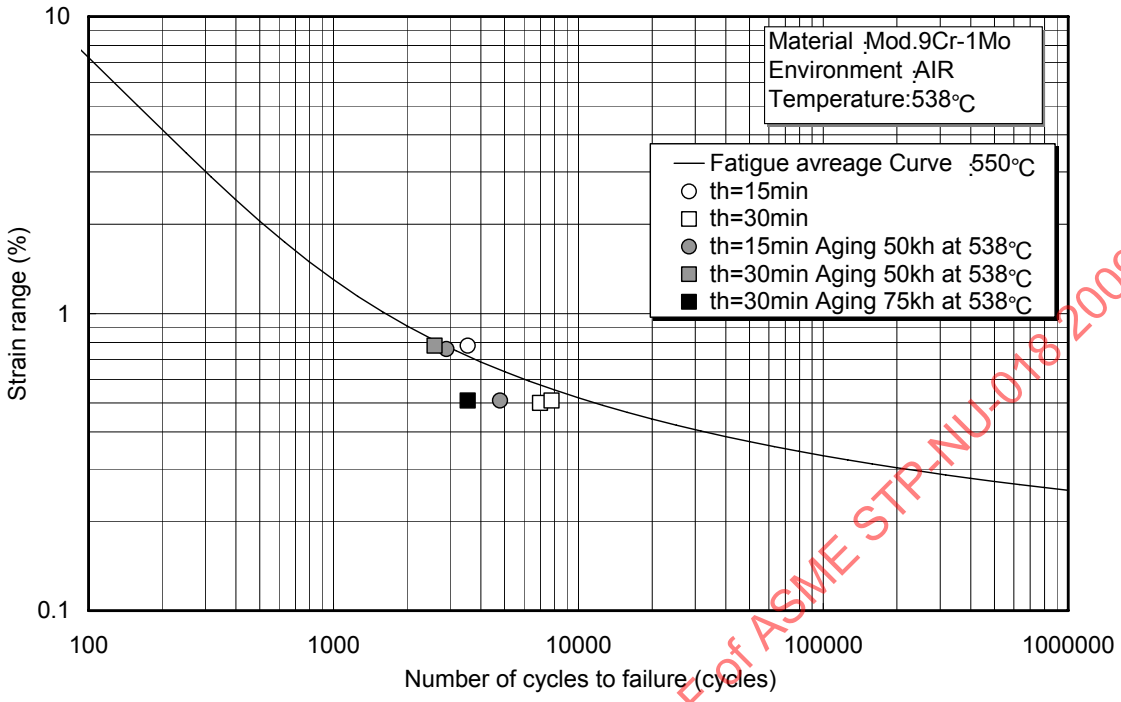


**Figure 74 - Comparison of Creep-Fatigue Life between Pre-Aged Material and Unaged Material at 550˚C**

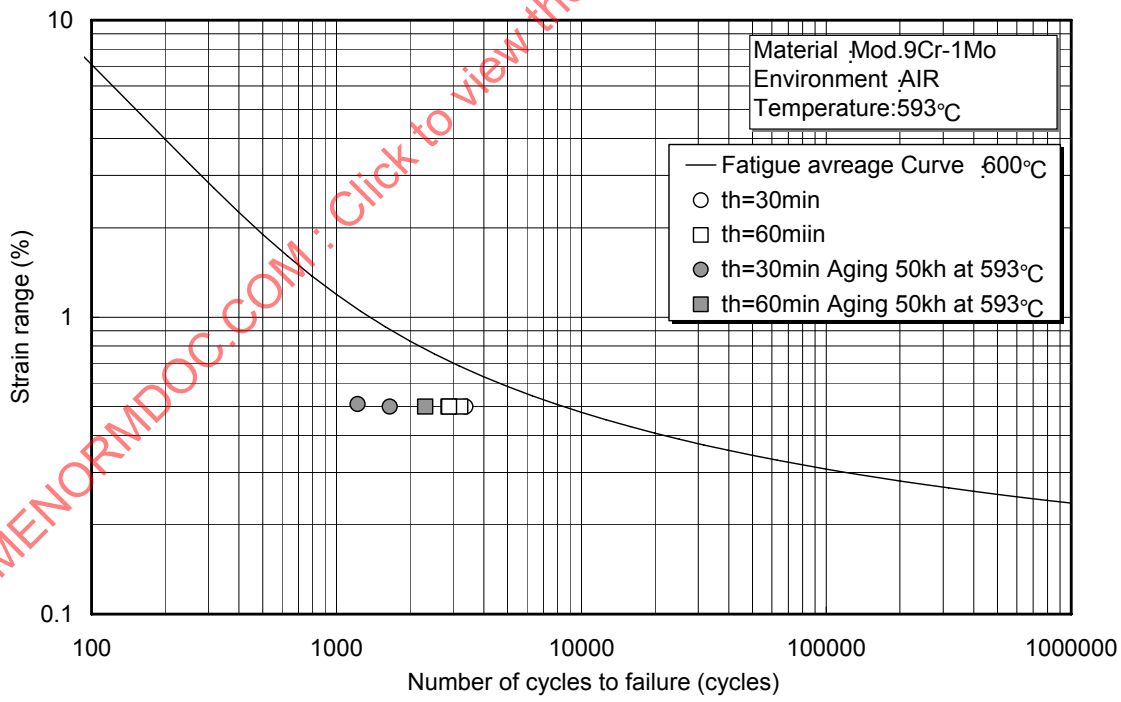


**Figure 75 - Comparison of Creep-Fatigue Life between Pre-Aged Material and Unaged Material at 600˚C**

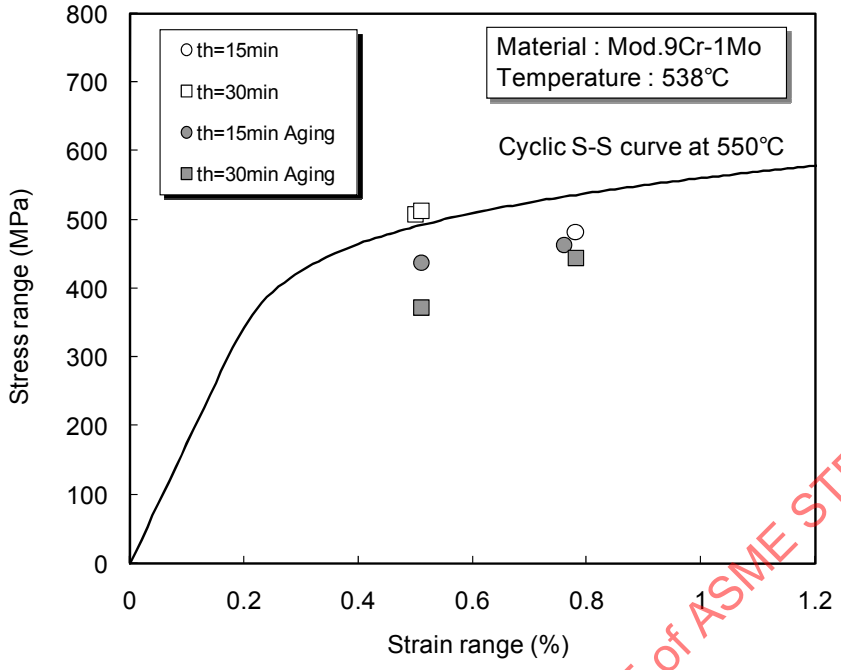


**Figure 76 - Comparison of Stress-Strain Response between Pre-Aged Material and Unaged Material at 550˚C**

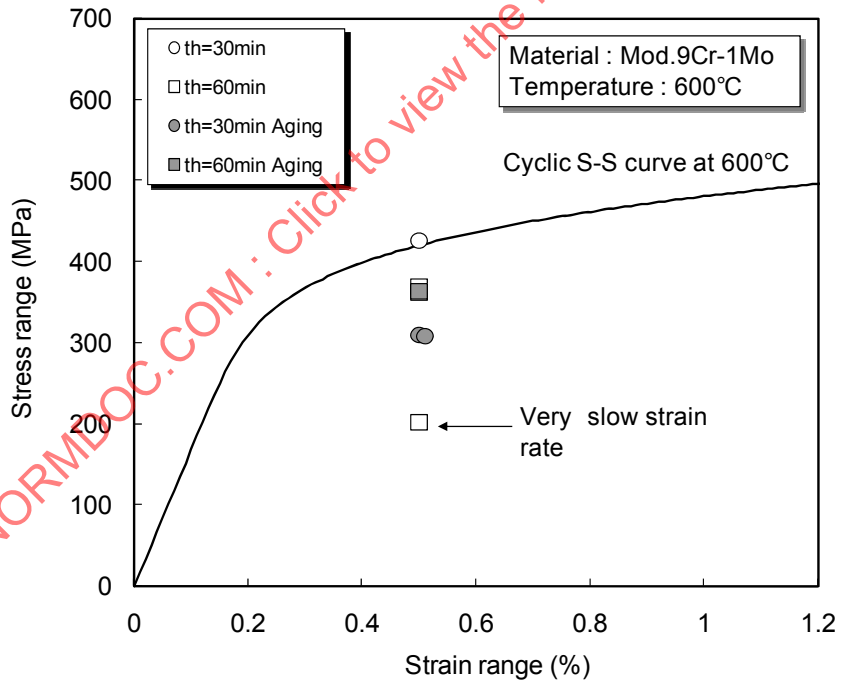


**Figure 77 - Comparison of Stress-Strain Response between Pre-Aged Material and Unaged Material at 600˚C**

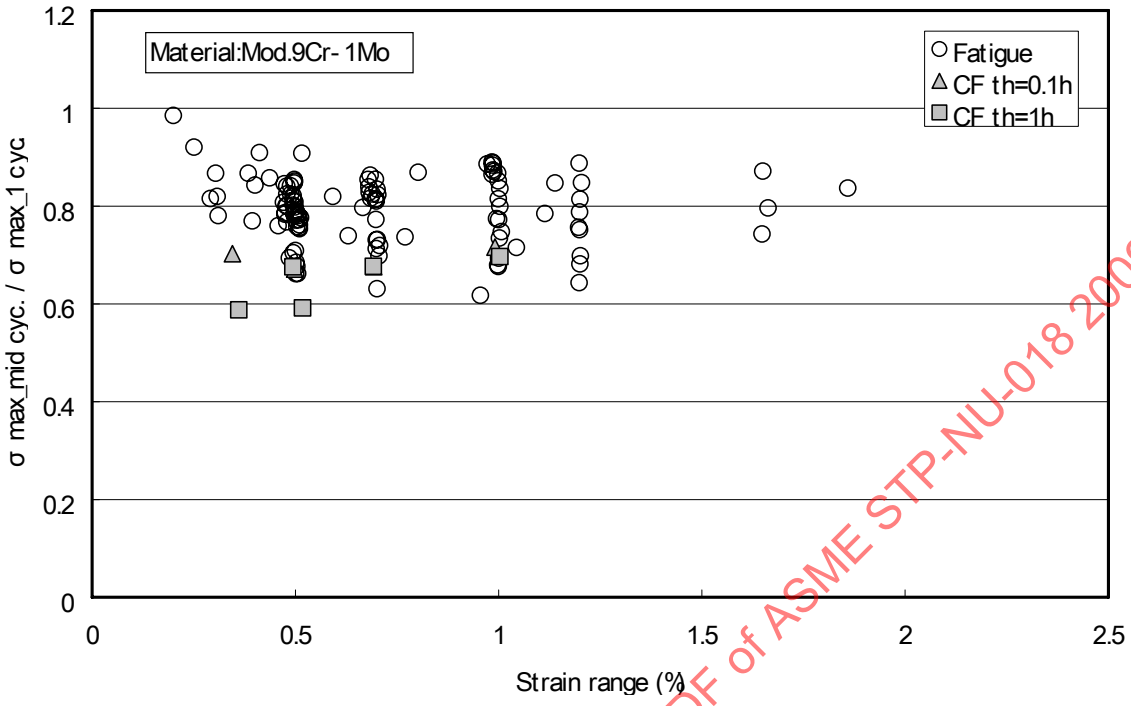


**Figure 78 - Ratio of Maximum Stress of Mid-Life to First Cycle**

# 3 SUGGESTIONS TO IMPROVE ASME-NH PROCEDURE AND R&D ITEMS

As pointed out in the previous sections, ASME-NH gives relatively conservative estimation of creep damage compared to other procedures. In this chapter, suggestions to improve the ASME-NH procedure are summarized and necessary research and development items are accordingly proposed.

## 3.1 Suggestions to Improve ASME-NH Procedure

In this section, suggestions to improve ASME-NH procedure are presented in two categories, i.e. items concerning the evaluation of creep damage and the evaluation of creep-fatigue life.

### 3.1.1 Evaluation of Creep Damage

In the previous section, reasons for the relatively large conservatism involved in the ASME-NH procedure were clarified. In this section, options to improve the procedure are suggested corresponding to the identified reasons of conservatism.

The suggested options for improvement of ASME-NH are summarized in Table 7. Their impacts on the evaluation of creep damage were investigated by calculating creep damage by five different methods corresponding to one of the options or a combination of options. The reference case corresponds to the current procedure and is the same as the calculation in Chapter 2.

In case (a), a modified strain amplitude, the modified strain range divided by two, is used instead of the modified strain range for the estimation of the initial stress of relaxation. In case (b), cyclic stress-strain curve is used instead of monotonic stress-strain curve. In case (c), a creep strain law and the strain hardening rule are used instead of the isochronous stress-strain curve for the estimation of stress relaxation behavior. Case (d) is the combination of cases (b) and (c). In case (e), the K' factor for this steel was changed from 0.67 to 0.9. The schematic illustration of calculation procedure is shown in Figure 79. The monotonic and cyclic stress-strain curves at 550˚C are shown in Figure 80 for information. Other conditions for calculation are the same as those used for the calculation of Figure 64.

The results of the evaluation are shown in Figure 81. In ASME-NH, lower bound stress is given by the core stress which is zero for Z=0. Therefore, to check the sensitivity of calculated creep damage to the lower bound stress, creep damage was calculated fictionally setting Z to 0, 0.3, 0.4, 0.5, as shown in Figure 82. It is understood form this figure that the effect of the value of Z on creep damage is small when elastically calculated stress is below 300 MPa approximately. Figure 83 shows the initial stresses estimated by various options. Case (a) shows a very large reduction in estimated creep damage due to the decrease of the initial stress of relaxation, particularly in lower stress ranges. This is because reduction of strain range is directly reflected to the reduction of the initial stress at regions close to an elastic region. Case (b) does not reduce the conservatism as far as isochronous curves are used, because although the initial stress is reduced by substituting monotonic stress-strain curves by cyclic stress-strain curves, the amount of stress relaxation estimated by the isochronous curves is reduced, due to the increased strain range, as shown in Figure 84 and Figure 85. The other three cases show some reduction in estimated creep damage, maintaining approximately the same degree of conservatism as RCC-MR or DDS. Corresponding results of creep-fatigue damage calculation of the experimental results are shown in Figure 86 to Figure 90.

From the above results, use of cyclic stress-strain curve, use of creep-strain law in conjunction with the strain hardening law, or the combination of both is recommended options for the improvement of the ASME-NH procedure. Which combination to choose depends on the conservatism necessary in the design of VHTR. If the material is to be applied to conditions under which sufficient data are not available, fairly large conservatism should be maintained.

### 3.1.2 Evaluation of Creep-Fatigue Life Based on Creep-Damage

As described in the previous chapter, the creep-fatigue damage envelope adopted in the ASME-NH procedure has a lot of conservatism. A damage envelope with an intersection point of (0.3, 0.3) can be adopted instead of (0.1, 0.01), as far as the experimental results analyzed in this investigation are concerned. It is to be kept in mind that the value of intersection point can only be determined by engineering judgment and theoretical derivation is most difficult. In other words, for employing different intersections for different materials, mechanistic explanation that only emerges from capturing the nature of each material is necessary, but it is normally difficult to prepare such basis.

## 3.2 Necessary R&D Items

In this section, R&D items that are necessary to improve the ASME-NH procedure to apply to VHTR conditions are summarized. They are categorized into short-term items and long-term items.

### 3.2.1 Short-Term Items

#### 3.2.1.1 Acquisition of Material Data

Creep-fatigue data of Grade 91 have been accumulated to the extent that design procedures for fast breeder reactors can be established. However, to apply this material to VHTR, more data at the temperature range expected in VHTR will be necessary. At temperatures higher than those encountered in fast breeder reactors, creep-fatigue life should naturally decrease. Therefore, the behavior of material should be captured more precisely to make the degree of conservatism optimum to ensure flexibility in design components and systems.

As described in the previous chapters, there are many factors that can affect the creep-fatigue life of Mod.9Cr-1Mo steel. Creep damage, tensile mean stress, oxidation, aging and loading sequence effects (creep rupture strength after cyclic softening) are among these factors. The effects of oxidation, aging and cyclic softening are not problematic in the case of austenitic steels but must be carefully addressed in the case of ferritic steels such as Grade 91.

It is not very practical to take every factor that can affect creep-fatigue life explicitly in a code procedure. Therefore, material tests should be performed systematically to identify relative importance of those factors. Very long term tests will not be necessary, tests to identify the limit where the effects of each factor saturates will be enough (For example, perform tensile hold tests and compressive hold tests until creep-fatigue life of tensile hold tests becomes shorter than that of compressive hold tests).

#### 3.2.1.2 Identification of Issues to be Addressed

Based on the material tests described above, decisions should be made as to how these effects, if they exist, should be incorporated into the creep-fatigue evaluation procedures. It would not be practical to introduce new factors into the code procedure. If additional phenomena that can reduce creep-fatigue life were identified, these should be accounted for in the conservatism in estimating either the initial stress or stress relaxation. It would be helpful to make a list of the phenomena of concern and the corresponding way to ensure conservatism (creep-fatigue life reduction due to aging is covered by which factor in the procedure, for example). In this case, attention should be paid to the possibility that relative importance may change in short-term region and long-term region in which we are interested.

### 3.2.2 Long-Term Items

#### 3.2.2.1 Long-Term Material Tests

In this perspective, more creep-fatigue data with longer hold times (10 hours, for example) either with a tensile hold time or a compressive hold time are desirable at strain ranges not larger than 0.5% to confirm the results obtained so far about the mechanisms of life reduction of creep-fatigue life reduction, i.e., the effects of creep, tensile mean stress and oxidation.

Recommended test conditions for VHTR design are shown in Table 8 and Table 9. The conditions in these tables are limited up to 600˚C because the design conditions of VHTR are not clear.

#### 3.2.2.2 Evaluation Method of Welded Joints

Another point which is very important in applying Grade 91 steel to VHTR is the treatment of welded joint. For fast breeder reactors, a mechanistic model has been developed and incorporated in the DDS procedure (Asada et. al., 1992, Asayama et. al., 1993, Taguchi et. al., 1996). The procedure in DDS accounts for the fatigue strength of weld metal, the increase of initial stress of relaxation due to harder stress-strain response of weld metal, and the increase of elastic follow-up as well.

At temperatures above 600˚C, Type IV cracking has been reported to occur. Tests should be performed at and above temperatures to which components of VHTR will be subjected. Therefore, a creep-fatigue evaluation method that can take into account Type IV cracking is also necessary.

#### 3.2.2.3 Extrapolating Experimental Data to the Design Regime

In design, extrapolating high stress/strain and relatively short hold time experimental data to the significantly lower stress and longer hold time design regime is inevitable primarily because of limitation of time, and this can be a problem particularly in evaluating margins we have in our design codes and procedures. Much research has been performed on this subject but no satisfactory definitive methods that can be applied to design evaluation have been proposed. A simple question whether or not saturation of creep-fatigue life reduction due to hold time occurs has yet to be answered. Therefore, full resolution of this problem would hardly be envisioned in the short or long terms.

However, there has been progress and important findings are beginning to be reported from recent researches in terms of mechanisms of deformation and failure of which understanding is a key to solve the issue. One approach is to use these results. For example, Kimura et. al. reported that “region splitting method” can be applied to predict long-term creep rupture strength of Grade 91. This method divides stress range by one half of yield strength at corresponding temperature and it correlates stress and rupture time in each region, with better accuracy compared to the case where one curve is applied to the whole region. This method is simple enough to be used in establishing material strength standards.

Another approach is to focus our attention precisely to the design regime. Grade 91 steels have relatively high yield strength and the magnitude of work hardening and ductility are less than austenitic stainless steels. Therefore it is anticipated that the materials will be used within the elastic region. This implies that cyclic softening may be small and we would be able to concentrate on softening that comes from hold time (and aging). This may lead to a finding that the possibility of degradation of creep properties due to cyclic softening can be ignored (no evidence at this point). From this viewpoint, tests focusing on material behavior rather than material strength could be prioritized because this type of tests can save significant time. The results of these tests would produce valuable information to determine the conditions of material strength tests that give maximum output with minimum resources.

### 3.2.2.4 Structural Tests for Validation

In establishing design code based on the information obtained from material tests, structural tests are indispensable for validation. The first step of structural tests will be a simple pipe subjected to cyclic thermal loading, for example. The next step will be tests with structural models that have more complex configurations that reproduce the essential features of VHTR components. If the components in VHTR may be thick, structural tests with thick structural test pieces are desirable, considering the possibility of Type IV cracking.

**Table 7 - Suggested Options for the Improvement of Creep-Fatigue Evaluation Procedure in ASME-NH**

| Case | Contents | S-S curve | Strain type | Description of relaxation | Note |
|---|---|---|---|---|---|
| Reference | Current procedure with k=1, $K_s$=1<br>Ratchet is not considered. | Monotonic | $\Delta\varepsilon_{mod}$ | Isochronous | |
| (a) | Initial stress is calculated based on half of the modified strain range | Monotonic | $\Delta\varepsilon_{mod}/2$ | Isochronous | |
| (b) | Cyclic stress-strain curve is used. | Cyclic | $\Delta\varepsilon_{mod}$ | Isochronous | |
| (c) | Strain hardening rule is used. | Monotonic | $\Delta\varepsilon_{mod}$ | Strain hardening rule | $q_c$=1 |
| (d) | Cyclic stress-strain curve is used.<br>Strain hardening rule is used. | Cyclic | $\Delta\varepsilon_{mod}$ | Strain hardening rule | $q_c$=1 |
| (e) | Stress factor on relaxation changed from 0.9 to 1.0. | Monotonic | $\Delta\varepsilon_{mod}$ | Isochronous | |

$q_c$: Elastic follow-up coefficient on relaxation behavior

**Table 8 - Recommended Creep Test Conditions**

| Temperature (˚C) | Stress (MPa) | Estimated time |
|---|---|---|
| 550 | 150 | 100,000 h |
| 600 | 100 | 50,000 h |

**Table 9 - Recommended Creep-Fatigue Test Conditions**

| $\Delta\varepsilon_t$ (%) | 500˚C | | 550˚C | | 600˚C | |
|---|---|---|---|---|---|---|
| | Hold time (h) | | Hold time (h) | | Hold time (h) | |
| | 1 | 10 | 1 | 10 | 1 | 10 |
| under 0.5 | ○ | ○ | ● | ☆ (18,000 at Δε=0.35%) | ☆(1,700 at Δε=0.35%) | ☆(11,000 at Δε=0.35%) |
| 0.5 ~ 1.0 | ● | ○ | ● | ●(compression)<br>☆(6,000 atΔε=0.7%) | ● | ☆(5,000 atΔε=0.7%) |
| 1.0 over | ● | ○ | ● | ○ | ● | ○ |

- ● Completion
- ○ Incompleteness
- ☆ Recommended test condition
- ( ) Estimated time by DDS average

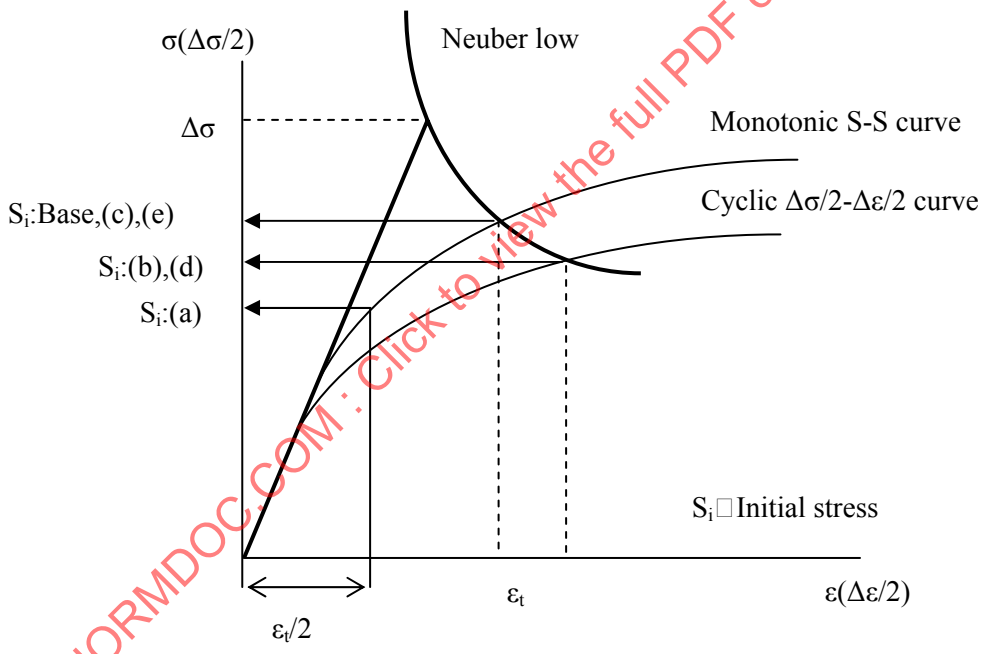


**Figure 79 - Calculation Procedure of Initial Stress Using Monotonic S-S Curve**

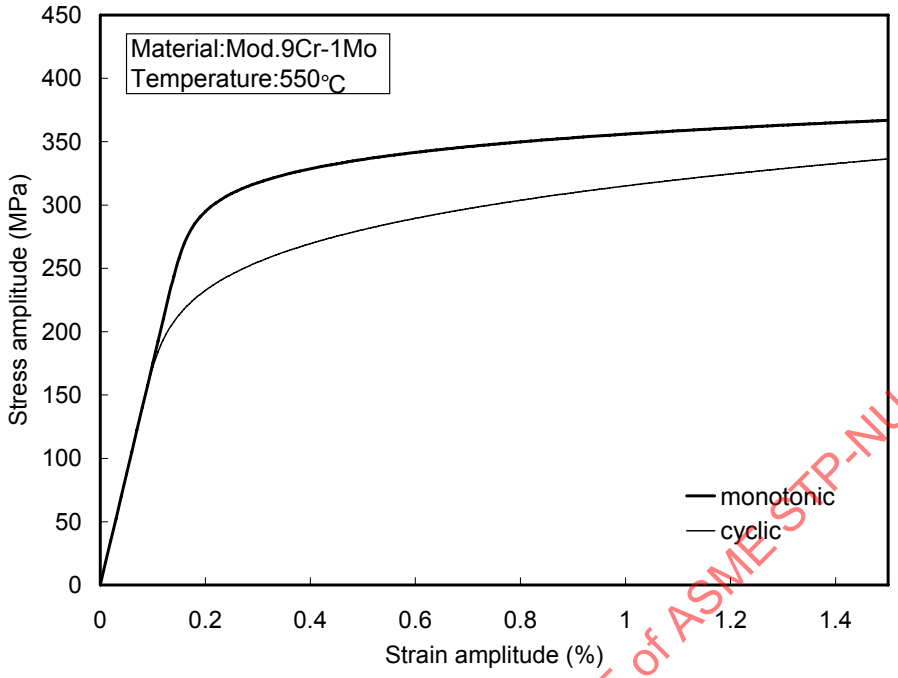


**Figure 80 - Monotonic and Cyclic Stress-Strain Relation at 550˚C**

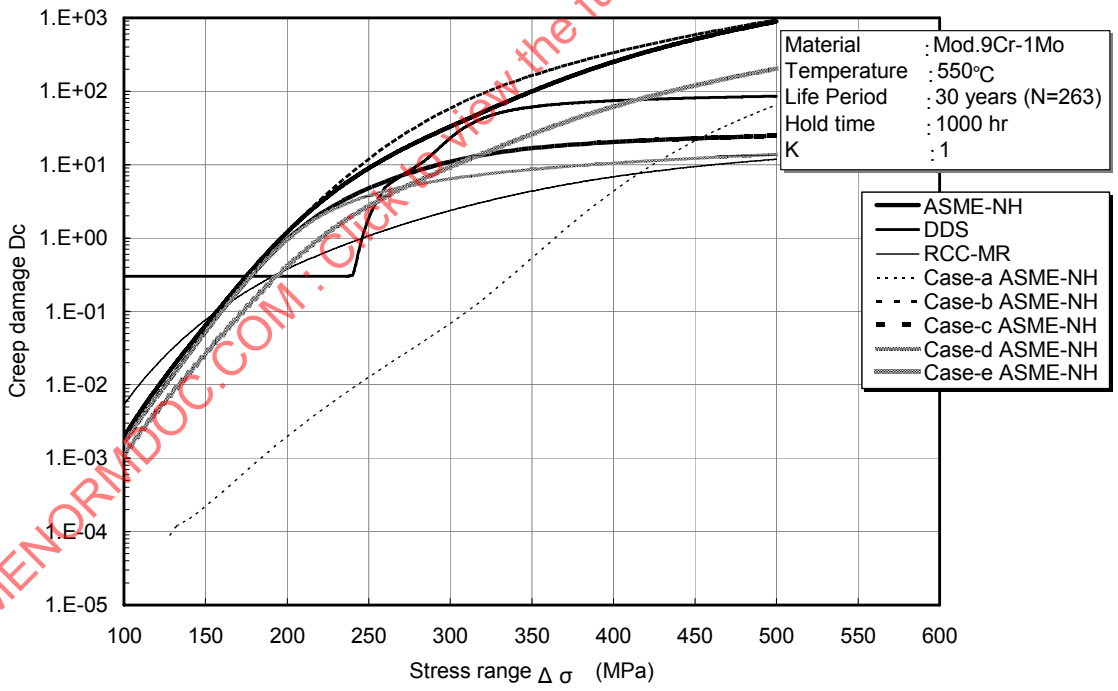


**Figure 81 - Creep Damage Calculated Based on Various Options**

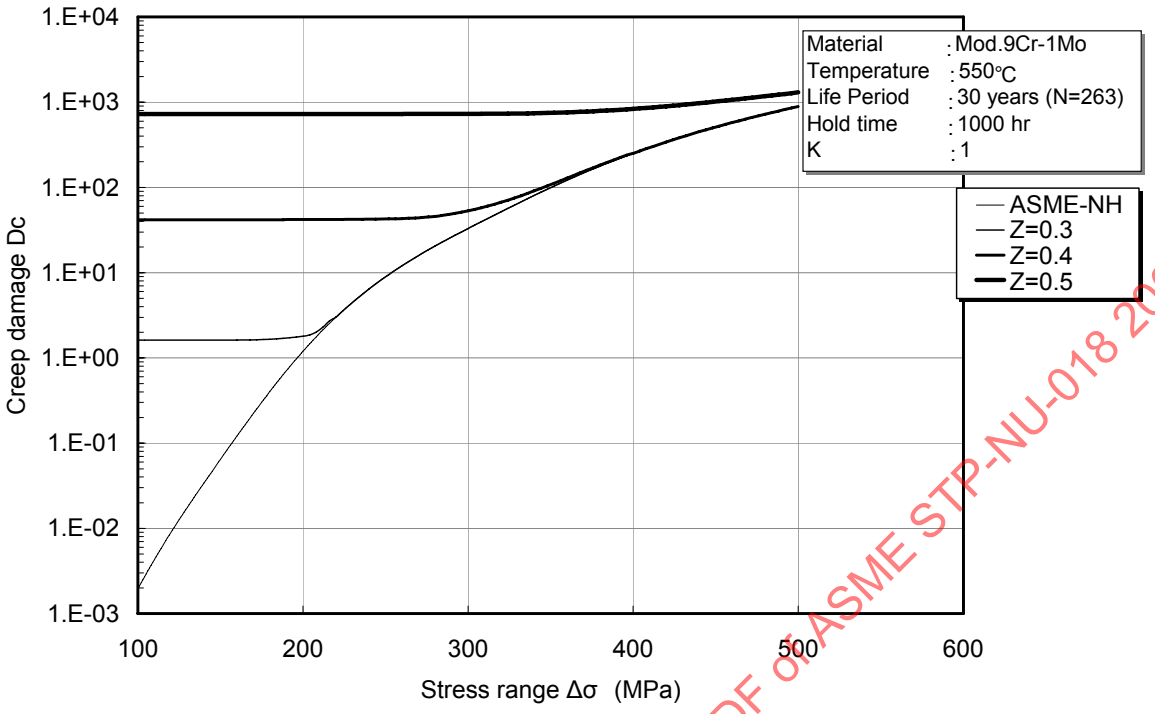


**Figure 82 - The Effect of the Value of Z on Creep Damage in ASME-NH**

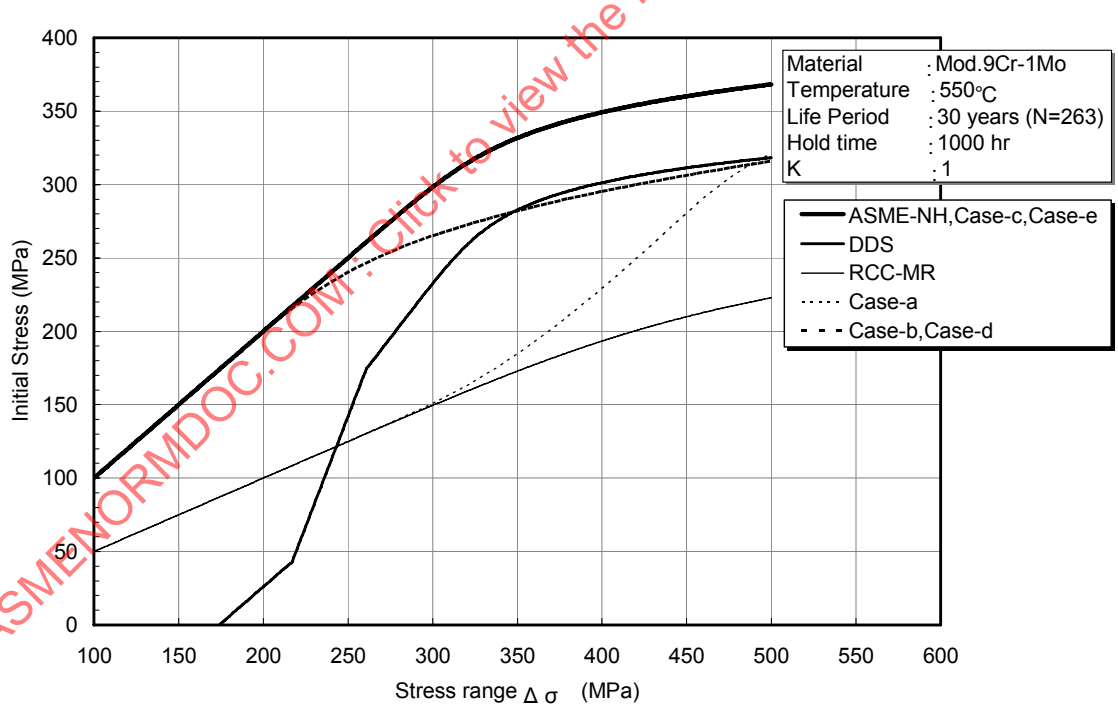


**Figure 83 - Comparison of Initial Stresses of Stress Relaxation**

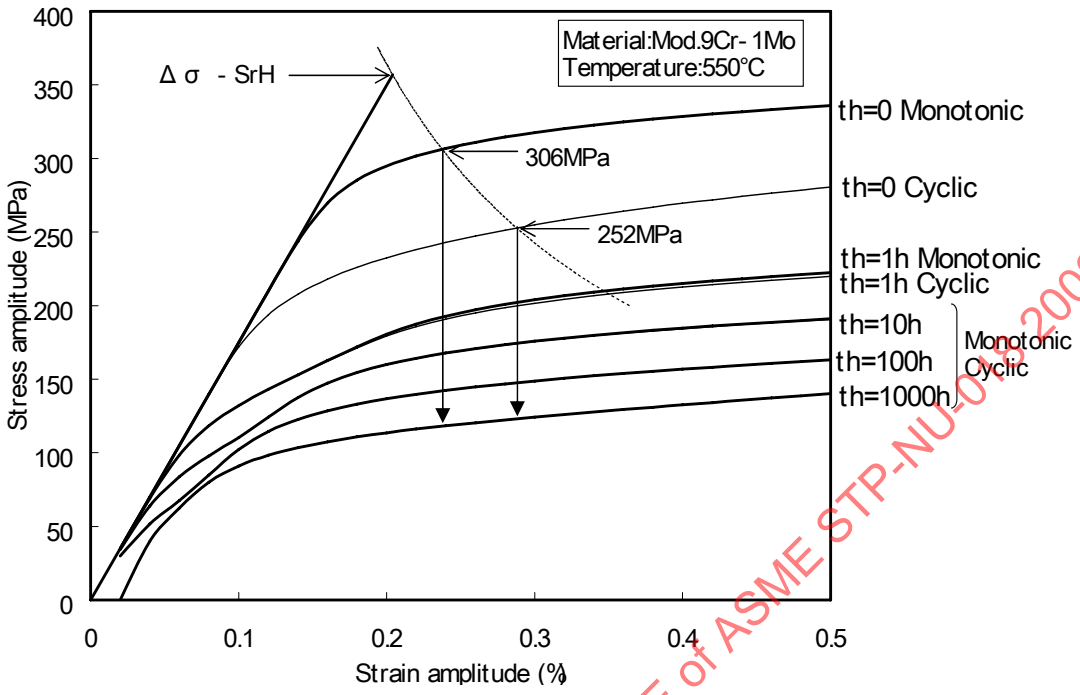


**Figure 84 - Monotonic and Cyclic Isochronous Curves at 550°C**

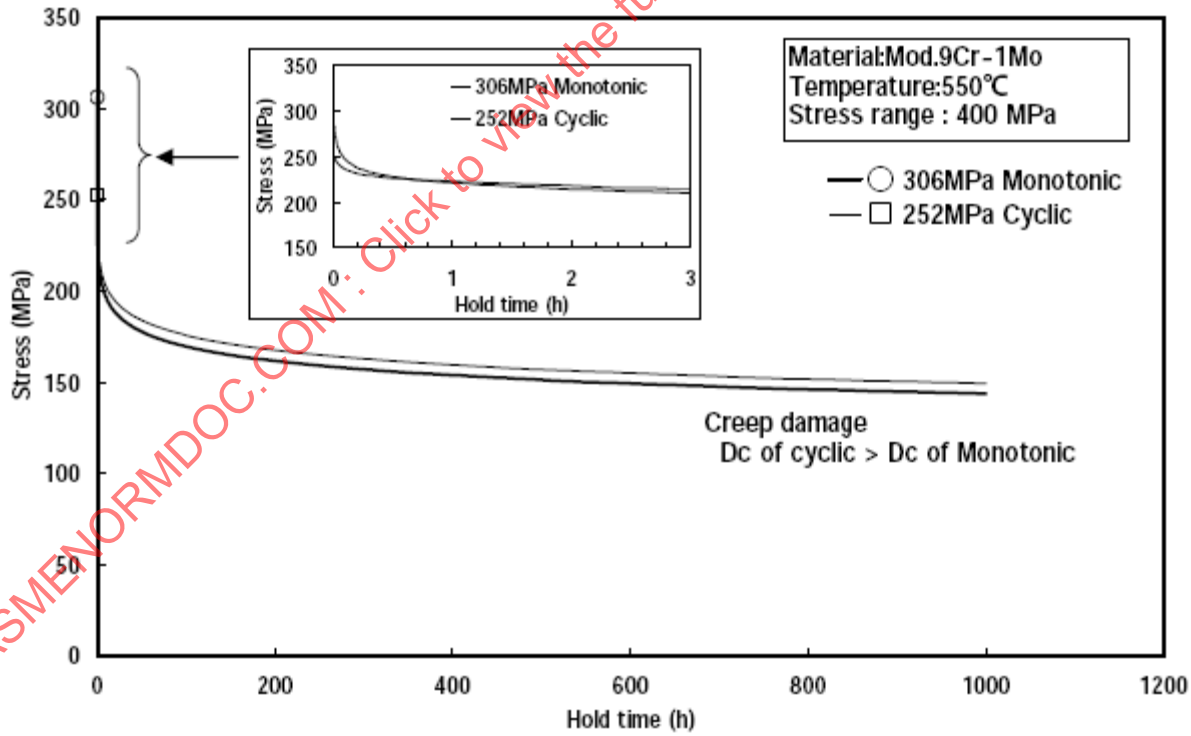


**Figure 85 - Comparison of Relaxation Behavior between Monotonic and Cyclic At 550°C**

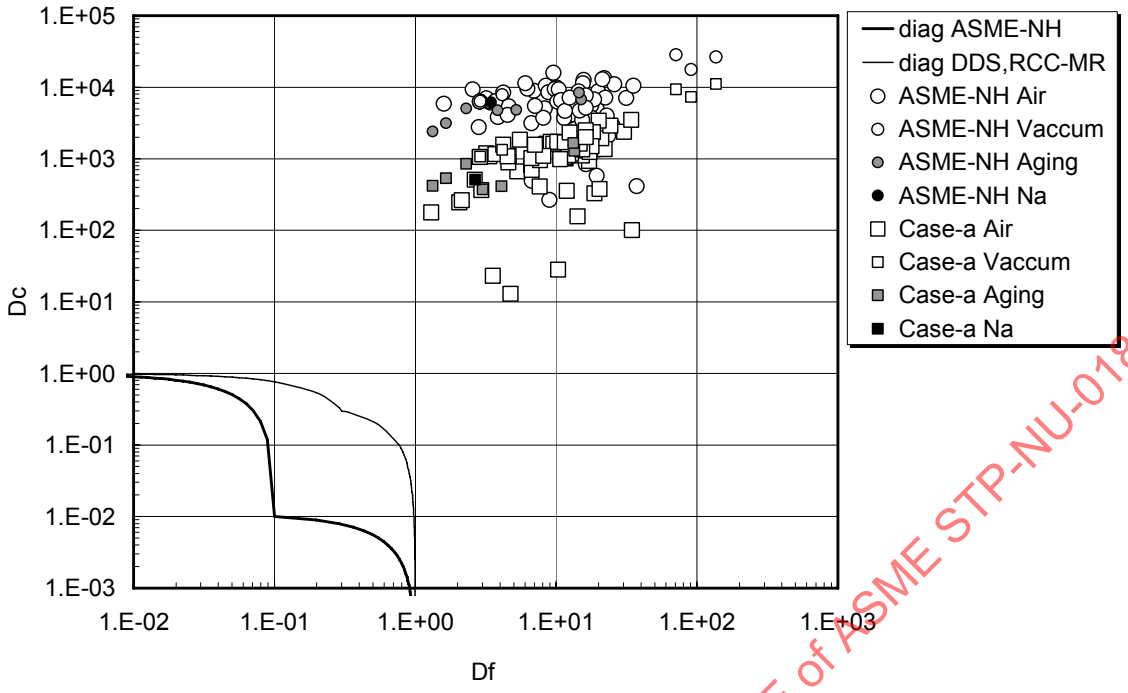


**Figure 86 - Creep-Fatigue Damage Calculated Based on Case (a)**

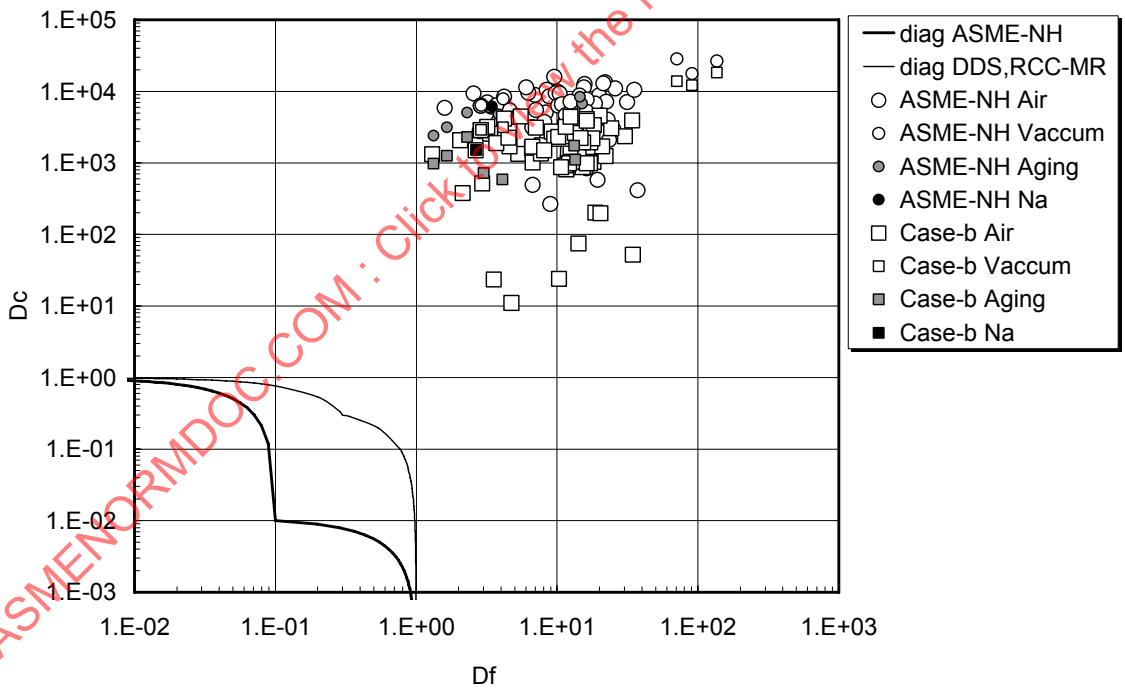


**Figure 87 - Creep-Fatigue Damage Calculated Based on Case (b)**

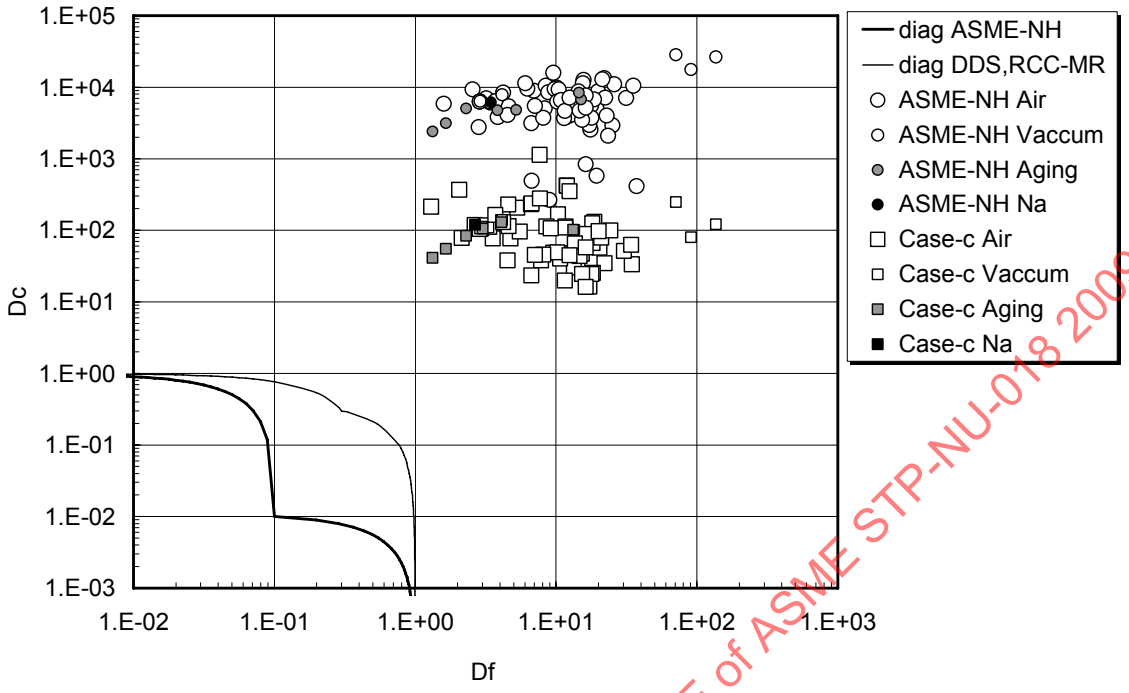


**Figure 88 - Creep-Fatigue Damage Calculated Based on Case (c)**

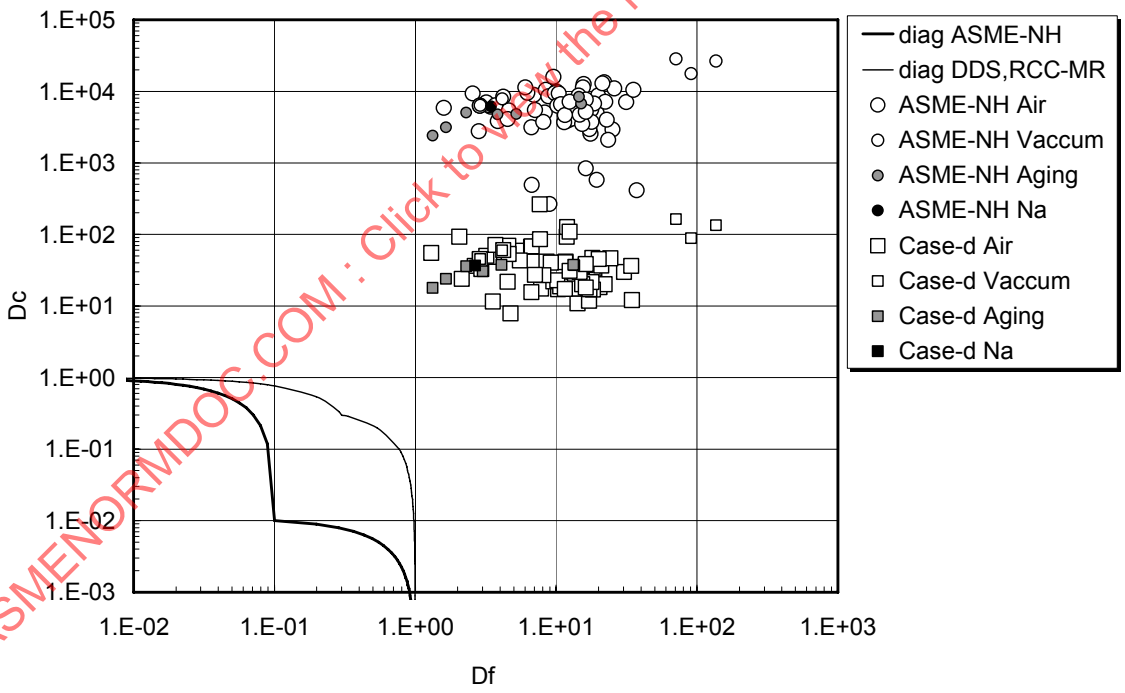


**Figure 89 - Creep-Fatigue Damage Calculated Based on Case (d)**

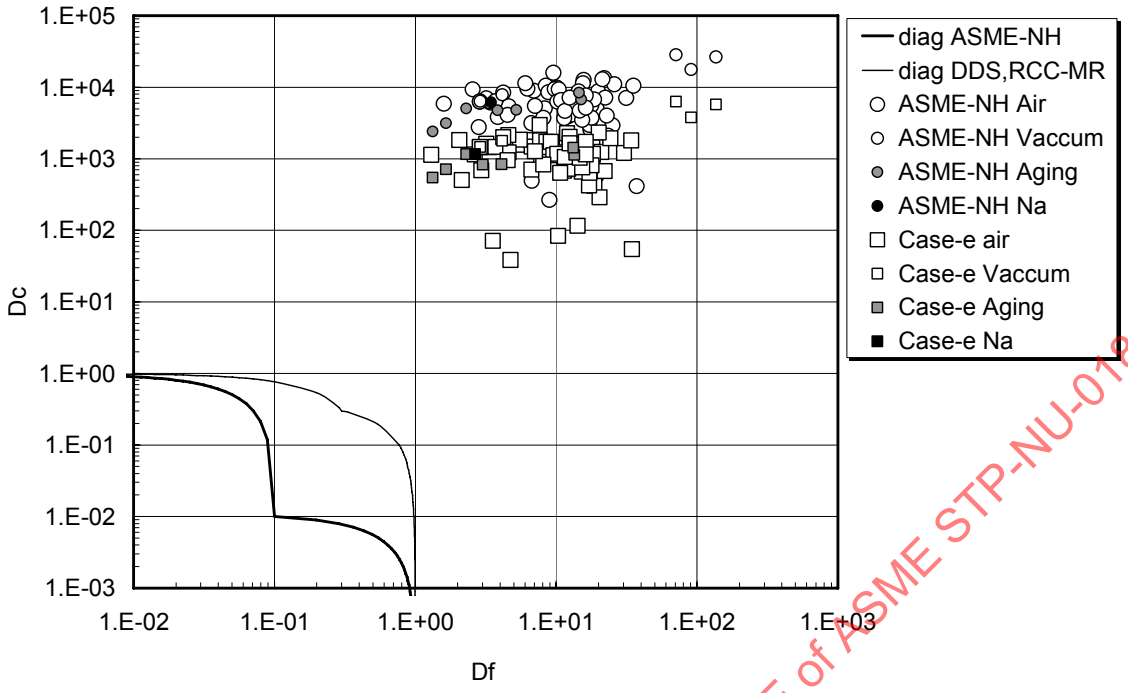


**Figure 90 - Creep-Fatigue Damage Calculated Based on Case (e)**

## REFERENCES


[1] ASME Boiler and Pressure Vessel Code, Division 1, Subsection NH, ASME, New York, 2004.

[2] Demonstration fast breeder reactor elevated temperature structural design guideline (DDS), Japan Atomic Power Co., (in Japanese), 1999.

[3] RCC-MR 2002, Design and Construction Rules for mechanical components of FBR nuclear islands and high temperature applications, AFCEN, 2002 Edition.

[4] K. Aoto, R. Komine, F. Ueno, H. Kawasaki and Y. Wada, Creep-Fatigue evaluation of normalized and tempered modified 9Cr1Mo, Nuclear Engineering and Design, Vol. 153, pp. 97-110, 1994.

[5] Y. Asada, K. Douzaki, M. Ueta, M. Ichimiya, K. Mori, M. Kitagawa, T. Nishida and T. Sukekawa, Research and Development on 9Cr-Steels for Steam Generator of DFBR in Japan (1) Fatigue properties, SMiRT11, Transactions Vol. L, L05/1, (1991a).

[6] Y. Asada, M. Ueta, M. Ichimiya, K. Douzaki, T. Nishida, T. Sakon, K. Mori and M. Sukekawa, Research and Development on 9Cr-Steels for Steam Generator of DFBR in Japan (2) Creep properties, SMiRT11, Transactions Vol. L, L05/1, (1991b).

[7] Y. Asada, M. Ueta, K. Douzaki, M. Sukekawa, K. Taguchi, and H. Koto, Creep, fatigue and creep-fatigue properties of modified 9Cr-1Mo steel and its weldments for steam generator of fast breeder reactor, PVP-Vol.230, p. 41, 1992.

[8] Y. Asada, K. Dozaki, M. Ueta, M. Ichimiya, K. Mori, K. Taguchi, M. Kitagawa, T. Nishida, T. Sakon and M. Sukekawa, Exploratory research on creep and fatigue properties of 9Cr-steels for the steam generator of an FBR, Nuclear Engineering and Design 139, p. 269, 1993.

[9] T. Asayama, S. Hasebe, K. Hirakawa and Y. Wada, Creep-fatigue evaluation method for Mod.9Cr-1Mo weldment, SMiRT12, Transactions Vol. L, L05/5, 1993.

[10] K. Taguchi, M. Ueta, K. Douzaki, M. Sukekawa, H. Koto and Y. Asada, Creep-fatigue life prediction for modified 9Cr-1Mo steel, PVP-Vol. 262, p. 175, 1993.

[11] K. Taguchi, M. Ueta, H. Koto and M. Sukekawa, Creep damage evaluation of modified 9Cr-1Mo steel based on a time-fraction concept, PVP-Book No. H0976B, p. 449, 1995.

[12] K. Taguchi, S. Maruyama, T. Fujioka, Y. Yamashita, K. Koto, K. Takahashi, Y. Toya and T. Sato, Creep, fatigue, and creep-fatigue properties of modified 9Cr-1Mo steel weldments, PVP-Vol. 336, p. 295, 1996.

[This page intentionally left blank]

# PART II
# HASTELLOY XR

# 1 DATA COLLECTION ON HASTELLOY XR

## 1.1 Development of Hastelloy XR

In 1970s, material selection tests of heat-resistant alloys for the High-Temperature Gas-cooled Reactor (HTGR) were performed as shown in Figure 59 mainly on long-term corrosion resistance in impure HTGR helium environment. Taking into account also service conditions of the intermediate heat exchanger (IHX) of the HTGR, a nickel-base Cr-Mo-Fe superalloy Hastelloy X, which has excellent accumulated experiences in jet engines was selected for the heat transfer tubes and the hot header in the IHX. Since Hastelloy X does not have sufficient compatibility with the primary helium coolant at very high temperatures, Hastelloy XR was developed from Hastelloy X to improve the compatibility.

It was found that for Hastelloy X, tightening the contents of some elements even within the specification of the chemical compositions results in remarkable improvements in the compatibility. The following modification items (a) and (b) were made on Hastelloy X to improve the compatibility and further modification items (c) and (d) were given to improve applicability to the HTGR.

*(a)* Optimizing manganese and silicon contents

Formation of stable and adherent oxidation films of $MnCr_2O_4$ spinel and $SiO_2$ is essential for the very high temperature components. Such an oxidation film is formed on the base metal through optimizing the Mn and Si contents for Hastelloy X (Shindo, 1982).

*(b)* Lowering aluminum and titanium contents

Internal oxidation and intergranular attack are suppressed through lowering the A1 and Ti contents (Shindo, 1982).

*(c)* Lowering cobalt content

Radioactive contamination in the primary cooling system by Co-containing corrosion products decreases to negligible levels through lowering the Co content (Shindo, 1982).

*(d)* Optimizing boron content

Addition of boron improves the creep strength for Hastelloy XR (Kurata, 1986), but causes contamination of the core and degradation in weldability. Optimization of the B content, therefore, is needed for a specific purpose. To a Tungsten-arc Inert-gas (TIG) welding wire, the addition of boron within 40-60 ppm was made to improve the creep strength of the welded joints.

JAEA in cooperation with Mitsubishi Materials Group developed Hastelloy XR with the modifications (a) to (c) above by 1976. Then, various tests were conducted on Hastelloy XR to construct an engineering database for design of the HTGR. In addition, quality of Hastelloy XR including creep strength was improved with the modification (d) above by 1984. Based on the engineering database of Hastelloy XR, JAEA developed high temperature structural design guidelines including design allowable limits on Hastelloy XR by 1990.

The specification of the improved version of Hastelloy X, which is called the nuclear grade alloy Hastelloy XR, is shown in Table 8, with a comparison to that of Hastelloy X. Hastelloy XR with optimization of boron content is called Hastelloy XR-II, when it is necessary to distinguish Hastelloy XR-II from Hastelloy XR. Heat transfer tubes, hot header, etc. of the intermediate heat exchanger of the High Temperature Engineering Test Reactor (HTTR) is made of Hastelloy XR-II.

Figure 92 shows results of long-term corrosion tests under severe thermal cycles, wherein superiority of Hastelloy XR to Hastelloy X is demonstrated as expected from the protective oxide film formed on Hastelloy XR.

**Table 10 - Specifications for Chemical Composition of Hastelloy XR and X**

| Material | Range | Chemical Compositions (wt%) | | | | | | | | | | | | | | |
|---|---|---|---|---|---|---|---|---|---|---|---|---|---|---|---|---|
| | | Elements | | | | | | | | | | | | | | |
| | | C | Mn | Si | P | S | Cr | Co | Mo | W | Fe | Ni | B | Al | Ti | Cu |
| Hastelloy XR | max | 0.15 | 1.00 | 0.50 | 0.040 | 0.030 | 23.00 | 2.50 | 10.00 | 1.00 | 20.00 | Remainder | 0.010 | 0.05 | 0.03 | 0.50 |
| | min | 0.05 | 0.75 | 0.25 | - | | 20.50 | - | 8.00 | 0.20 | 17.00 | Remainder | - | - | - | - |
| Hastelloy X | max | 0.15 | 1.00 | 1.00 | 0.040 | 0.030 | 23.00 | 2.50 | 10.00 | 1.00 | 20.00 | Remainder | 0.010 | 0.50 | 0.15 | 0.50 |
| | min | 0.05 | - | - | - | - | 20.50 | 0.50 | 8.00 | 0.20 | 17.00 | Remainder | - | - | - | - |

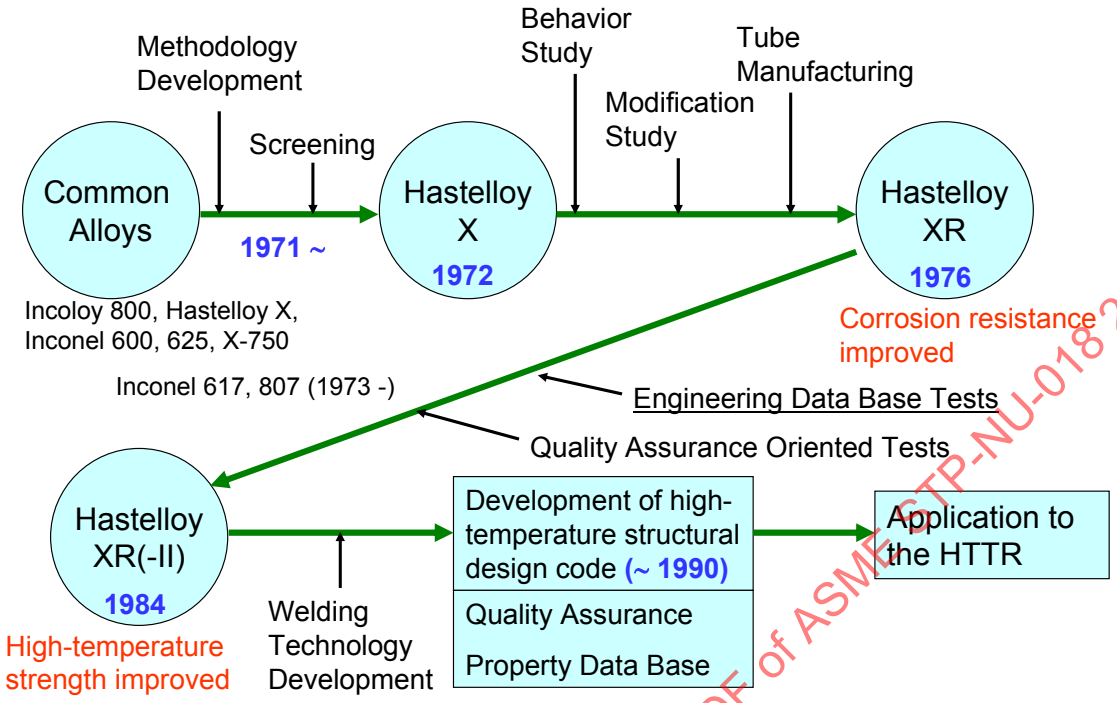


**Figure 91 - Development of Hastelloy XR**

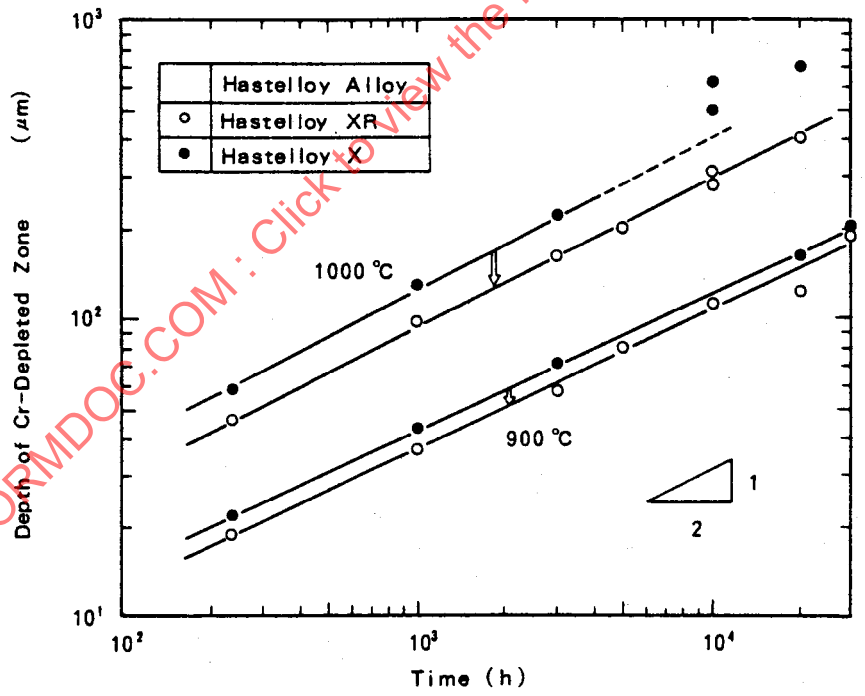


**Figure 92 - Comparison of Environmental Effect in Cr-Depleted Zone Depth between Hastelloy XR and Hastelloy X**

## 1.2 Data of Hastelloy XR

### 1.2.1 Creep fatigue

Creep fatigue test data of Hastelloy XR is shown in Table 11 and Table 12 and Figure 92 and Figure 94.

Table 11 shows results of low cycle fatigue tests with symmetric triangular strain waveform on Hastelloy X and Hastelloy XR at 900°C in simulated HTGR helium called JAERI-type B helium environment with impurity contents indicated in Table 13. Chemical composition of these materials is shown in Table 14.

Table 12 shows results of low cycle fatigue tests with trapezoidal strain waveform on Hastelloy XR at 900˚C in JAERI-type B helium environment.

Figure 94 shows relation between total strain range and fatigue life under different strain rates arranging the data in Table 11. No significant difference in fatigue strength was observed between Hastelloy X and Hastelloy XR under the given conditions.

Figure 94 shows low cycle fatigue and creep fatigue data on Hastelloy XR at 900˚C in JAERI-type B helium environment, which was used for development of high temperature structural design guidelines. Among the three different types of loadings with trapezoidal strain waveform, the creep fatigue life was reduced most effectively in tensile hold-time tests. Similar tendency is reported by Meurer et. al. (1984) on Incoloy 800H at 850˚C and Inconel 617 at 950˚C.

### 1.2.2 Creep

Creep rupture test data of Hastelloy XR from 800˚C to 1050˚C in air and in simulated HTGR helium, which was used for determination of design allowable limits in high temperature structural design guideline, is shown in Figure 95. Trends in stress dependence and data scattering of the creep rupture strength are judged to be quite similar at 1000˚C to those at lower temperatures. Therefore, it was concluded that Hastelloy XR is stable at 1000˚C or below.

Most of the data in Figure 63 was obtained in cooperative research of JAEA and National Institute for Materials Science (NIMS). Creep rupture test data of the cooperative research in air and in simulated HTGR helium (JAERI-type B helium) is shown in Table 15–Table 18 and Table 19, respectively. Figure 96 shows the creep rupture test data in air in Table 15–Table 18. Figure 97 shows comparison of the creep test data in air and JAERI-type B helium. No environmental effect can be observed by Figure 97. Chemical composition of Hastelloy XR used for the tests is shown in Table 18.

Creep rupture test data of Hastelloy XR-II from 700˚C to 1000˚C in air and in JAERI-type B helium is shown in Table 21–Table 23 and Table 24, respectively. The data was obtained in cooperative research of JAEA and NIMS. Figure 98 shows the creep rupture test data in air in Table 21–Table 23. Figure 99 shows comparison of the creep test data in air and JAERI-type B helium. Again, no environmental effect can be observed by Figure 67. Chemical composition of Hastelloy XR-II used for the tests is shown in Table 23.

Comparison of creep rupture test data on Hastelloy XR and Hastelloy XR-II is shown in Figure 100. Creep rupture time of Hastelloy XR-II is much larger than that of Hastelloy XR under the same condition.

### 1.2.3 Fatigue

In addition to the low cycle fatigue tests with symmetric triangular strain waveform in simulated HTGR helium described above, similar low cycle fatigue tests in air at various temperatures from

room temperature to 1000˚C were conducted on Hastelloy XR so as to determine design allowable limits (Design fatigue strain range) in high temperature structural design guidelines.

**Table 11 - Results of Low Cycle Fatigue Tests with Symmetric Triangular Strain Waveform on Hastelloy X And Hastelloy XR at 900˚C In JAERI-Type B Helium Environment**

| Material | $\dot{\varepsilon}t$ (1/s) | $\Delta\varepsilon t$ % | $\Delta\varepsilon in$ (at 1/2 $N_f$) % | $N_f$ |
|---|---|---|---|---|
| Hastelloy X | $1x10^{-3}$ | 0.28 | 0.07 | 56701 |
| | | 0.40 | 0.17 | 5590 |
| | | 0.80 | 0.58 | 1899 |
| | | 1.20 | 0.97 | 512 |
| | $1x10^{-4}$ | 0.28 | 0.12 | 11535 |
| | | 0.40 | 0.23 | 4535 |
| | | 0.80 | 0.60 | 1351 |
| | $2x10^{-5}$ | 0.40 | 0.28 | 2974 |
| | | 0.80 | 0.68 | 530 |
| Hastelloy XR | $1x10^{-3}$ | 0.28 | 0.08 | 32238 |
| | | 0.40 | 0.18 | 9978 |
| | | 0.80 | 0.62 | 1326 |
| | | 0.80 | 0.57 | 1664 |
| | | 1.20 | 0.98 | 511 |
| | $1x10^{-4}$ | 0.28 | 0.11 | 18160 |
| | | 0.40 | 0.23 | 5856 |
| | | 0.80 | 0.64 | 1103 |
| | $2x10^{-5}$ | 0.40 | 0.28 | 1918 |
| | | 0.40 | 0.28 | 2326 |
| | | 0.80 | 0.67 | 551 |

**Table 12 - Results of Low Cycle Fatigue Tests with Trapezoidal Strain Waveform on Hastelloy XR at 900°C in JAERI-Type B Helium Environment**

| Holdtime | | $\Delta\varepsilon t$ | $\Delta\varepsilon in$ (at 1/2 $N_f$) | $N_f$ |
|---|---|---|---|---|
| Tension Side | Compression Side | % | % | |
| 1 min | 0 | 0.8 | 0.64 | 641 |
| 10 min | 0 | 0.8 | 0.67 | 451 |
| 10 min | 0 | 0.8 | 0.67 | 365 |
| 0 | 1 min | 0.8 | 0.65 | 1427 |
| 0 | 10 min | 0.8 | 0.66 | 1349 |
| 1 min | 1 min | 0.8 | 0.74 | 837 |
| 10 min | 10 min | 0.81 | 0.76 | 786 |

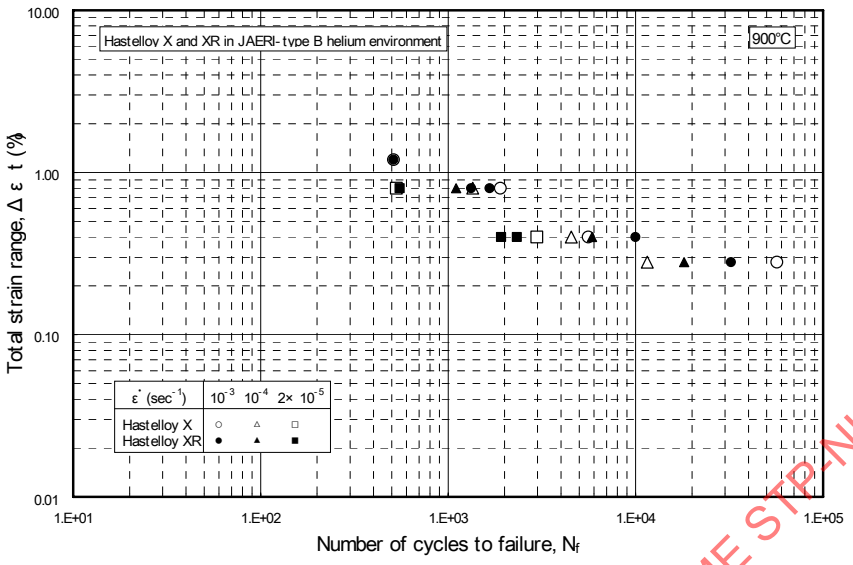


**Figure 93 - Relation between Total Strain Range and Fatigue Life Under Different Strain Rates**

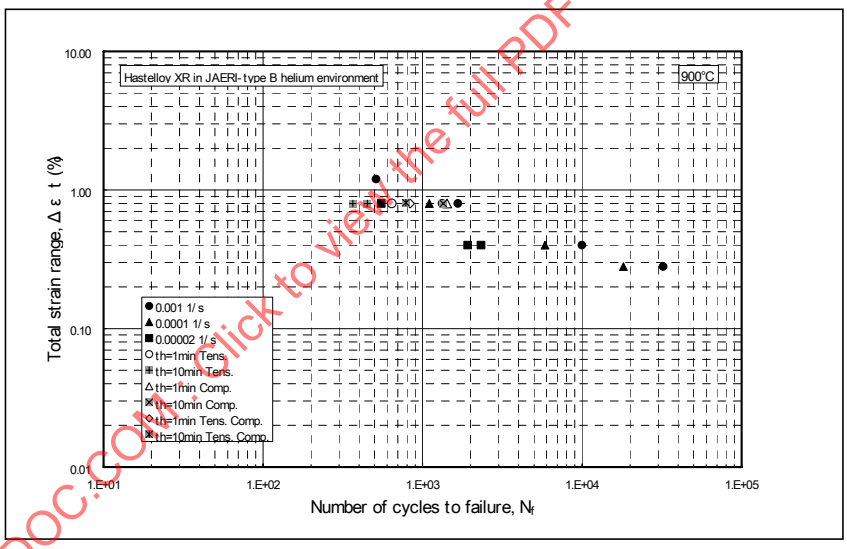


**Figure 94 - Creep Fatigue Test Data on Hastelloy XR**

**Table 13 - Impurity Levels of Simulated HTGR Helium Called JAERI-Type B Helium**

| Impurity Levels (Pa) | | | | |
|---|---|---|---|---|
| H2 | H2O | CO | CO2 | CH4 |
| 20 to 21 | 0.08 to 0.12 | 10 to 11 | 0.2 to 0.3 | 0.5 to 0.6 |

**Table 14 - Chemical Composition of the Materials Hastelloy X and Hastelloy XR**

| Material | Chemical Compositions (wt%) | | | | | | | | | | | | |
|---|---|---|---|---|---|---|---|---|---|---|---|---|---|
| | C | Mn | Si | P | S | Cr | Co | Mo | W | Fe | Ni | B | Al | Ti |
| Hastelloy X | 0.07 | 0.61 | 0.39 | 0.012 | <0.001 | 21.26 | 1.71 | 8.89 | 0.57 | 18.98 | Bal. | 0.00085 | 0.25 | <0.01 |
| Hastelloy XR | 0.07 | 0.83 | 0.32 | <0.005 | 0.006 | 21.84 | 0.19 | 9.06 | 0.53 | 18.26 | Bal. | 0.0001 | 0.02 | <0.01 |

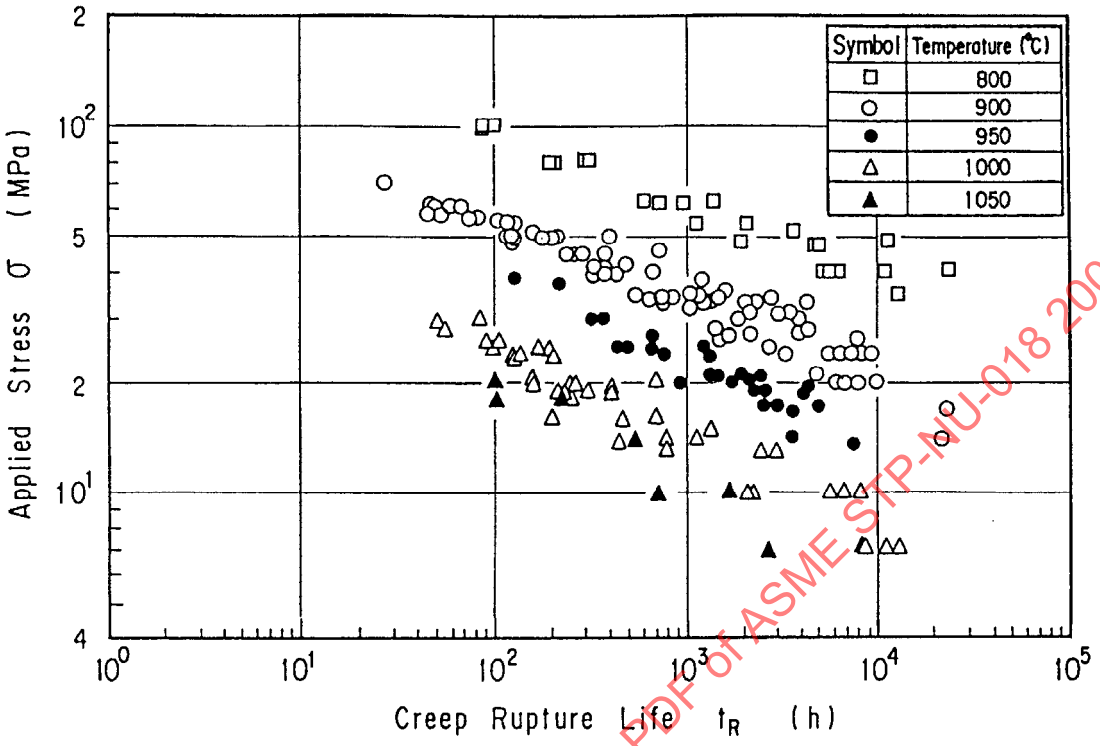


**Figure 95 - Creep Rupture Life for Hastelloy XR**

**Table 15 - Results of Creep Tests for Hastelloy XR in Air (Tube)**

| Specimen No. | Temp (°C) | Stress (MPa) | $t_R$ (h) | El (%) | RA (%) | $e_0$ (%) | $\dot{e}_m$ (%/h) | $t_{1\%}$ (h) | $t_3$ (h) | $e_3$ (%) |
|---|---|---|---|---|---|---|---|---|---|---|
| XRT14 | 800 | 98.1 | 88.9 | 23.9 | 28.6 | 0.070 | 9.38E-02 | 9.8 | 29.2 | 3.020 |
| XRT18 | | 60.8 | 608.6 | 38.5 | 15.1 | 0.043 | 3.08E-03 | 187.0 | 173.8 | 0.885 |
| XRT28 | | 53.0 | 1119.2 | 15.5 | 13.4 | 0.038 | 1.95E-03 | 317.2 | 290.8 | 0.858 |
| XRT20 | | 47.1 | 1952.0 | 11.4 | 12.3 | 0.035 | 4.53E-04 | 782.0 | 475.0 | 0.430 |
| XRT26 | | 39.2 | 5624.6 | 8.7 | 11.7 | 0.028 | 4.67E-04 | 1901.0 | 3828.0 | 2.100 |
| XRT16 | | 39.2 | 6455.4 | 7.7 | 12.7 | 0.028 | 4.46E-04 | 1973.0 | 4384.8 | 2.270 |
| XRT10 | | 33.3 | 12884.8 | 5.2 | 9.1 | 0.023 | 1.27E-04 | 5794.0 | 10526.0 | 1.800 |
| XRT21 | 850 | 39.2 | 1569.3 | 10.2 | 13.7 | 0.028 | 8.23E-04 | 530.4 | 331.6 | 0.525 |
| XRT11 | 900 | 49.0 | 123.0 | 17.4 | 17.6 | 0.035 | 6.38E-02 | 14.6 | 40.3 | 2.840 |
| XRT03 | | 39.2 | 412.9 | 11 | 18.6 | 0.030 | 6.40E-03 | 95.3 | 77.8 | 0.776 |
| XRT23 | | 33.3 | 764.8 | 10.2 | 11.6 | 0.026 | 4.57E-03 | 201.8 | 341.0 | 1.815 |
| XRT07 | | 26.5 | 1675.6 | 9.1 | 11.6 | 0.020 | 1.53E-03 | 614.0 | 990.0 | 1.780 |
| XRT27 | | 23.5 | 3345.3 | 10.8 | 10.6 | 0.018 | 6.86E-04 | 1056.0 | 1720.0 | 1.640 |
| XRT08 | | 19.6 | 6434.7 | 8.1 | 9.5 | 0.015 | 2.02E-04 | 3475.0 | 3460.0 | 0.990 |
| XRT06 | | 13.7 | 21396.0 | 6.7 | 5.3 | 0.012 | 9.53E-05 | 6210.0 | 12480.0 | 1.800 |
| XRT29 | 950 | 19.6 | 928.9 | 10.3 | 13.7 | 0.016 | 3.27E-03 | 222.0 | 210.6 | 0.906 |
| XRT19 | 1000 | 18.6 | 316.9 | 15.1 | 12.3 | 0.018 | 5.74E-03 | 78.8 | 60.8 | 0.579 |
| XRT09 | | 13.7 | 795.7 | 12 | 13 | 0.013 | 3.71E-03 | 213.1 | 222.0 | 1.060 |
| XRT17 | | 9.8 | 2124.8 | 18.4 | 8.4 | 0.010 | 6.55E-04 | 849.0 | 739.0 | 0.792 |
| XRT02 | | 6.9 | 10920.6 | 27.3 | 11.6 | 0.007 | 4.67E-04 | 480.0 | 3726.0 | 3.068 |
| XRT12 | 1050 | 17.7 | 105.0 | 18.8 | 17.6 | 0.020 | 1.65E-02 | 18.3 | 10.5 | 0.420 |
| XRT15 | | 9.8 | 718.5 | 10.2 | 10.6 | 0.012 | 1.55E-03 | 371.0 | 363.0 | 0.963 |
| XRT04 | | 6.9 | 2641.6 | 38.2 | 2.1 | 0.008 | 1.75E-03 | 437.0 | 922.0 | 2.050 |

**Table 16 - Results of Creep Tests for Hastelloy XR in Air (Plate)**

| Specimen No. | Temp (°C) | Stress (MPa) | $t_R$ (h) | El (%) | RA (%) | $e_0$ (%) | $\dot{e}_m$ (%/h) | $t_{1\%}$ (h) | $t_3$ (h) | $e_3$ (%) |
|---|---|---|---|---|---|---|---|---|---|---|
| XRS07 | 800 | 78.5 | 314.6 | 19.6 | 22.8 | 0.057 | 8.35E-03 | 82 | 81 | 0.97 |
| XRS02 | | 60.8 | 1409.9 | 10.1 | 14.4 | 0.042 | 8.28E-04 | 550 | 448 | 0.67 |
| XRS15 | | 53 | 2105.1 | 8.9 | 10.6 | 0.038 | 6.70E-04 | 786 | 636 | 0.72 |
| XRS12 | | 47.1 | 4981.4 | 7.7 | 9.9 | 0.033 | 2.29E-04 | 2292 | 1464 | 0.56 |
| XRS09 | | 39.2 | 23593.6 | 8.9 | 14 | 0.028 | 6.37E-05 | 9620 | 17126 | 1.70 |
| XRS05 | 900 | 49 | 177.7 | 18.4 | 23.5 | 0.038 | 3.23E-02 | 22 | 24 | 1.08 |
| XRS03 | | 33.3 | 1479.2 | 9.4 | 11.9 | 0.027 | 2.36E-03 | 388 | 582 | 1.60 |
| XRS16 | | 26.5 | 4019.8 | 7.1 | 5.2 | 0.022 | 4.69E-04 | 1685 | 3000 | 1.70 |
| XRS20 | | 23.5 | 9487.7 | 5.7 | 10.9 | 0.018 | 1.18E-04 | 6110 | 6254 | 1.05 |
| XRS01 | | 19.6 | 9909 | 5.2 | 8.4 | 0.015 | 1.40E-04 | 4618 | 6322 | 1.43 |
| XRS13 | | 16.7 | 23521.6 | 6.8 | 7.7 | 0.013 | 5.94E-05 | 12720 | 14208 | 1.20 |
| XRS08 | 1000 | 23.5 | 208.3 | 17 | 20.2 | 0.022 | 4.00E-03 | 60 | 38 | 0.40 |
| XRS18 | | 18.6 | 435.4 | 13 | 26.4 | 0.018 | 5.71E-03 | 103 | 91 | 0.78 |
| XRS19 | | 13.7 | 1124.7 | 11 | 9.1 | 0.013 | 1.97E-03 | 341 | 384 | 1.22 |
| XRS11 | | 9.8 | 5849.5 | 15 | 14 | 0.010 | 4.77E-04 | 751 | 2760 | 2.24 |
| XRS17 | 1050 | 17.7 | 225.1 | 14.9 | 18.6 | 0.020 | 5.50E-03 | 69 | 54 | 0.53 |
| XRS04 | | 13.7 | 550.7 | 15.5 | 15.7 | 0.015 | 8.99E-03 | 66 | 151 | 1.99 |
| XRS06 | | 9.8 | 1696.4 | 9.8 | 9.5 | 0.012 | 2.02E-03 | 313 | 894 | 2.38 |
| XRS14 | | 6.9 | 8608.1 | 15.6 | 19.3 | 0.008 | 1.93E-04 | 361 | 4416 | 2.94 |

**Table 17 - Results of Creep Tests for Hastelloy XR in Air (Bar)**

| Specimen No. | Temp (°C) | Stress (MPa) | $t_R$ (h) | El (%) | RA (%) | $e_0$ (%) | $\dot{e}_m$ (%/h) | $t_{1\%}$ (h) | $t_3$ (h) | $e_3$ (%) |
|---|---|---|---|---|---|---|---|---|---|---|
| XRB09 | 800 | 78.5 | 307.9 | 25.6 | 24.7 | 0.057 | 1.78E-02 | 48 | 79 | 1.75 |
| XRB04 | | 47.1 | 5063.0 | 14.1 | 16.5 | 0.033 | 7.08E-04 | 1038 | 1145 | 1.11 |
| XRB06 | 900 | 49.0 | 203.0 | 46.1 | 46.9 | 0.038 | 3.17E-02 | 20 | 17 | 0.80 |
| XRB10 | | 23.5 | 5611.9 | 25.8 | 32.0 | 0.018 | 2.09E-03 | 382 | 1314 | 3.16 |
| XRB11 | 1000 | 18.6 | 263.5 | 38.5 | 45.9 | 0.018 | 4.55E-02 | 16 | 36 | 2.45 |
| XRB07 | | 9.8 | 5928.1 | 37.1 | 34.1 | 0.010 | 2.61E-03 | 242 | 1327 | 4.01 |

**Table 18 - Results of Creep Tests for Hastelloy XR in Air (Subsize Specimen Machined from Tube)**

| Specimen No. | Temp (°C) | Stress (MPa) | $t_R$ (h) | El (%) | RA (%) |
|---|---|---|---|---|---|
| XRM2 | 800 | 39.2 | 5070.1 | 4.8 | 9.8 |
| XRM7 | 900 | 39.2 | 377.4 | 7.3 | 14.3 |
| XRM3 | | 19.6 | 6821.1 | 7.0 | 13.9 |
| XRM4 | 1000 | 19.6 | 265.8 | 11.4 | 17.7 |
| XRM5 | | 9.8 | 6610.7 | 37.0 | 23.5 |

**Table 19 - Results of Creep Tests for Hastelloy XR in JAERI-Type B Helium Environment**

| Temp (°C) | Stress (MPa) | $t_R$ (h) | El (%) | RA (%) | $t_{1\%}$ (h) | $t_3$ (h) | $e_3$ (%) |
|---|---|---|---|---|---|---|---|
| 800 | 98.1 | 104.4 | 41.3 | 36.1 | 8 | 35 | 4.3 |
| | 78.5 | 298.5 | 31.2 | 23.7 | 41 | 105 | 3 |
| | 60.8 | 980.7 | 18 | 16 | 135 | 580 | 6.8 |
| | 51 | 3706.8 | 16 | 13.6 | 360 | 2180 | 5 |
| | 47.1 | 11485.8 | 26 | 24.2 | 360 | 6500 | 8.5 |
| | 39.2 | 10944.1 | 32 | 36 | 360 | 4050 | 6.2 |
| 900 | 58.8 | 62 | 47.3 | 55.3 | 4 | 30 | 9.1 |
| | 51 | 160.7 | 55.3 | 44.2 | 10 | 69 | 8.6 |
| | 49 | 217.8 | 43.3 | 41.2 | 18 | 110 | 12 |
| | 44.1 | 283.7 | 50 | 37.1 | 20 | 140 | 11 |
| | 39.2 | 694.7 | 41.7 | 36 | 48 | 360 | 12.6 |
| | 34.3 | 1579.6 | 35.8 | 30.6 | 130 | 860 | 9 |
| | 29.4 | 3839.7 | 24.6 | 21.3 | 210 | 2000 | 7.7 |
| | 26.5 | 3999.7 | 22 | 17.8 | 660 | 2400 | 7.6 |
| | 23.5 | 7447.1 | 26 | 30 | 720 | 4130 | 9 |
| | 19.6 | 7936.6 | 34 | 30 | 720 | 3300 | 7 |
| 1000 | 24.5 | 196.2 | 55 | 43.2 | 22 | 112 | 16.3 |
| | 19.6 | 410.6 | 42.3 | 33.4 | 36 | 212 | 12.5 |
| | 15.7 | 699.2 | 41 | 32.2 | 43 | 350 | 10.8 |
| | 12.7 | 2498.3 | 35.3 | 24.6 | 250 | 1380 | 12 |
| | 9.8 | 2247.3 | 45.3 | 35.5 | 500 | 1100 | 7.1 |
| | 9.8 | 8111.1 | 34 | 22 | 1160 | 2650 | 4.1 |

**Table 20 - Chemical Composition of Hastelloy XR for Creep Tests**

| Material | Chemical Compositions (wt%) | | | | | | | | | | | | | |
|---|---|---|---|---|---|---|---|---|---|---|---|---|---|---|
| | C | Mn | Si | P | S | Cr | Co | Mo | W | Fe | Ni | B | Al | Ti |
| Hastelloy XR | 0.07 | 0.88 | 0.27 | <0.005 | <0.005 | 21.9 | Tr | 9.1 | 0.47 | 18.2 | Bal. | 0.00028 | 0.03 | 0.02 |

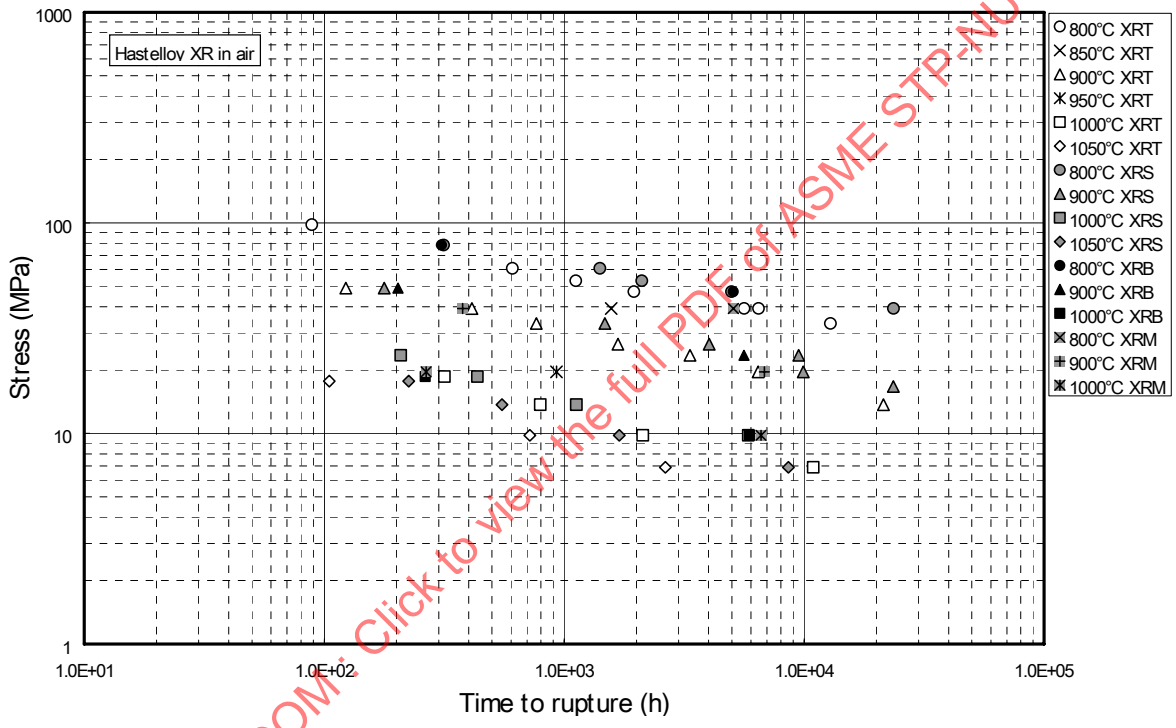


**Figure 96 - Results of Creep Tests for Hastelloy XR in Air**

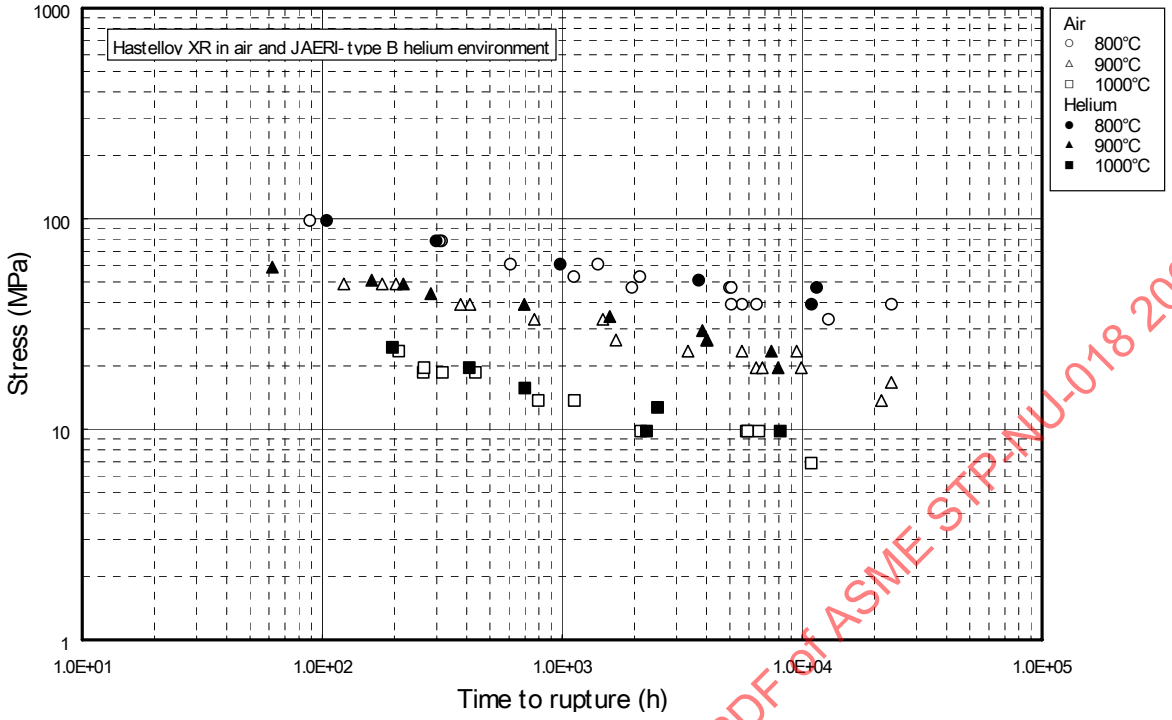


**Figure 97 - Results of Creep Tests for Hastelloy XR in Air and in JAERI-Type B Helium Environment**

**Table 21 - Results of Creep Tests for Hastelloy XR-II in Air (Plate: ϕ10mm)**

| Specimen No. | Temp (°C) | Stress (MPa) | $t_R$ (h) | El (%) | RA (%) | $e_0$ (%) | $\dot{e}_m$ (%/h) | $t_{1\%}$ (h) | $t_3$ (h) |
|---|---|---|---|---|---|---|---|---|---|
| XR2P10 | | 225.6 | 129.0 | 97.1 | 76.8 | 0.412 | 1.65E-01 | 4.7 | 41.5 |
| XR2P11 | | 196.1 | 329.6 | 111.5 | 81.5 | 0.171 | 8.52E-02 | 10.8 | 98.0 |
| XR2P12 | 700 | 176.5 | 796.8 | 86.1 | 85.3 | 0.132 | 3.32E-02 | 20.2 | 354.0 |
| XR2P13 | | 147.1 | 3016.4 | 103.3 | 87.2 | 0.109 | 8.75E-03 | 49.5 | 1404.0 |
| XR2P14 | | 117.7 | 26733.4 | 69.4 | 86.4 | 0.077 | 3.09E-04 | 207.0 | 9984.0 |
| XR2P16 | | 117.7 | 164.5 | 75.3 | 92.3 | 0.091 | 1.51E-01 | 4.2 | 67.0 |
| XR2P01 | | 98.1 | 651.6 | 62.7 | 88.0 | 0.069 | 2.77E-02 | 21.5 | 292.0 |
| XR2P02 | 800 | 85.3 | 1418.2 | 83.2 | 87.9 | 0.066 | 1.18E-02 | 35.0 | 566.4 |
| XR2P03 | | 75.5 | 4341.1 | 35.1 | 67.3 | 0.048 | 2.30E-03 | 222.0 | 1680.0 |
| XR2P15 | | 68.6 | 7148.2 | 67.7 | 77.8 | 0.049 | 1.53E-03 | 327.0 | 1896.0 |
| XR2P17 | | 68.6 | 70.8 | 66.2 | 91.8 | 0.057 | 2.33E-01 | 4.0 | 13.8 |
| XR2P18 | | 58.8 | 197.7 | 109.1 | 82.9 | 0.043 | 9.08E-02 | 8.0 | 27.5 |
| XR2P04 | 900 | 44.1 | 917.1 | 80.3 | 83.4 | 0.031 | 1.62E-02 | 54.5 | 68.0 |
| XR2P05 | | 39.2 | 2486.4 | 45.3 | 71.7 | 0.023 | 1.99E-03 | 286.0 | 193.5 |
| XR2P06 | | 31.4 | 8218.5 | 39.4 | 57.1 | 0.024 | 7.63E-04 | 1223.0 | 1872.0 |
| XR2P20 | | 29.4 | 112.0 | 80.1 | 89.3 | 0.022 | 3.55E-02 | 19.0 | 16.0 |
| XR2P07 | | 22.6 | 623.8 | 55.9 | 50.9 | 0.018 | 2.56E-03 | 127.0 | 88.0 |
| XR2P08 | 1000 | 16.7 | 1462.5 | 66.2 | 55.8 | 0.014 | 1.11E-03 | 266.0 | 214.5 |
| XR2P09 | | 11.8 | 4437.8 | 53.8 | 34.6 | 0.006 | 1.45E-04 | 824.0 | 573.0 |
| XR2P19 | | 7.8 | 16194.7 | 34.0 | 36.8 | 0.004 | 9.41E-06 | 4423.0 | 3408.0 |

**Table 22 - Results of Creep Tests for Hastelloy XR-II in Air (Plate: ϕ6mm)**

| Specimen No. | Temp (°C) | Stress (MPa) | $t_R$ (h) | El (%) | RA (%) | $e_0$ (%) | $\dot{e}_m$ (%/h) | $t_{1\%}$ (h) | $t_3$ (h) |
|---|---|---|---|---|---|---|---|---|---|
| XR2S3 | 700 | 117.7 | 24651.5 | 41.3 | 85.1 | 0.077 | 2.58E-04 | 168.0 | 9408.0 |
| XR2S5 | 800 | 75.5 | 4116.6 | 60.6 | 74.5 | 0.065 | 2.88E-03 | 162.5 | 1656.0 |
| XR2S6 | | 68.6 | 8459.0 | 76.8 | 73.4 | 0.053 | 1.29E-03 | 354.5 | 2376.0 |
| XR2S8 | 900 | 39.2 | 2895.7 | 56.8 | 65.7 | 0.027 | 1.16E-03 | 345.5 | 215.8 |
| XR2S9 | | 31.4 | 8590.2 | 40.9 | 48.4 | 0.023 | 7.62E-04 | 1167.0 | 1560.0 |
| XR2S10 | 950 | 29.4 | 829.5 | 71.9 | 77.7 | 0.050 | 2.98E-03 | 140.0 | 111.0 |
| XR2S10 | | 22.6 | 2647.6 | 62.9 | 56.1 | 0.032 | 1.38E-03 | 335.5 | 280.0 |

**Table 23 - Results of Creep Tests for Hastelloy XR-II in Air (Tube)**

| Specimen No. | Temp (°C) | Stress (MPa) | $t_R$ (h) | El (%) | RA (%) | $e_0$ (%) | $\dot{e}_m$ (%/h) | $t_{1\%}$ (h) | $t_3$ (h) |
|---|---|---|---|---|---|---|---|---|---|
| XR2T1 | 700 | 225.6 | 135.7 | 109.9 | 75.0 | 0.668 | 1.94E-01 | 2.7 | 44.0 |
| XR2T11 | | 196.1 | 355.8 | 106.3 | 78.8 | 0.183 | 7.18E-02 | 12.1 | 88.0 |
| XR2T12 | | 176.5 | 622.1 | 66.0 | 84.5 | 0.127 | 3.81E-02 | 24.7 | 202.0 |
| XR2T13 | | 147.1 | 3237.4 | 59.7 | 84.1 | 0.101 | 6.14E-03 | 78.5 | 1200.0 |
| XR2T15 | 800 | 117.7 | 178.3 | 87.6 | 91.8 | 0.091 | 1.27E-01 | 6.6 | 62.5 |
| XR2T16 | | 98.1 | 604.2 | 70.8 | 86.0 | 0.071 | 3.44E-02 | 21.8 | 247.0 |
| XR2T01 | | 85.3 | 1387.4 | 71.2 | 79.5 | 0.060 | 1.36E-02 | 45.0 | 556.8 |
| XR2T02 | | 75.5 | 3446.1 | 57.4 | 71.1 | 0.052 | 4.81E-03 | 142.5 | 1152.0 |
| XR2T03 | | 68.6 | 6196.2 | 41.4 | 61.6 | 0.049 | 2.01E-03 | 445.5 | 1536.0 |
| XR2T17 | 900 | 68.6 | 101.4 | 67.7 | 86.5 | 0.052 | 1.02E-01 | 8.5 | 13.0 |
| XR2T18 | | 58.8 | 201.6 | 51.7 | 77.7 | 0.046 | 4.96E-02 | 16.5 | 19.5 |
| XR2T04 | | 44.1 | 1231.7 | 42.4 | 61.9 | 0.037 | 2.57E-03 | 164.0 | 127.2 |
| XR2T05 | | 39.2 | 2285.1 | 34.8 | 60.4 | 0.027 | 1.51E-03 | 279.0 | 1207.2 |
| XR2T06 | | 31.4 | 7830.8 | 33.5 | 54.5 | 0.022 | 6.92E-04 | 692.0 | 3120.0 |
| XR2T19 | 1000 | 29.4 | 215.0 | 50.5 | 64.6 | 0.027 | 6.00E-03 | 42.0 | 24.2 |
| XR2T20 | | 22.6 | 737.5 | 46.3 | 56.1 | 0.021 | 2.28E-03 | 199.0 | 178.5 |
| XR2T07 | | 16.7 | 2021.6 | 47.3 | 45.2 | 0.013 | 6.85E-04 | 415.0 | 1156.8 |
| XR2T08 | | 11.8 | 6308.3 | 34.3 | 28.6 | 0.019 | 2.48E-04 | 941.5 | 3312.0 |

**Table 24 - Results of Creep Tests for Hastelloy XR-II In JAERI-Type B Helium Environment (Plate: ϕ6mm)**

| Specimen No. | Temp (°C) | Stress (MPa) | $t_R$ (h) | El (%) | RA (%) | $e_0$ (%) | $\dot{e}_m$ (%/h) | $t_{1\%}$ (h) | $t_3$ (h) |
|---|---|---|---|---|---|---|---|---|---|
| 60P21 | 700 | 225.6 | 117.5 | 70.0 | 66.8 | 0.540 | 1.77E-01 | 3.4 | 54.0 |
| 60PH12 | | 196.1 | 301.7 | 69.2 | 79.9 | 0.177 | 7.35E-02 | 17.5 | 128.5 |
| 60P10A | | 176.5 | 784.8 | 64.7 | 71.1 | 0.125 | 2.94E-02 | 24.0 | 433.0 |
| 60P12 | | 147.1 | 3167.0 | 56.1 | 71.5 | 0.105 | 5.32E-03 | 50.0 | 2140.0 |
| 60P07 | 800 | 117.7 | 123.0 | 80.8 | 75.2 | 0.085 | 1.00E-02 | 5.0 | 22.0 |
| 60P09 | | 98.1 | 443.1 | 64.7 | 69.1 | 0.071 | 3.30E-02 | 18.5 | 89.5 |
| 60P10 | | 85.3 | 1287.4 | 55.9 | 63.7 | 0.062 | 9.45E-03 | 43.0 | 272.0 |
| 60P11 | | 75.5 | 4851.6 | 43.9 | 56.4 | 0.056 | 1.40E-03 | 208.0 | 1520.0 |
| 60P19W | | 68.6 | 10175.8 | 24.8 | 29.3 | 0.051 | 4.87E-04 | 490.0 | 3520.0 |
| 60P22 | 900 | 68.6 | 75.2 | 88.3 | 74.5 | 0.051 | 2.61E-01 | 3.4 | 16.7 |
| 60P06 | | 58..8 | 191.2 | 72.3 | 60.6 | 0.044 | 1.01E-01 | 6.8 | 56.0 |
| 60P25W | | 44.1 | 1787.3 | 62.4 | 60.4 | 0.034 | 2.84E-03 | 138.0 | 117.0 |
| 60P13 | | 39.2 | 2683.0 | 31.1 | 44.4 | 0.031 | 9.19E-04 | 230.0 | 655.0 |
| 60P14 | | 31.4 | 10056.3 | 24.5 | 20.5 | 0.025 | 1.36E-04 | 3500.0 | 3660.0 |
| 60P24 | 1000 | 29.4 | 183.5 | 49.1 | 53.7 | 0.024 | 1.35E-02 | 35.5 | 33.7 |
| 60P23 | | 22.6 | 504.4 | 39.7 | 32.6 | 0.016 | 2.84E-03 | 100.0 | 37.0 |
| 60P16 | | 16.7 | 1754.3 | 38.3 | 28.2 | 0.015 | 1.22E-03 | 347.0 | 274.0 |

**Table 25 - Chemical Composition of Hastelloy XR-II for Creep Tests**

| Material | Chemical Compositions (wt%) | | | | | | | | | | | | | |
|---|---|---|---|---|---|---|---|---|---|---|---|---|---|---|
| | C | Mn | Si | P | S | Cr | Co | Mo | W | Fe | Ni | B | Al | Ti |
| Hastelloy XR-II (tube) | 0.07 | 0.86 | 0.32 | <0.01 | <0.01 | 21.98 | 0.05 | 8.83 | 0.51 | 17.70 | Bal. | 0.005 | 0.02 | 0.01 |
| Hastelloy XR-II (plate) | 0.07 | 0.88 | 0.33 | <0.001 | 0.001 | 21.99 | 0.06 | 8.73 | 0.63 | 17.80 | Bal. | 0.006 | 0.03 | 0.01 |

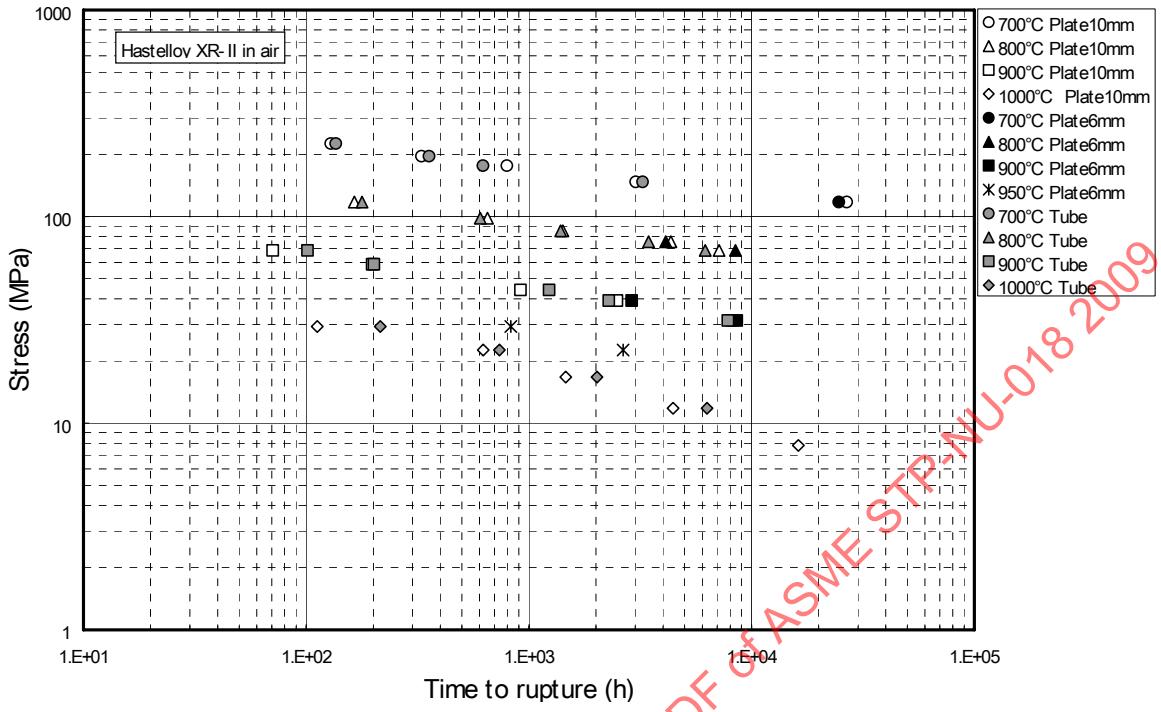


**Figure 98 - Results of Creep Tests for Hastelloy XR-II in Air**

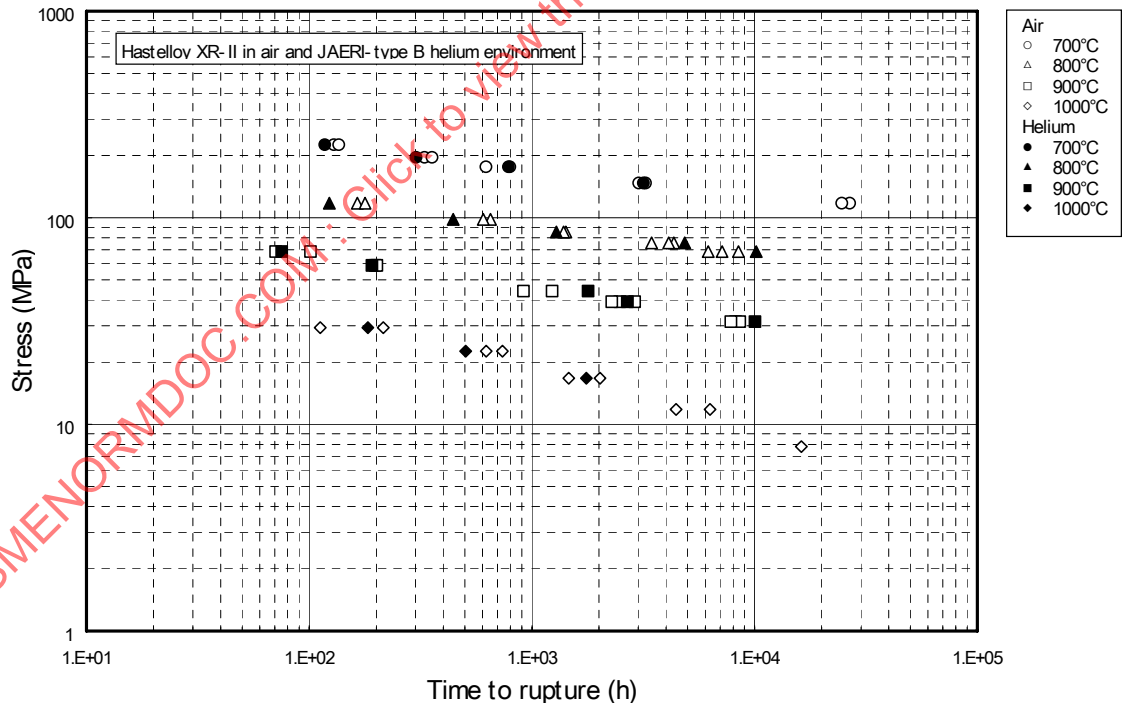


**Figure 99 - Results of Creep Tests for Hastelloy XR-II in Air and in JAERI-Type B Helium Environment**

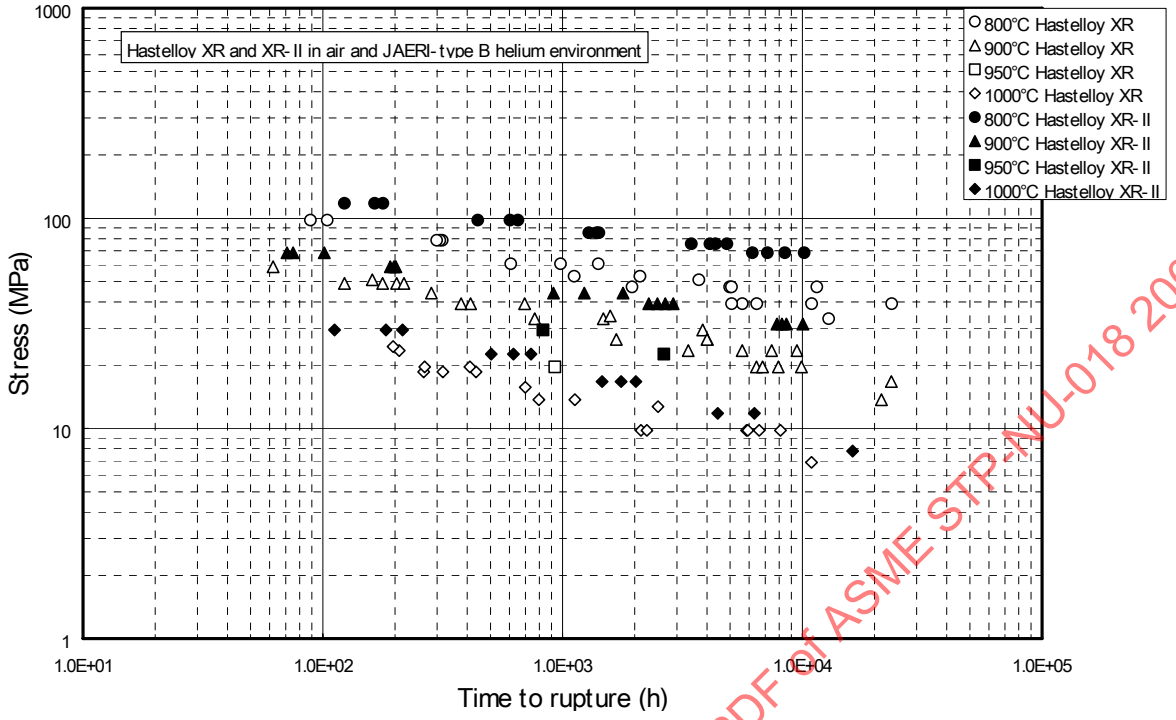


**Figure 100 - Comparison of Creep Test Data for Hastelloy XR and Hastelloy XR-II**

# 2 CREEP-FATIGUE CRITERIA ON HASTELLOY XR

## 2.1 High Temperature Structural Design Guideline for HTGR

### 2.1.1 Introduction

The primary cooling system components and related components that serve as the reactor coolant pressure boundaries of the HTTR are used at high temperatures in creep regime. Figure 101 shows cooling system of the HTTR. In particular, the heat transfer tubes and hot header of the intermediate heat exchanger (IHX) are subjected to temperatures above 900°C. The reactor pressure vessel as well as the metallic core support structures are exposed to the reactor coolant at temperatures of around 400°C under an irradiation condition. High temperature structural materials are chosen for the high temperature components of the HTTR, taking into careful considerations the service conditions and safety functions of the components. The material used are as follows.

- A nickel-base corrosion and heat resistant superalloy Hastelloy XR
- A normalized and tempered (NT) 2 1/4Cr-1Mo steel
- Two types of austenitic stainless steel, SUS321TB and SUS316
- 1Cr-0.5Mo-V steel, an alloy steel bolting material for high temperature service.

Some of the high temperature materials and their service temperatures are beyond the well-established high temperature structural design codes such as the Elevated Temperature Structural Design Guide for the Prototype Fast Breeder Reactor "Monju" (abbreviated as FBR Code) and the ASME Boiler and Pressure Vessel Code Case N-47 (ASME, 1986). Accordingly, development of a new high temperature structural design guideline was necessary for these materials at their service temperatures. Moreover, at the very high temperatures, where creep deformation is significant, component design based on elastic analysis is not possible.

Thus, extensive R&D was carried out not only in JAEA but also in national and private research organizations in Japan to establish a reliable high temperature structural design guideline.

### 2.1.2 Identification of Failure Modes

A high temperature structural design guideline provides design limits and rules for guarding high temperature components against failure modes. Development of a new high temperature structural design guideline, therefore, requires

*(a)* Identification of failure modes under exposure to service environments within the guideline application temperature range for each material, and

*(b)* Development of design limits and rules for guarding against each failure mode with appropriate safety margins.

From reviewing material test results and information on failures at commercial plants and experimental facilities, the following failure modes were identified.

*(a)* Ductile rupture by short-term loading

*(b)* Creep rupture by long-term loading

*(c)* Buckling by short-term loading

*(d)* Creep buckling by long-term loading

*(e)* Creep fatigue failure

*(f)* Gross distortion by incremental collapse and ratcheting

*(g)* Loss of function by excessive deformation.

These failure modes are the same as those considered in well-established high temperature structural design codes. It should be noted here that the long-term loading means loading at high temperatures that develops significant creep effect over a long period.

### 2.1.3 Developments of Design Limits and Rules

The fact that the failure modes for the new materials are the same as for those of the well-established codes suggests the possibility that fundamental philosophies on design limits and rules of the well-established codes can be applicable to the new material, Hastelloy XR. Among the well-established high temperature structural design codes, the FBR Code was the only one that had been authorized by the Japanese government, and so it was the most appropriate for discussion on applicability to the new material. We came to the conclusion that design limits and rules for the above-mentioned seven failure modes can be developed on the basis of the fundamental philosophies of the FBR Code as shown in Table 26.

On this conclusion, the detailed design limits and rules were developed based on experimental data on material properties and structural mechanics behavior under multi-axial stress states, referring to those of the FBR Code, as described below.

### 2.1.4 Material Characterization on Hastelloy XR

The maximum metal temperature of Hastelloy XR in the HTTR reaches about 900°C even during the normal operation and is likely to exceed 950°C but less than 1000°C in events such as a loss of secondary cooling.

Taking into account the service temperature conditions, material tests and structural mechanics tests for both base metals and TIG-weld joints were conducted at temperatures ranging from room temperature to 1050˚C, mainly in JAEA but also in the National Institute for Materials Science (NIMS) and research laboratories of private nuclear power companies. Test conditions of major material property tests for the base metals are briefly listed in Table 27. Test specimens were taken from product forms of tubes, plates, forging cylinders and bars simulating application to the HTTR high temperature components.

By carefully reviewing the experimental data, the following results were derived.

*(a)* Tensile property

At low or intermediate temperatures up to 800˚C, Hastelloy XR is work-hardening under monotonic loadings at the strain rate of 0.3%/min which is specified for tensile tests by the Japan Industrial Standards (JIS), and has hardening ratios of two or above, similarly to austenitic stainless steels (the hardening ratio is defined as a ratio of ultimate tensile strength to yield strength). On the other hand, at high temperatures above 850˚C, an abrupt decrease in load or a wavy stress-strain curve under straining at this strain rate is observed due to dynamic recrystallization, as shown in Figure 102.

Taking into consideration that dynamic recrystallization is not observed at higher strain rates of about 100%/min as shown in Figure 103, the strain rate for the tensile tests was changed for Hastelloy XR from 0.3%/min to 100%/min at high temperatures over 800˚C. Time-independent allowable limits were generated from the tensile test data at this higher strain rate.

*(b)* Creep property

Since many commercial superalloys are known to lose their stability of mechanical strength at very high temperatures above 1000˚C, the maximum temperature by which high temperature strengths, in particular creep rupture strength, are stable for Hastelloy XR is required to be identified. Figure 103 shows that trends in stress dependence and data scattering of the creep rupture strength are quite similar at 1000˚C to those at lower temperatures. Therefore, it was concluded that Hastelloy XR is stable up to 1000˚C.

Concerning the helium environmental effect on creep rupture strength, Figure 104 shows creep rupture lives under a specific stress in various helium environments. Hastelloy XR suffers no degradation in creep rupture strength except in a decarburizing environment. In this figure, a helium environment is characterized fairly well in the stability diagram for Cr (acr=0.8) which is expressed by a carbon activity ac and oxygen partial pressure $PO_2$. Atmospheres denoted as the areas I and II lead to rapid decarburization with or without oxidation, while in the areas IV and V rapid carburization occurs. In area III, mild carburization occurs. In Figure 104, a creep rupture life at a specified helium environment is scaled to lengths of the bar located on the stability diagram. A detailed description of this diagram is given in Kurata, Y. et. al., (1989). The primary coolant of the HTTR shall be in the area III where any significant degradation in creep rupture life is not observed for Hastelloy XR. Then, it is not necessary to consider helium environment effects on design allowable limits for Hastelloy XR.

*(c)* Creep-fatigue interaction

Creep-fatigue interaction for Hastelloy XR is quite similar to those for austenitic stainless steels such as SUS304 and 316. Degradations in lifetime are more pronounced due to holds in tension than those in compression. Figure 105 and Figure 106 show the applicability of the well-known cycle and time fraction rule proposed by Robinson (1952) and Taira (1962), which is adopted in the FBR Code. The accumulated fatigue and creep damage fractions in the figures were calculated with design parameters. It can be concluded form these figures that the linear summation rule of cycle and time fractions is applicable to Hastelloy XR with a great deal of safety margins even at very high temperatures.

*(d)* Applicability of the Fast Breeder Reactor Code

As discussed above, the material properties for Hastelloy XR were observed to be basically similar to those for austenitic stainless steels. These observations lead to the conclusion that the FBR Code is, in principle, applicable to Hastelloy XR at the temperatures ranging to 1000°C, with a modification to the tensile test procedure.

*(e)* Structural mechanics behavior

The high temperature structural design guideline for class 1 components of the HTTR was established on the basis of component-wise structural mechanics behavior data as well as material property data referring to the FBR Code. The emphasis of the structural mechanics research works was placed on the applicability of the FBR Code to Hastelloy XR under the service conditions of the very high temperature components. Research works for Hastelloy XR include experiments on multiaxiality of creep rupture strength and creep-fatigue interaction, and on creep buckling. Further research works were carried out for establishment of creep analysis methods for Hastelloy XR.

*(1)* Multiaxiality of creep rupture strength and creep fatigue damage

Since the very high temperature components are exposed to multiaxial loading conditions, multiaxial formulations are required for high temperature strengths of Hastelloy XR. In the FBR Code, the stress intensity criterion, i.e., the maximum shear stress criterion, is adopted

as the multiaxial formulation for primary stresses, while Von Mises' stresses is that for primary + secondary stresses in evaluating a creep damage. Figure 107 shows the applicability of Von Mises' criterion to that of creep rupture strength. The experiments were carried out in such a manner that a tubular test specimen was subjected to a combination of axial and torsional loads. From this figure, it was concluded that the Von Mises' criterion predict the creep rupture life on the safe side. Consequently, the multiaxial formulations, which were given in the FBR Code, were demonstrated to be applicable to Hastelloy XR

*(2)* Creep buckling

Heat transfer tubes of the IHX shall not fail by a creep buckling at a piping rupture accident in the secondary cooling system. Component-wise experiments, therefore, were conducted at the Helium Engineering Demonstration Loop (HENDEL) at JAERI so as to demonstrate the structural integrity of the tubes against the creep buckling and the applicability of a design rule given in the design code. The creep bucking data demonstrated the structural integrity with a great safety margin. A finite element calculation predicted the creep buckling time in good agreement with the experimental data, i.e., within an accuracy of 50%.

*(3)* Creep analysis method

Key items for establishing an appropriate creep analysis method are as follows:

- Generation of an appropriate creep constitutive equation,
- Definition of correct safety margins for uncertainties in predicting creep behavior, and
- A procedure to define loading sequences or combinations

For item one several research experiments were carried out to clarify a hardening rule and a flow rule under multiaxial stress states and also statistical analyses were made to formulate a creep equation, i.e., a correlation of creep data from constant uniaxial load tests under isothermal conditions. The experimental data showed the applicability of strain hardening rule and Von Mises' flow rule to Hastelloy XR. The statistical analyses revealed that the time function proposed by Garofalo, et al (1963) correlates the creep curve data in the superior agreement to the rational time function (Booker, 1977). Figure 108 shows the superiority of Garofalo's expression.

For item two, principles to define the safety margins for variations in creep behavior of a high temperature structure were established through sensitivity analysis of a creep constitutive equation. The analytical results clarified that the variations might be covered with those in fundamental creep property such as creep strain curves.

For item three, creep analyses of the very high temperature components were conducted, taking into account a unique feature of thermal transient behavior of the components.

Finally, the design limits and rules for Hastelloy XR in the HTTR high temperature structural design guideline were developed referring to those of the FBR Code, with exceptions.

Table 26 - HTGR High Temperature Structural Design Guideline Features

| Materials | Code features |
|---|---|
| Hastelloy XR | Referred to the FBR Code (Elevated Temperature Structural Design Guide for Class 1 Components of Prototype Fast Breeder Reactor "Monju"), design and limits are established from material properties and component test data. |
| 2 1/4Cr-1Mo steel and Austenitic stainless steels (SUS321 and SUS316 ) | Design rules and limits are the same as those of the FBR Code. Helium environment and neutron irradiation effects are newly added to the design limits. |
| 1Cr-0.5Mo-V steel | Design rules and limits are established from material properties data, taken into account the semi-creep service conditions in the HTTR |

Table 27 - Mechanical Properties Data on Hastelloy XR Obtained for High Temperature Structural Design Guideline

| Test item | Test conditions |
|---|---|
| Tensile tests | Temperatures : RT to 1000 °C, every 25 °C<br>Strain rates : 0.3 %/min to 100 %/min |
| Creep tests | Temperatures : 500 to 1050 °C, every 50 °C<br>Maximum test time : about 38,000 hours<br>Total number of tests : about 300 |
| Fatigue and creep-fatigue interaction tests | Temperatures : RT to 1000 °C, every 50 °C at high temperatures<br>Strain rates : $2\times10^{-5}$ to $1\times10^{-3}$ /s<br>Hold times : 0 to 1 hour<br>Materials : as-received and thermally aged |
| Fracture toughness tests | Thermal aging conditions<br>Temperatures : 800 to 1000 °C<br>Maximum aging time : 2,000 hours<br>Test items : V-notch charpy, fracture toughness and fatigue crack propagation rate |
| Corrosion tests | Environment : HTTR coolant gas-simulated helium<br>Temperatures : 900 to 1000 °C<br>Maximum test time : 30,000 hours |
| Others | Poisson's ratio, thermal expansion and so on |

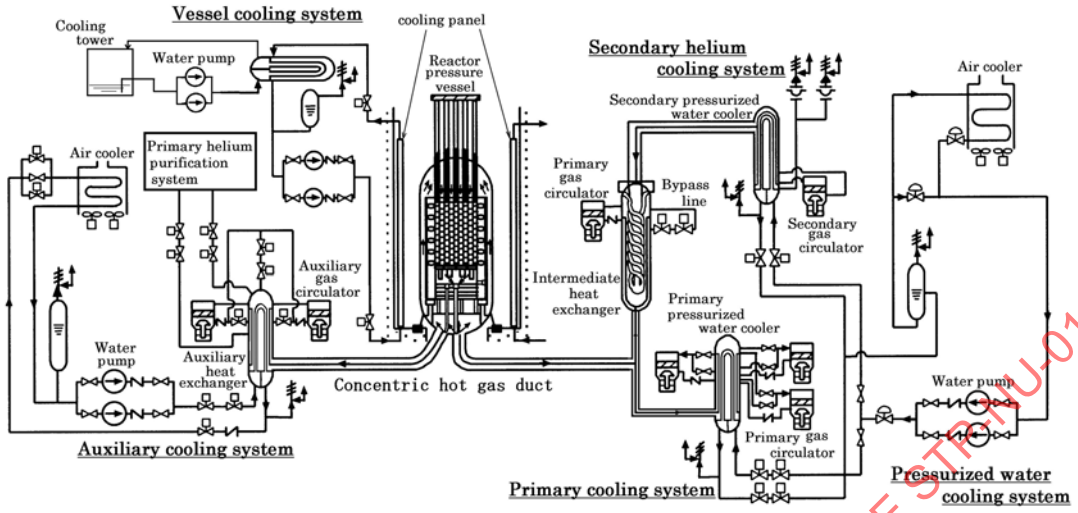


**Figure 101 - Cooling System of the HTTR**

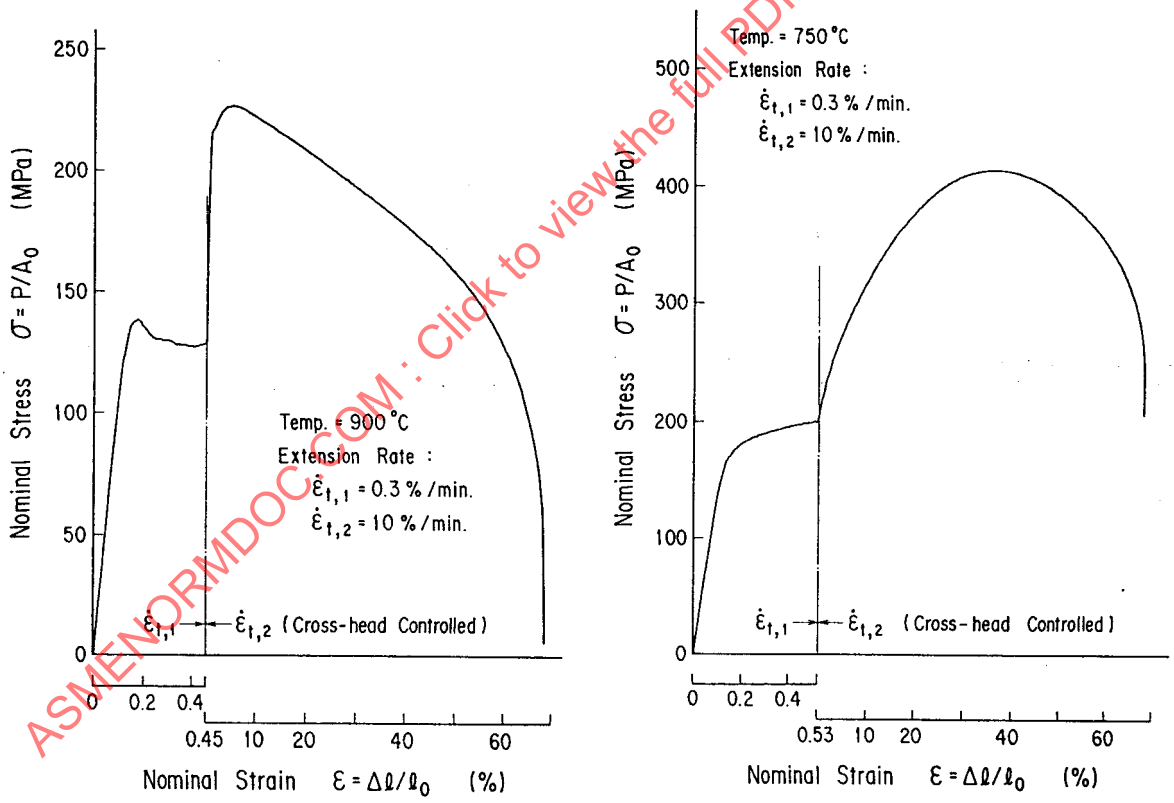


**Figure 102 - Tensile Stress-Strain Curves for Hastelloy XR at the Strain Rates of JIS**

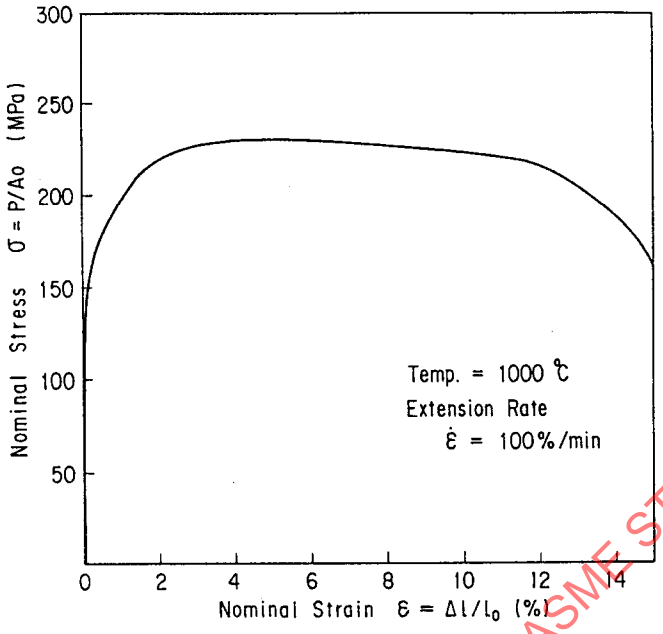


**Figure 103 - Stress-Strain Curve for Hastelloy XR (1000˚C, Extension Rate = 100%/Min)**

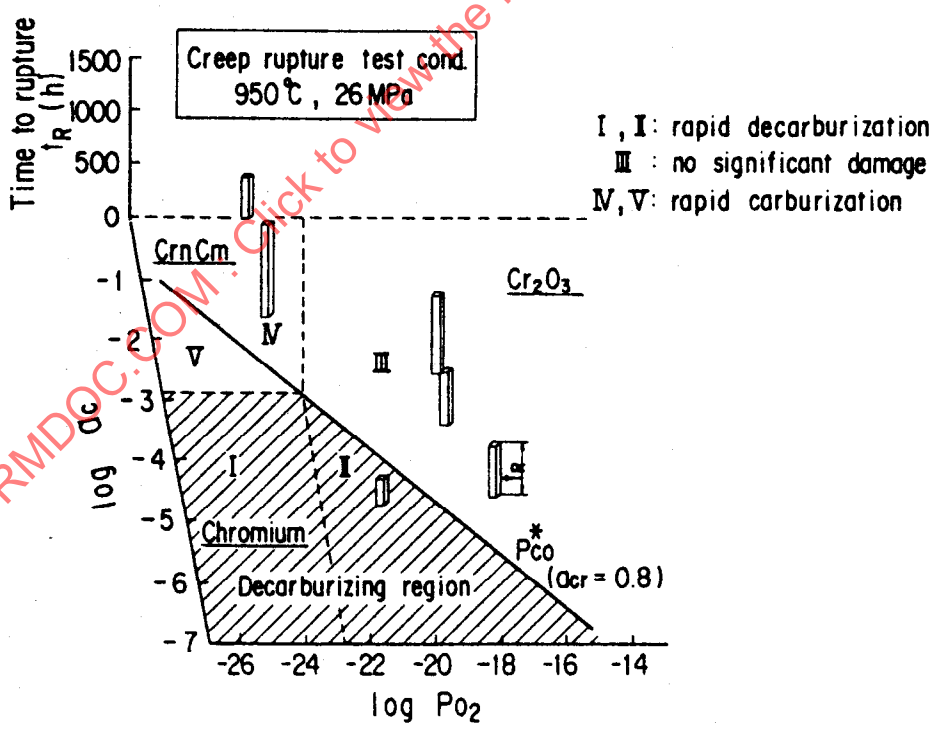


**Figure 104 - Comparison of Creep Rupture Lives for Hastelloy XR in Several Different Helium Environments on the Stability Diagram for Cr ($A_{cr}$=0.8) At 950˚C Under 26MPa**

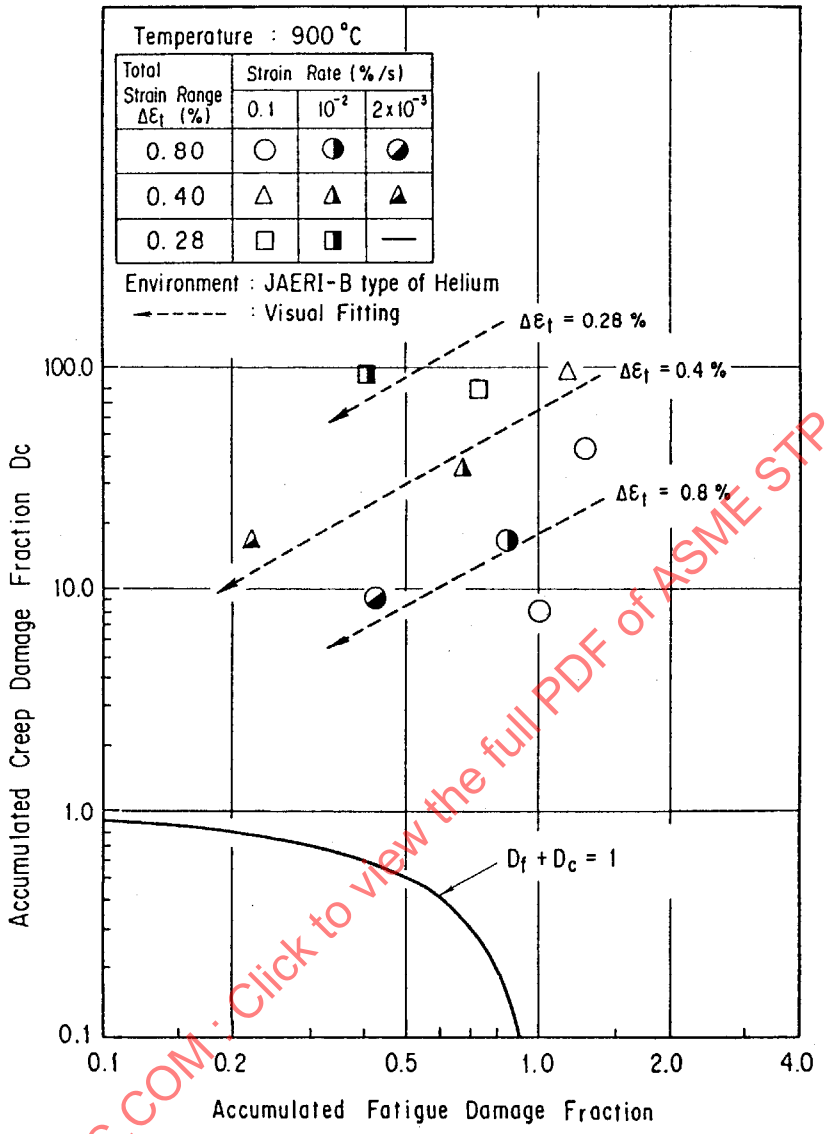


**Figure 105 - Strain Rate Effect on Creep-Fatigue Interaction for Hastelloy XR**

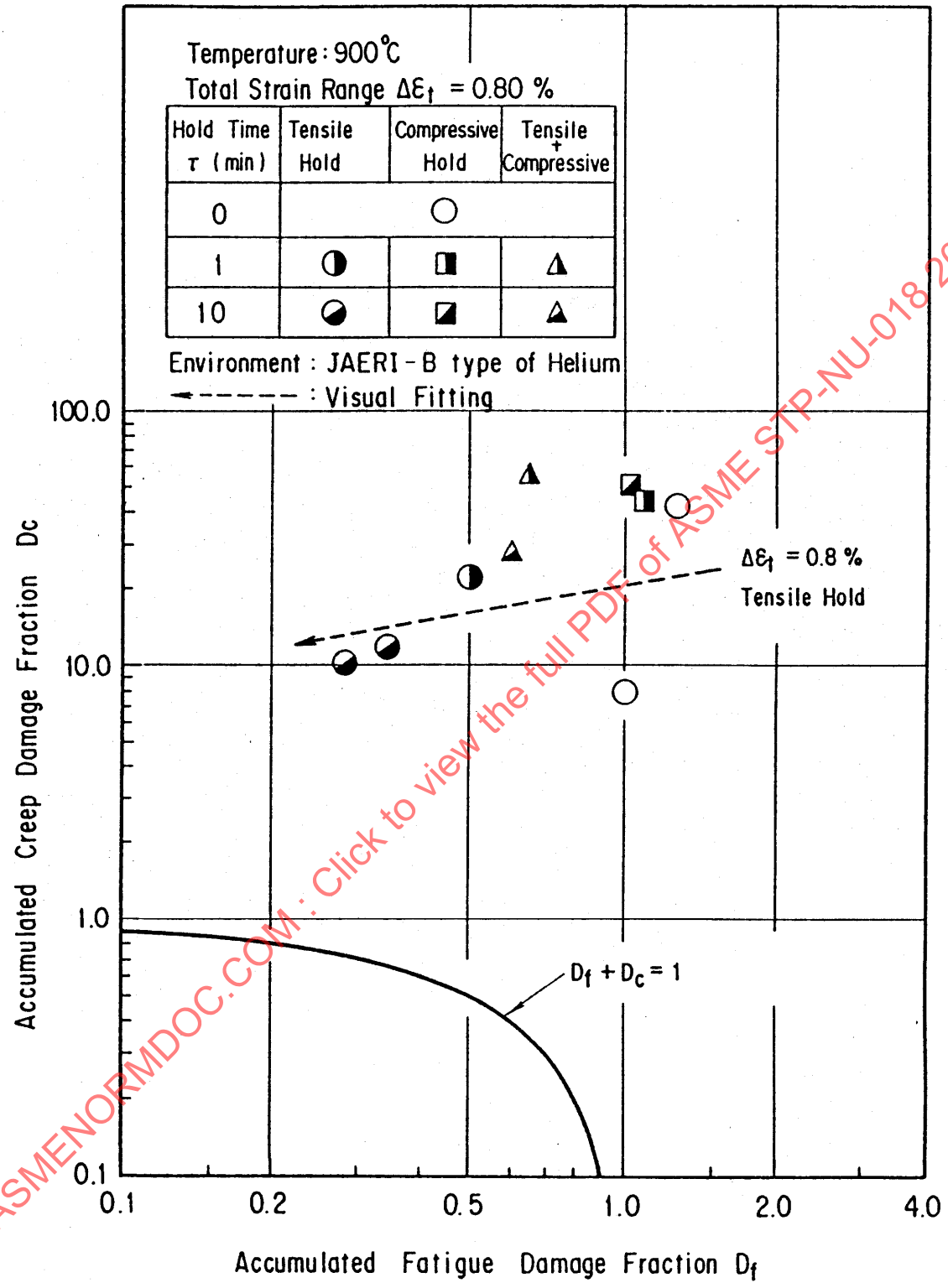




**Figure 106 - Hold Time Effect on Creep-Fatigue Interaction for Hastelloy XR**

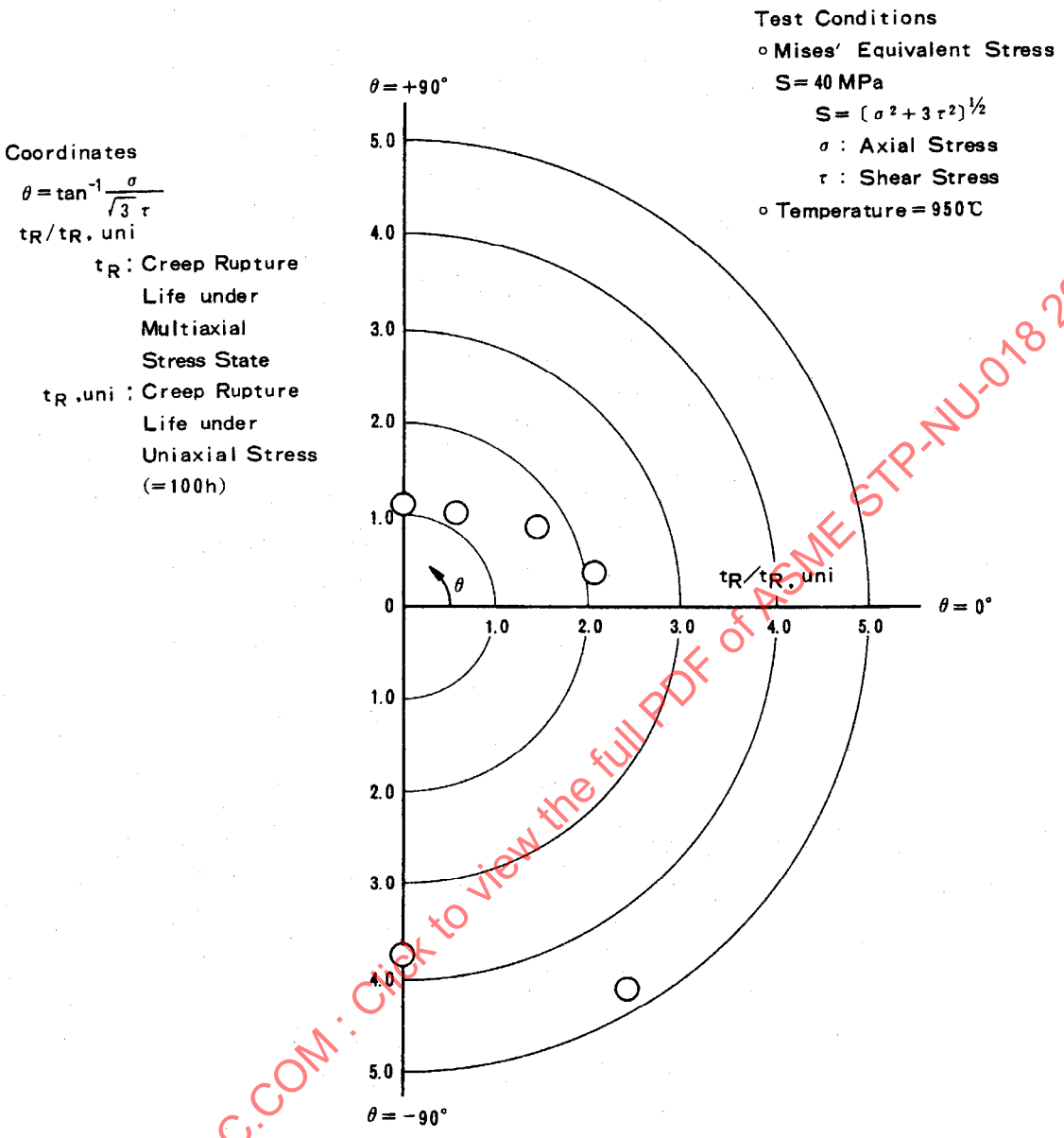


**Figure 107 - Creep Rupture Life under Multi-Axial Stress States for Hastelloy XR**

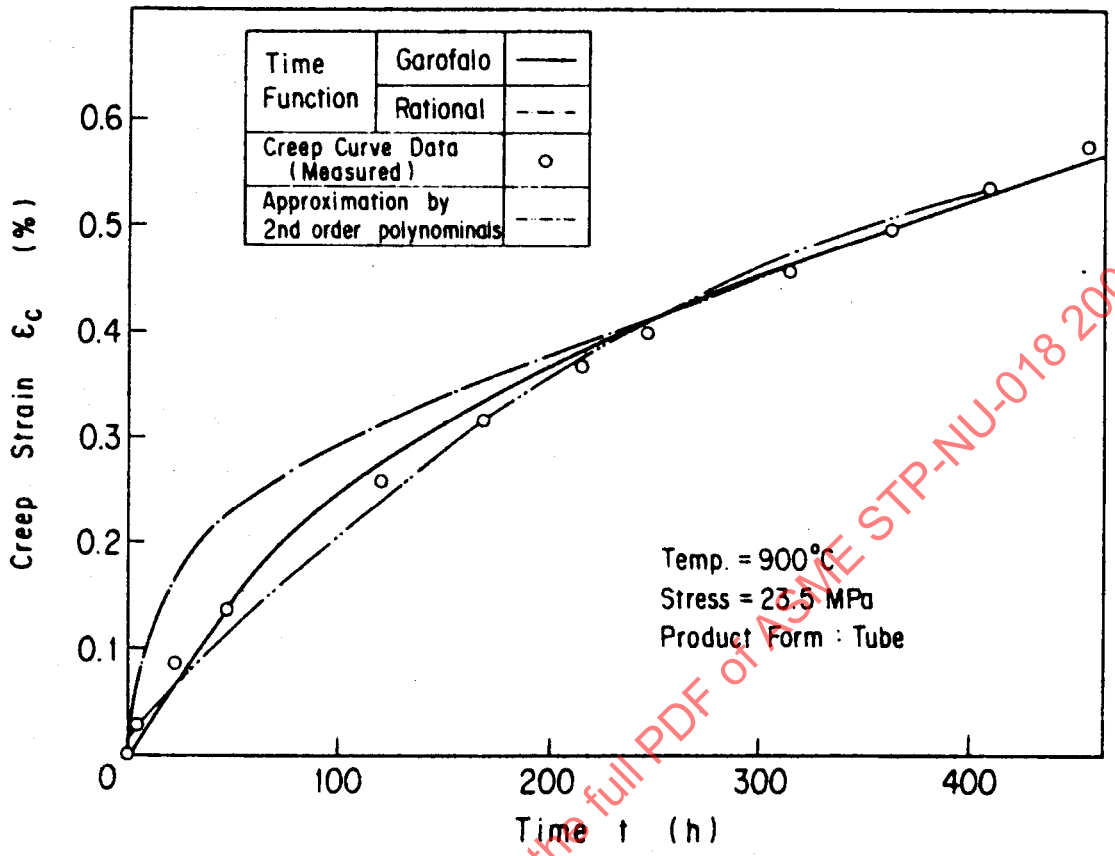


**Figure 108 - Applicability of Time Functions to Hastelloy XR**

## 2.2 Inelastic Analysis of the Intermediate Heat Exchanger (IHX) for HTTR

### 2.2.1 Intermediate Heat Exchanger (IHX) for the HTTR

The IHX is a vertical helically-coiled counter flow type heat exchanger in which primary helium gas flows on the shell side and secondary helium gas in the tube side as shown in Figure 109. Table 28 shows the major specifications of the IHX.

Primary helium gas enters the IHX through the inner pipe of the primary concentric hot gas duct. It is deflected under a hot header and discharged around the heat transfer tubes to transfer the heat to the secondary helium cooling system. It flows to the primary gas circulator via the upper outlet nozzle and flows back to the annular space between the inner and outer shells.

Secondary helium gas flows downwards in the heat transfer tubes and upwards in the central hot gas duct through the hot header. The inner insulation is installed inside the inner shell to maintain its temperature below 440˚C. The insulation outside and inside the central hot gas duct restrain the heat transfer so that high efficiency can be obtained. In addition, it also keeps the temperature of the central duct below 940˚C.

Primary helium gas is contained only in the primary cooling system because the pressure in the secondary helium cooling system is adjusted somewhat higher than that in the primary cooling system.

The tube support assemblies hold the heat transfer tubes. Both the central hot gas duct and the heat transfer tube support assemblies are hung from the vessel top so that the thermal expansion is not constrained.

The material of the heat transfer tubes and the hot header is Hastelloy XR and the inner and outer shells are made of 2 1/4Cr–1Mo steel.

The IHX has a bypass line, which prevents natural circulation from the reactor core to the IHX during the single loaded operation. The forced circulation from the Primary Pressurized Water Cooler (PPWC) through the bypass line occurs and keeps the temperature of the outer shell below 430˚C. Primary helium gas flows from the PPWC and enters into annulus space between the inner and outer shells and then flows inside the inner shell through the bypass line. It returns to the PPWC through the IHX and the primary concentric hot gas duct. The shutoff valve stops this forced circulation during the parallel loaded operation and in case of a scram when the auxiliary cooling system is activated.

The inner structures such as the heat transfer tubes, the central hot gas duct and the hot header are operated beyond 900˚C. A design method based on the elastic analysis cannot meet the criteria of the high temperature structural design guideline for the HTGR class 1 components. Therefore, the design method based on a creep analysis is used for evaluation of their structural integrity. The creep fatigue damage was properly evaluated and is capable of meeting the criteria.

### 2.2.2 Structural Integrity Evaluation of the HTTR IHX

Hastelloy XR is used for the heat transfer tubes, the center pipe and the hot header of the IHX. The heat transfer tubes, the center pipe and the hot header form the boundary of primary helium and secondary helium. The material creep becomes remarkably large at operation temperatures higher than 900˚C. Therefore, creep strain and creep damage was evaluated by inelastic analysis, i.e., elastic creep analysis in the structural integrity evaluation. The elastic creep analysis was employed, because at the high temperature around 900˚C where creep deformation is dominant, it is meaningless and impossible to separate creep and plastic deformation. Thus, only creep strain is treated as inelastic strain.

#### 2.2.2.1 Creep analysis method

As a uni-axial creep constitutive equation, the following Garofalo's expression is used as described above:

$$\varepsilon_c = \varepsilon_t\left(1 - e^{-rt}\right) + \dot{\varepsilon}_{\min} \cdot t$$

where:

$\varepsilon_c$ : creep strain

$\varepsilon_t$ : maximum primary creep strain

$r$ : inverse number of time constant for primary creep

$t$ : time

$\dot{\varepsilon}_{\min}$ : minimum creep strain rate

The material constants of Hastelloy XR are shown in Table 29.

For the flow rule, the following flow rule of Mises is used:

$$\dot{\varepsilon}_{cij} = \lambda \cdot s_{ij} = \frac{3\dot{\varepsilon}_{ceq}}{2\sigma_{eq}} s_{ij}$$

where:

$\dot{\varepsilon}_{cij}$ : creep strain rate tensor

$\dot{\varepsilon}_{ceq}$ : equivalent creep strain rate

$\sigma_{eq}$ : equivalent stress

$s_{ij}$ : stress deviator tensor

For the hardening rule, strain hardening rules was adopted and ORNL rule was used when stress reversal occurs.

#### 2.2.2.2 Evaluation of cumulative inelastic strain

In the high temperature structural design guideline for HTGR, it is required to limit cumulative principal inelastic strain (membrane) lower than 0.01 and cumulative principal inelastic strain (membrane + bending) lower than 0.02.

In the first step, some events with severer thermal transients were selected, their order and duration time was considered, and loading hysteresis was determined. Then, elastic creep analysis of selected parts of the IHX was performed according to the loading hysteresis, and creep strain was derived.

In order to obtain cumulative inelastic strain at the end of lifetime of the IHX, creep strain at certain evaluation points in the first several (at least three) cycles of the loading hysteresis were calculated, and then extrapolated using the following equation:

$$\varepsilon_{ji}(eoh) = \varepsilon_{ji}(last) + \{\varepsilon_{ji}(last) - \varepsilon_{ji}(last-1)\} \times (N - last)$$

where

$\varepsilon_{ji}$ : cumulative creep strain in the loading hysteresis $j$ ($i$ = 1 to 6)

$eoh$ : end of the loading hysteresis $j$

$last$: the last cycle number (three or larger) analyzed in the loading hysteresis $j$

$N$ : number of cycles in the loading hysteresis $j$

The equation above is applicable when:

$$\{\varepsilon_{ji}(last) - \varepsilon_{ji}(last-1)\} \leq \{\varepsilon_{ji}(last-1) - \varepsilon_{ji}(last-2)\}$$

Finally, the cumulative creep strain was derived using the following equation:

$$\varepsilon_i(eoh) = \sum_j \varepsilon_{ji}(eoh)$$

#### 2.2.2.3 Evaluation of cumulative creep fatigue damage factor

In the high temperature structural design guideline for HTGR, it is required to limit cumulative creep fatigue damage factor as follows:

$$D_f + D_c \leq D$$

where

$D_f$: cumulative fatigue damage factor

$D_c$ : cumulative creep damage factor

$D$ : 1 (Allowable limit)

and

$$D_c = 2\int_0^{t^*} \frac{dt}{T_d} \quad D_f = \sum_i \frac{n_i}{N_{di}}$$

where:

$N_{di}$: number of design allowable cycles (Figure 110)

$T_d$: allowable time duration derived from stress-to-rupture curve (Figure 111)

Similarly to the process of evaluation of cumulative creep strain, in the first step of evaluating creep damage, some events with severer thermal transient were selected, their order and duration time was considered, and loading hysteresis was determined. Then, elastic creep analysis of selected parts of the IHX was performed according to the loading hysteresis, and Mises equivalent stress at certain evaluation points in the first several (at least three) cycles of the loading hysteresis was calculated using the following equation:

$$(D_c)_{cycle} = 2\sum\left(\frac{\Delta t_i}{T_{di}^*}\right)$$

where:

$(D_c)_{cycle}$ = creep damage factor of a certain cycle number

$T_{di}^*$: $T_d(T, \sigma_{eq}^*)$; allowable time duration for temperature $T$ and Mises eq stress $\sigma_{eq}^*$

$\sigma_{eq}^*$: max ($\sigma_{eq,i}$, $\sigma_{eq,i+1}$)

$\sigma_{eq,i}$: Mises equivalent stress at time point $i$

$\sigma_{eq,i+1}$: Mises equivalent stress at time point $i+1$

$\Delta t_i$: time increment from time point $i$ to time point $i+1$

Then, the creep damage factor was extrapolated to the end of lifetime using the following equation:

$$(D_c)_{eoh,j} = \sum_1^{last} (D_c)_{cycle,j} + (D_c)_{last,j} \times (N - last)$$

where:

$(D_c)_j$: creep damage factor of the loading hysteresis $j$

$(D_c)_{cycle,j}$: creep damage factor of a certain cycle number in the loading hysteresis $j$

*eoh*: end of the loading hysteresis $j$

*last*: the last cycle number (three or larger) analyzed in the loading hysteresis $j$

$N$: number of cycles in the loading hysteresis $j$

The equation above is applicable when:

$$(D_c)_{last,j} \leq (D_c)_{cycle,j}$$

Finally, the cumulative creep damage factor was derived using the following equation:

$$(D_c)_{eoh} = \sum_j (D_c)_{eoh,j}$$

On the other hand, cumulative fatigue damage factor was derived by elastic analysis procedure in the high temperature structural design guideline for HTGR and added to the cumulative creep damage factor.

The thermal stress in the first layer of heat transfer tube is evaluated since it becomes possibly the maximum value. This originates due to the short horizontal distance to the first bend from the hot header and due to the temperature gradient between the center pipe and the heat transfer tube. Table 30 shows evaluation results of the heat transfer tube. The cumulative principal creep strain is calculated to be 0.0013 for membrane and 0.0021 for the sum of membrane and bending, respectively. The cumulative creep and fatigue factors reach 0.26. These results satisfy the allowable limits, which were established in the high temperature structural design code for the HTGR class 1 components.

Figure 112 shows a vertical view of a lower reducer of the center pipe in the intermediate heat exchanger. Table 31 shows evaluation results for the lower reducer of the center pipe. The maximum cumulative principal creep strain is calculated to 0.0011 for membrane and 0.0032 for the sum of membrane and bending, respectively. The cumulative creep and fatigue factors reach 0.28. These results also satisfy the allowable limits in the same structural design code.

**Table 28 - Major Specifications of the Intermediate Heat Exchanger for HTTR**

| Type | Vertical helically-coiled counter flow | |
|---|---|---|
| Design pressure | | |
| Outer shell | 4.7 MPa | |
| Heat transfer tube | 0.29 MPa (differential pressure) | |
| Design temperature | | |
| Outer shell | 430 °C | |
| Heat transfer tube | 955 °C | |
| Operating condition | Rated operation | High temperature test operation |
| Flow rate of primary helium gas (maximum) | 15 t/h | 12 t/h |
| Inlet temperature of primary helium gas | 850 °C | 950 °C |
| Outlet temperature of primary helium gas | 390 °C | 390 °C |
| Flow rate of secondary helium gas | 14 t/h | 12 t/h |
| Inlet temperature of secondary helium gas | 300 °C | 300 °C |
| Outlet temperature of secondary helium gas | 775 °C | 860 °C |
| Heat capacity | 10 MW | |
| Heat transfer tube | | |
| Number | 96 | |
| Outer diameter | 31.8 mm | |
| Thickness | 3.5 mm | |
| Length | 30 m | |
| Outer diameter of shell | 2.0 m | |
| Total height | 11.0 m | |
| Material | | |
| Outer and inner shell | 2 1/4Cr-1Mo steel | |
| Heat transfer tube | Hastelloy XR | |
| Hot header and center pipe | Hastelloy XR | |

**Table 29 - Material Constants of the Creep Constitutive Equation for Hastelloy XR**

$$\varepsilon_c = \varepsilon_t\left(1 - e^{-rt}\right) + \dot{\varepsilon}_{\min} \cdot t$$

where

$\varepsilon_c$ = creep strain (mm/mm)

$\varepsilon_t$ = maximum primary creep strain (mm/mm)

$r$ = inverse number of time constant for primary creep (1/h)

$t$ = time (h)

$\dot{\varepsilon}_{\min}$ = minimum creep strain rate (mm/mm/h)

and

$\sigma$ = stress (kg/mm$^2$)

$T$ = temperature (°C)

**$\varepsilon_t$**

$4.0 < \sigma$ : $\varepsilon_t = 0.056 \times 10^{-2}$

$2.0 < \sigma \leq 4.0$ : $\varepsilon_t = (-0.0578 + 0.454 / \sigma) \times 10^{-2}$

$0.5 < \sigma \leq 2.0$ : $\varepsilon_t = 0.169 \times 10^{-2}$

$\sigma \leq 0.5$ : $\varepsilon_t = \{0.169 \cdot (\sigma / 0.5)\} \times 10^{-2}$

**$r$**

$0.5 \leq \sigma$ : $r = 10^{p(\sigma,T)}$

$\sigma < 0.5$ : $r = 10^{p(\sigma=0.5,T)} \cdot (\sigma / 0.5)$

where

$p(\sigma, T) = f_1(T) + f_2(T) \cdot \sigma$

$f_1(T) = 4.854 - 2.415 \times 10^{-2} \cdot T + 1.674 \times 10^{-5} \cdot T^2$

$f_2(T) = 3.399 - 9.898 \times 10^{-3} \cdot T + 7.693 \times 10^{-6} \cdot T^2$

**$\dot{\varepsilon}_{\min}$**

$0.5 \leq \sigma$ : $\dot{\varepsilon}_{\min} = 10^{fa(\sigma,T)} \times 10^{-2}$

$0.1 \leq \sigma < 0.5$ : $\dot{\varepsilon}_{\min} = 10^{fb(\sigma,T)} \times 10^{-2}$

$\sigma < 0.1$ : $\dot{\varepsilon}_{\min} = 10^{fb(\sigma=0.1,T)} \cdot (\sigma / 0.1) \times 10^{-2}$

where

$fa(\sigma, T) = 14.326 + 3.222 (\log_{10}\sigma) + 2.400 (\log_{10}\sigma)^2 - 2.246 \times 10^4 / (T + 273.15)$

$fb(\sigma, T) = 1.777 (\log_{10}\sigma + 0.30103) + 13.574 - 2.246 \times 10^4 / (T + 273.15)$

**Table 30 - Cumulative Principal Creep Strain, Cumulative Creep and Fatigue Damage Factors of the Heat Transfer Tubes at First Layer in the Intermediate Heat Exchanger**

| Evaluation items | | Evaluation result | Allowable limit |
|---|---|---|---|
| $\varepsilon_c$ | Membrane | 0.0013 | 0.01 |
| | Membrane+Bending (inner surface) | 0.0021 | 0.02 |
| | Membrane+Bending (outer surface) | 0.0005 | 0.02 |
| $D_c$ | Inner surface | 0.187 | - |
| | Outer surface | 0.106 | - |
| $D_f$ | Inner surface | 0.072 | - |
| | Outer surface | 0.066 | - |
| $D_c+D_f$ | Inner surface | 0.26 | 1.0 |
| | Outer surface | 0.18 | 1.0 |

Note:

$\varepsilon_c$: cumulative principal creep strain.
$D_c$: cumulative creep damage factor.
$D_f$: cumulative fatigue damage factor.

**Table 31 - Cumulative Principal Creep Strain, Cumulative Creep and Fatigue Damage Factors of the Lower Reducer of the Center Pipe in the Intermediate Heat Exchanger**

| EC | Evaluation items | | Evaluation result | Allowable limit |
|---|---|---|---|---|
| 1 | $\varepsilon_c$ | Membrane | 0.0008 | 0.01 |
| | | Membrane+Bending (inner surface) | 0.0004 | 0.02 |
| | | Membrane+Bending (outer surface) | 0.0009 | 0.02 |
| | $D_c$ | Inner surface | 0.076 | - |
| | | Outer surface | 0.111 | - |
| | $D_f$ | Inner surface | 0.001 | - |
| | | Outer surface | 0.001 | - |
| | $D_c+D_f$ | Inner surface | 0.08 | 1.0 |
| | | Outer surface | 0.12 | 1.0 |
| 2 | $\varepsilon_c$ | Membrane | 0.0007 | 0.01 |
| | | Membrane+Bending (inner surface) | 0.0006 | 0.02 |
| | | Membrane+Bending (outer surface) | 0.0008 | 0.02 |
| | $D_c$ | Inner surface | 0.078 | - |
| | | Outer surface | 0.107 | - |
| | $D_f$ | Inner surface | 0.001 | - |
| | | Outer surface | 0.001 | - |
| | $D_c+D_f$ | Inner surface | 0.08 | 1.0 |
| | | Outer surface | 0.11 | 1.0 |
| 3 | $\varepsilon_c$ | Membrane | 0.0011 | 0.01 |
| | | Membrane+Bending (inner surface) | 0.0006 | 0.02 |
| | | Membrane+Bending (outer surface) | 0.0012 | 0.02 |
| | $D_c$ | Inner surface | 0.076 | - |
| | | Outer surface | 0.110 | - |
| | $D_f$ | Inner surface | 0.001 | - |
| | | Outer surface | 0.001 | - |
| | $D_c+D_f$ | Inner surface | 0.08 | 1.0 |
| | | Outer surface | 0.12 | 1.0 |

Note: EC: Evaluation cross section. $\varepsilon_c$: cumulative principal creep strain.
$D_c$: cumulative creep damage factor. $D_f$ :cumulative fatigue damage factor.

| EC | Evaluation items | | Evaluation result | Allowable limit |
|---|---|---|---|---|
| 4 | $\varepsilon_c$ | Membrane | 0.0009 | 0.01 |
| | | Membrane+Bending (inner surface) | 0.0027 | 0.02 |
| | | Membrane+Bending (outer surface) | 0.0013 | 0.02 |
| | $D_c$ | Inner surface | 0.077 | - |
| | | Outer surface | 0.081 | - |
| | $D_f$ | Inner surface | 0.001 | - |
| | | Outer surface | 0.001 | - |
| | $D_c+D_f$ | Inner surface | 0.08 | 1.0 |
| | | Outer surface | 0.09 | 1.0 |
| 5 | $\varepsilon_c$ | Membrane | 0.0006 | 0.01 |
| | | Membrane+Bending (inner surface) | 0.0032 | 0.02 |
| | | Membrane+Bending (outer surface) | 0.0023 | 0.02 |
| | $D_c$ | Inner surface | 0.259 | - |
| | | Outer surface | 0.080 | - |
| | $D_f$ | Inner surface | 0.002 | - |
| | | Outer surface | 0.001 | - |
| | $D_c+D_f$ | Inner surface | 0.27 | 1.0 |
| | | Outer surface | 0.09 | 1.0 |
| 6 | $\varepsilon_c$ | Membrane | 0.0010 | 0.01 |
| | | Membrane+Bending (inner surface) | 0.0014 | 0.02 |
| | | Membrane+Bending (outer surface) | 0.0007 | 0.02 |
| | $D_c$ | Inner surface | 0.270 | - |
| | | Outer surface | 0.096 | - |
| | $D_f$ | Inner surface | 0.001 | - |
| | | Outer surface | 0.001 | - |
| | $D_c+D_f$ | Inner surface | 0.28 | 1.0 |
| | | Outer surface | 0.10 | 1.0 |

Note: EC: Evaluation cross section. $\varepsilon_c$: cumulative principal creep strain.
$D_c$: cumulative creep damage factor. $D_f$: cumulative fatigue damage factor.

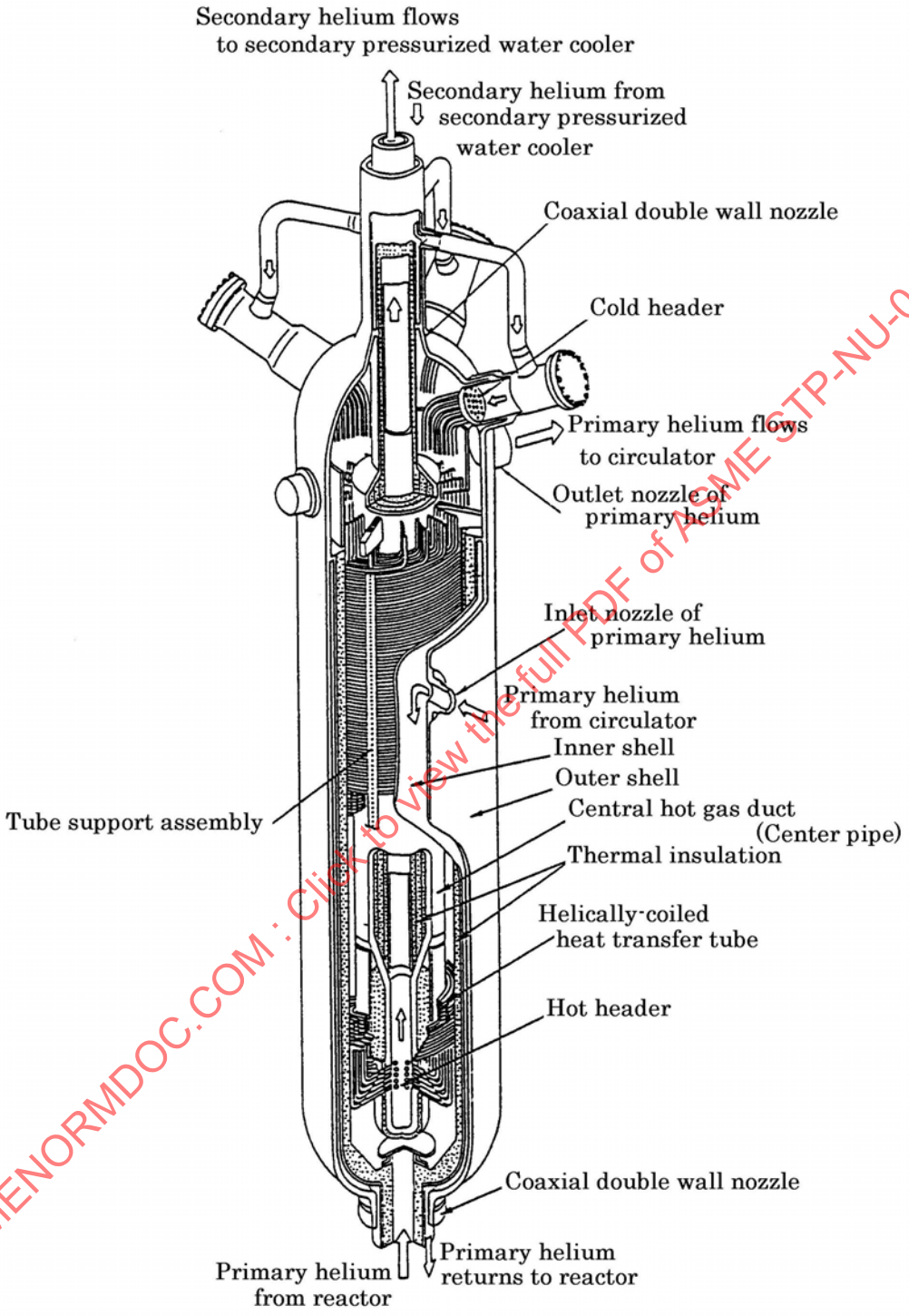




**Figure 109 - Intermediate Heat Exchanger (IHX) for HTTR**

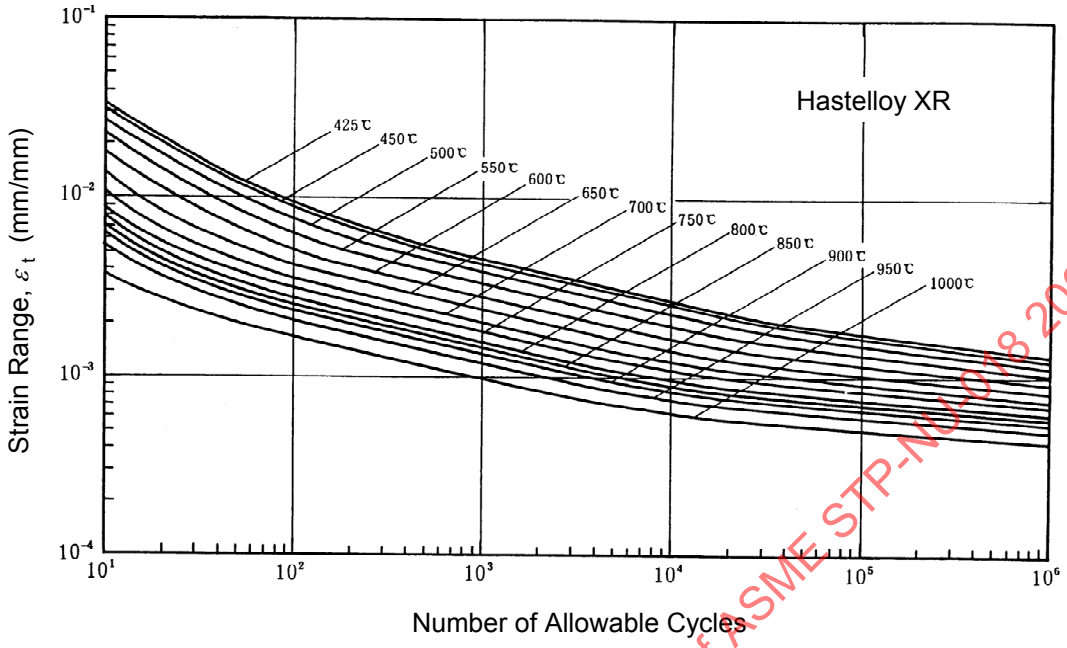


**Figure 110 - Design Fatigue Strain Range for Hastelloy XR**

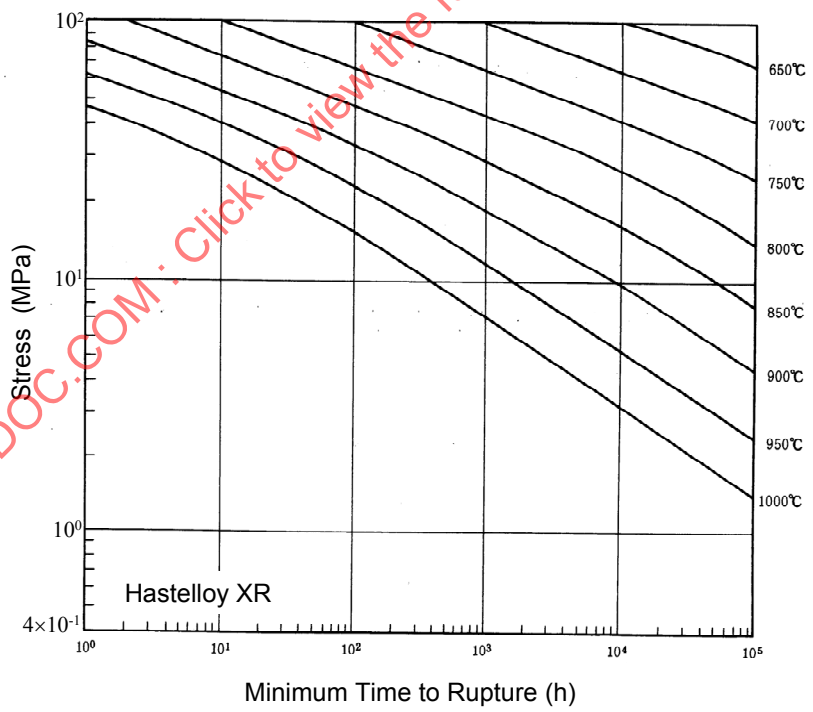


**Figure 111 - Stress-to-Rupture Curve for Hastelloy XR**

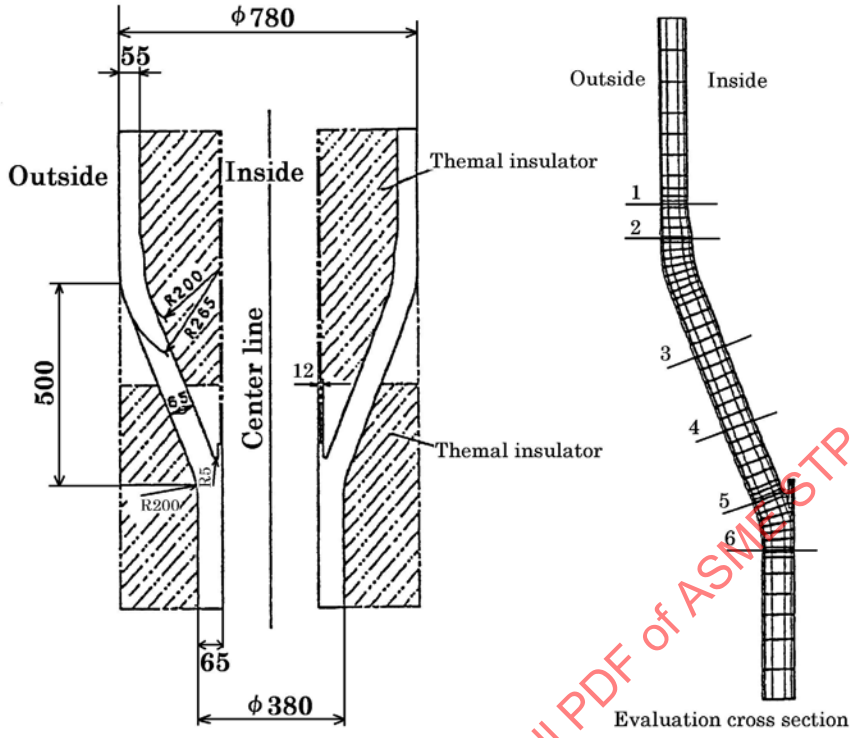


**Figure 112 - Vertical View of the Lower Reducer of the Center Pipe in the IHX**

## 2.3 Summary of Creep-Fatigue Criteria on Hastelloy XR

From a screening of commercial and experimental superalloys available in the 1970s, Hastelloy X was selected for the very high temperature structures such as the heat transfer tubes of the IHX. Since Hastelloy X does not have sufficient compatibility with the primary helium coolant, the improved version of Hastelloy X, which is called Hastelloy XR, was developed through optimizing or lowering contents of several elements.

Since some of the high temperature materials and their service temperatures were out of scope of the existing FBR Code, many research works on material characterizations and structural mechanics behavior were made in order to establish a high temperature structural design code for both materials.

Material characterizations for Hastelloy XR suggested that special considerations should be taken into account for dynamic recrystallization at high temperatures. A new tensile test procedure with a change in strain rate to 100%/min at temperatures over 800°C was proposed to obtain the time-independent elastic-plastic property for Hastelloy XR. The further material characterization and component-wise structural mechanics research works revealed that design rules for austenitic stainless steels can be applied to Hastelloy XR, and, therefore, the high temperature structural design guideline was established, referring to the FBR Code. A creep analysis method was established for Hastelloy XR through several research works. In the creep analysis method, the creep equation was generated from Garofalo's type of the time function, and it was also demonstrated that the strain hardening rule and Von Mises' flow rule is applicable to Hastelloy XR.

In the design of the intermediate heat exchanger (IHX) for HTTR, inelastic analysis was conducted to evaluate cumulative creep strain and cumulative creep and fatigue damage factors based on the high temperature structural design guideline.

# 3 NECESSARY RESEARCH AND DEVELOPMENT ITEMS IN RELATION TO CREEP-FATIGUE EVALUATION FOR GEN IV AND VHTR REACTORS

## 3.1 Linear Summation Rule of Cycle and Time Fractions

As described in section 1.1 and 2.1, creep fatigue tests on Hastelloy XR by JAEA were performed in order to confirm conservativeness of conventional linear summation rule of cycle and time fractions (fatigue and creep damage factors) with the allowable limit $D$ of 1. It was concluded in section 2.1 that the linear summation rule is applicable to Hastelloy XR with a great deal of safety margins even at very high temperatures.

It is envisaged that the linear summation rule is similarly applicable to other Ni-base superalloys like Inconel 617 and Haynes 230. However, creep fatigue tests on Inconel 617 and Haynes 230 will be needed to confirm conservativeness of conventional linear summation rule or to develop new methods.

## 3.2 Inelastic Constitutive Equations

In the design of the intermediate heat exchanger (IHX) for HTTR, inelastic analysis was necessary to evaluate creep strain and creep damage at very high temperatures. Similarly, in the design of high temperature components such as IHX made of Inconel 617 and Haynes 230, inelastic analysis will be inevitable. In the design of HTTR IHX, conventional Garofalo's expression was used as a creep constitutive equation because the high temperature structural design guideline was developed in 1980s. Recently, a lot of constitutive equations using so called unified theory have been developed by Chaboche, Krempl, etc. In the future design of high temperature components, applicability of unified inelastic constitutive equations should be investigated.

## 3.3 Helium Environmental Effect

Impurities in the primary coolant of the HTTR must be controlled so that primary coolant shall be in area III of Figure 104, where mild carburization occurs. For this purpose, research and developments are underway in the HTTR to develop methods to control helium purification system.

Similarly, research and developments will be needed for future HTGRs on Inconel 617 and Haynes 230 to determine optimum level of impurities in the primary coolant as well as to develop methods of controlling helium purification system to keep the optimum level.